

AALBORG UNIVERSITY

---

**RELIABILITY ANALYSIS OF FATIGUE  
IN COMPOSITE TENSION  
REINFORCEMENT BARS  
IN A BRIDGE STRUCTURE**

---

MASTER THESIS, M.SC. IN STRUCTURAL AND CIVIL ENGINEERING



---

CHRISTIAN HJORTH &  
FREDERIK BOYSEN  
AALBORG UNIVERSITY  
SCHOOL OF ENGINEERING  
AND SCIENCE

---

TURNED IN: 10/06/2015

---

© Aalborg University, spring 2015

Christian Hjorth and Frederik Boysen

The content of this report is freely accessible, however publication  
(with source references) is only allowed upon agreement with the authors.

This report is typeset in Times New Roman 11pt.  
Layout and typography by the authors using L<sup>A</sup>T<sub>E</sub>X.

---

**Master Thesis, Master of Science  
at the School of Civil Engineering**

**AALBORG UNIVERSITY**  
STUDENT REPORT

Sofiendalsvej 9-11  
9200 Aalborg SV  
Telephone 9940 8484  
Fax 9940 8552  
<http://www.ses.aau.dk/>

**Synopsis:**

**Title:**

Reliability Analysis of Fatigue  
in Composite Reinforcement  
Tension Bars in a Bridge Structure

**Project period:**

4<sup>th</sup> semester M.Sc, spring 2015

**Supervisors:**

John Dalgaard Sørensen  
Henrik Stensgaard Toft

**Report circulation:** 3

**Report page numbers:** 1-131

**Appendix page numbers:** 133-149

**Turned in:** 10<sup>th</sup> June 2015

Fiber-reinforced polymer composites have been used in civil engineering for years, as replacement material for traditional materials and are becoming more used in structures. This raises the need for a design standard for fiber reinforced polymer composites. However no Eurocode is available for fiber reinforced polymer composites.

In this report, fatigue of fiber-reinforced polymer is investigated in order to calibrate partial safety factors using probabilistic methods for a traffic bridge system. The traffic bridge system is mainly composed of composites. Characterization of strengths is achieved through static and fatigue tests using statistical analysis. Traffic loads are applied according to DS/EN 1991-2 and uncertainties regarding the traffic load is modeled as stochastic variables. The fatigue limit state is investigated along with a sensitivity analysis. Based on the fatigue limit state and corresponding design equation, the partial safety factors are calibrated to the target reliability levels for bridges according DK NA.

**Participants:**

---

Christian Hjorth

---

Frederik Boysen



---

# Preface

This report presents the work from the 4<sup>th</sup> semester master program in *Structural and Civil Engineering* at Aalborg University by Christian Hjorth and Frederik Boysen. The subject is "*Reliability Analysis of Fatigue in Composite Reinforcement Tension Bars in a Bridge Structure*". The project was made during the spring semester of 2015 and delivered on 10.06.2015 under guidance from supervisors, John Dalsgaard Sørensen and Henrik Stensgaard Toft.

## Reading Guidelines

References throughout the report are collected in a bibliography at the back of the report, where all the sources of knowledge are mentioned with the needed data. Sources are presented using the *Harvard Method*, wherein a reference is given as: [Author, Year].

In each chapter of the main report, tables, pictures, and equations are used. They are given a reference numbers, starting with the number of the chapter. For equations the numbering will only occur if the equation has been referred to. Also, if needed, commentary text is added below figures/tables for easier understanding for the reader.

Important appendixes coupled to the report are found at the back of the report. A digital appendix is placed on a CD attached to the report. The digital appendix contains *MATLAB* scripts, Excel-documents and the report as a PDF version. References inside the report to the Appendix-CD are done as [Appendix-CD, "*Document Name*"].



## Abstract

Fiber-forstærket polymer kompositter har været anvendt som udskiftningsmateriale for traditionelle materialer såsom stål og beton i mange år, men bliver nu anvendt i større grad som konstruktionsmateriale. Dette skaber behov for en designnorm for fiber-forstærket kompositter, men der er ikke i skrivende stund en Eurocode eller dansk anneks tilgængelig for fiber-forstærker polymer kompositter.

I denne rapport undersøges udmattelse af fiber-forstærket polymer kompositter med mål at kalibrere partialkoefficienter for et brosystem ved brug af probabilistiske metoder. Brosystemet består hovedsageligt af kompositmateriale.

Til karakterisering af materialeegenskaber anvendes statiske forsøg samt udmattelsesforsøg, hvor Maximum-Likelihood metoden anvendes til at bestemme materialeparametre til  $S-N$ -kurven samt statistiske usikkerheder. Ydermere undersøges forskellige constant life diagrammer på baggrund af tilgængeligt eksperimentelt data.

Brosystemet påvirkes af trafiklasten. Til at estimere trafiklasten anvendes udmattelseslastmodel 4 iht. DS/EN 1991-2. Yderligere påføres stokastiske usikkerheder til trafiklasten for at tage højde for varierende vægt og placering samt dynamiske effekter.

I forbindelse med undersøgelse af udmattelse af fiber-forstærket polymer kompositter undersøges udmattelsesgrænsetilstanden ved en pålidelighedsanalyse. I pålidelighedsanalysen opstilles en ligning for grænsetilstanden, der tager højde for usikkerhed på laster og materiale. Ydermere foretages et følsomhedsstudie af udmattelsesgrænsetilstanden for at vurdere, hvilke stokastiske variable er mest betydningsfulde for sikkerhedsindekset. Designligninger opstilles for forskellige constant life diagrammer, hvor partialkoefficienter og karakteristiske værdier er anvendt. Partialkoefficienter kalibreres iht. årlige sikkerhedsindekser for trafikbroer iht. dansk anneks, hvorfra anbefalede partialkoefficienter til brug i det undersøgte kompositmateriale bestemmes.



---

# Contents

<b>Preface</b>	<b>iii</b>
Reading Guidelines . . . . .	iii
<b>Notation list</b>	<b>ix</b>
<b>1 Introduction</b>	<b>1</b>
1.1 Statement of Intent . . . . .	3
<b>2 A Short Introduction to Composites</b>	<b>5</b>
2.1 Fatigue in Composites . . . . .	8
2.2 Fiber-Reinforced Composites in Codes . . . . .	21
<b>3 Bridge System</b>	<b>23</b>
3.1 Design Criteria . . . . .	23
3.2 Static System . . . . .	23
3.3 Static Loads . . . . .	25
<b>4 Uncertainty Modeling</b>	<b>29</b>
4.1 Experimental Characterization of Fiber-Reinforced Composite Materials . . . . .	30
4.2 Uncertainty of Transverse Positioning of Vehicles . . . . .	44
4.3 Uncertainty for Variable Loads . . . . .	45
4.4 Uncertainty in Calculation of Stresses . . . . .	45
4.5 Damage Accumulation Model . . . . .	46
4.6 Overview of Uncertainties and Stochastic Variables . . . . .	46
<b>5 Fatigue Loads</b>	<b>49</b>
5.1 Critical Fatigue Points . . . . .	59
5.2 Estimation of Adequate Amount of Lorry Crossings . . . . .	76
5.3 Precision of Discretization . . . . .	78
5.4 Concluding Remarks . . . . .	81
<b>6 Reliability Analysis</b>	<b>85</b>
6.1 Basic Concept of Probabilities in Civil Engineering . . . . .	85
6.2 Reliability Assessment Methods . . . . .	89

---

6.3	Target Reliability . . . . .	92
6.4	Overview of Reliability Analysis . . . . .	94
6.5	Fatigue Limit State . . . . .	95
6.6	Sensitivity Analysis . . . . .	101
6.7	Correlation between $\log K$ for Different $R$ -ratios . . . . .	106
<b>7</b>	<b>Reliability-Based Calibration of Partial Safety Factors</b>	<b>109</b>
7.1	Partial Safety Factors as DS/INF 172 . . . . .	109
7.2	Partial Safety Factors as Germanischer Lloyd . . . . .	114
7.3	Fatigue Design Factor as DS/INF 172 . . . . .	116
7.4	Reduction of Characteristic Value of Miner's Rule . . . . .	117
7.5	The Bridge Spans Influence on Reliability Level . . . . .	117
<b>8</b>	<b>Discussion</b>	<b>121</b>
<b>9</b>	<b>Conclusion</b>	<b>125</b>
	<b>Bibliography</b>	<b>129</b>
	<b>Appendix</b>	<b>135</b>
<b>A</b>	<b>Comparison of Fatigue Life Prediction Methods</b>	<b>135</b>
<b>B</b>	<b>Calculation of Concrete Beam</b>	<b>143</b>
<b>C</b>	<b>Approximate Fatigue Design</b>	<b>149</b>

## Notation list

$\alpha$	Cyclic strain amplitude	$\gamma_m$	Partial safety factor for fatigue strength
$\alpha$	Relation between reinforcement and concrete's E-modulus	$\gamma_G$	Partial safety factor for dead load
$\alpha$ -vector	Normalized vector at design point in $u$ -space	$\gamma_{Load}$	Partial safety factor related to realized uncertainties: $X_{Load}$ , $X_{Dyn}$ and $X_{Pos}$
$\bar{x}_{ln}$	Logarithmic mean of sample	$\gamma_{M0}$	Partial safety factor
$\beta$	Reliability index	$\gamma_{Mat}$	Partial safety factor related to the material uncertainty
$\beta_a$	Annual reliability index	$\gamma_{Ma}$	Partial safety factor defined by Germanischer Lloyd
$\beta_t$	Target reliability index	$\gamma_{Mb}$	Partial safety factor defined by Germanischer Lloyd
$\rho_{R=-1}$	Correlation coefficient matrix for $S-N$ curve at $R = -1$	$\gamma_{Model}$	Partial safety factor related to $X_{Model}$
$\rho_{R=0.1}$	Correlation coefficient matrix for $S-N$ curve at $R = 0.1$	$\gamma_Q$	Partial safety factor for load
$\Delta M$	Rotational moment range	$\gamma_{Stat}$	Partial safety factor related to the statistical uncertainty
$\Delta$	Uncertainty for Miner's rule	$\mathbf{C}_{\log K, m, \sigma_\epsilon}$	Covariance matrix for $\log K$ , $m$ and $\sigma_\epsilon$
$\epsilon$	Error term in $S-N$ curve	$\mathbf{H}_{\log K, m, \sigma_\epsilon}$	Hessian matrix with second order derivatives of the log-Likelihood function
$\eta$	Cyclic mean strain	$\mathbf{U}$	Stochastic variables in $u$ -space
$\gamma$	Partial safety factor	$\mu$	Mean value
$\gamma_3$	Partial safety factor for consequence class		
$\gamma_c$	Partial safety factor for concrete strength		
$\gamma_f$	Partial safety factor for fatigue load		

$\mu_{\log K}$	Mean of $\log K$	$F$	Distribution Function
$\Phi()$	Standard Normal distribution	$f_c$	Strength of concrete
$\rho_{\log K, \sigma_\epsilon}$	Correlation coefficient between $\log K$ and $\sigma_\epsilon$	$f_X$	Probability density
$\rho_{\log K, m}$	Correlation coefficient between $\log K$ and $m$	$FDF$	Fatigue design factor
$\rho_{m, \sigma_\epsilon}$	Correlation coefficient between $m$ and $\sigma_\epsilon$	$G$	Design equation
$\sigma$	Standard deviation	$g(\mathbf{U})$	Limit state equation in $u$ -space
$\sigma_\epsilon$	Standard deviation of $\epsilon$	$g(\mathbf{X})$	Limit state equation/Safety margin
$\sigma_{\log K}$	Standard deviation of $\log K$	$g(\mathbf{x})$	Limit state function
$\sigma_{\sigma_\epsilon}$	Standard deviation of $\sigma_\epsilon$	$G_{Asphalt}$	Dead load of asphalt
$\sigma_{ln}$	Logarithmic standard deviation of sample	$G_{Beam}$	Dead load of concrete beam
$\sigma_m$	Standard deviation of $m$	$G_{Deck}$	Dead load of bridge deck
$\theta$	Statistical parameters	$h$	Height
$\zeta$	Omission sensitivity factor	$I$	Moment of inertia
$A$	Area	$i_{step}$	Step size
$a_A$	Distance from $x = 0$ to $P_A$	$K$	Material parameter
$a_C$	Distance from $y = 0$ to $P_C$	$K_{FI}$	Consequence class factor
$b$	Width	$L()$	Likelihood function
$b_A$	Distance from $x = 0$ to investigated point in Along-system	$L_A$	Length of section in Along-system
$b_C$	Distance from $y = 0$ to investigated point in Cross-system	$L_C$	Length of section in Cross-system
$C_i$	Coefficient by Germanischer Lloyd	$M$	Rotational moment
$COV$	Coefficient of variation	$m$	Material parameter
$D$	Damage	$M_A$	Rotational moment in Along-system
$d$	Effective height	$M_a$	Amplitude rotational moment
$E$	Modulus of elasticity	$M_C$	Rotational moment in Cross-system
$e_p$	Reliability elasticity coefficient	$M_m$	Mean rotational moment
		$N$	Number of cycles to failure
		$n$	Number of cycles
		$N_{obs}$	Vehicles per year
		$P_A$	Point load in the Along-system

$P_C$	Point load in the Cross-system	$S_{u,t}$	Ultimate tensile stress
$P_f$	Probability of failure	$STC$	Static compression test
$Q$	Point load	$STT$	Static tension test
$Q$	Tire force	$t$	Time
$q_A$	Line load on Along-system	$t_F$	Failure year
$q_C$	Line load on Cross-system	$u^*$	Design point in $u$ -space
$Q_{ik}$	Axle load	$u_{R=-1}$	Standard Normal distribution
$q_{ik}$	Area traffic load	$u_{R=0.1}$	Standard Normal distribution
$R$	Ratio between $S_{min}$ and $S_{max}$	$W$	First moment of area
$R_{cb}$	Reaction	$X$	Stochastic variable
$S_a$	Cyclic stress amplitude	$x, y, z$	Global coordinate system defined in figure 3.1
$S_c$	Stress in concrete	$x^*$	Design point in physical space
$S_m$	Cyclic mean stress	$x_i$	Sample no. $i$
$S_R$	Stress in reinforcement bar	$X_{Dyn}$	Stochastic uncertainty related to dynamic effects
$S_{eq}$	Equivalent stress amplitude	$X_{Load}$	Stochastic uncertainty related to loads
$S_{max}$	Maximum stress	$X_{Model}$	Stochastic uncertainty related to the model
$S_{min}$	Minimum stress	$X_{Pos}$	Stochastic uncertainty related to vehicle position
$S_{u,c,c}$	Characteristic ultimate compression stress	$z$	Design parameter
$S_{u,c,c}$	Rebar characteristic ultimate compression strength	LN	Lognormal distribution
$S_{u,c}$	Ultimate compression stress	N	Normal distribution
$S_{u,t,c}$	Characteristic ultimate tensile stress		
$S_{u,t,c}$	Rebar characteristic ultimate tension strength		



---

# Introduction

During the last 100 years, architects have been constrained in their efforts to create futuristic concepts due to the small collection of materials available for their designs, most commonly timber, steel, concrete and masonry. Now, advanced composite materials such as fiber-reinforced polymer composites are revolutionizing the industry by replacing the traditional materials. [Premier Composite Technologies, 2015] In civil engineering, fiber-reinforced polymer composites are increasingly being used in various areas ranging from replacement of internal reinforcement to their use as a cost effective replacement material during repairs and externally reinforcement of deteriorated concrete components to their use in bridge deck and bridges fully constructed in composites. [V. M. Karbhari, 2000]

In contrast to steel, fiber-reinforced polymer composites have several advantages such as higher resistance to corrosion leading to increased durability and lifespan, higher tensile and compression capacity, and high strength-to-weight ratio resulting in less dead load and more efficient structural designs e.g. larger spans in bridges. Additionally, fiber-reinforced polymer composites are non-conductive for electricity as well as non-magnetic. This is ideal for structures near or in seawater or other corrosive environments [Alsayed et al., 2015]. However compared to steel, fiber-reinforced polymer is characterized with lower Young's modulus and more sensitive to creep. During production, the energy consumption is lower compared to traditional building materials such as steel, concrete and aluminum. Compared to both steel and concrete, fiber-reinforced polymer composites also have higher thermal efficiency meaning lower thermal bridging and thereby energy cost savings.

Even though fiber-reinforced polymer composites provide several benefits compared to traditional building materials, a number of problems must be addressed before fiber-reinforced polymer composites can be used as a standard construction material. One of the problems is the lack of well documented data, similar to that available for grades of steel and concrete used in civil engineering. In relation to traditional construction materials, the countless combinations in fiber-reinforced polymer composites in regard to fiber and matrix systems makes the material attractive, but it can be a limitation in an industry where standardizations are key. The numerous combinations of fiber-reinforced polymer composite layups makes it difficult to predict fatigue life accurately due to its already

complex fatigue behavior. Partially, because of fatigue failure in composites consists of multiple failure mechanics and partially due to the complex stress state within the material. [Premier Composite Technologies, 2015]

Because fiber-reinforced polymer is a new material compared the conventional civil construction materials, there are challenges to overcome in the process of standardizing it. Fiber-reinforced polymer has been used as a construction material for several years, and there are multiple examples of clever use of the material characteristics. An example is the Fiberline Composites A/S bicycle and pedestrian bridge in Nørre Aaby on Funen built entirely in composites shown in figure 1.1. Here the low density of the material allowed for a prefabricated bridge that was rapidly installed. In comparison to a similar bridge in concrete, the composite bridge weighs 6 t and the concrete bridge would weigh about 20 times more, 120 t. As development and investigation continues, more data and knowledge arise and composites could in the near future be used as the primary as well as secondary construction material for train as well as car bridges, where low weight allow for longer span and fewer substructures. [Fiberline Composites A/S, 2014]



Figure 1.1. Pedestrian and cyclist bridge in Nørre Aaby on Funen.

This development will likely not be brought on by a single construction, but rather a change in the general tendency. However when change in construction material arise, new conflict points will as well. For example; replacing a concrete slab with a composite deck might lead to fatigue becoming a critical design point. This leaves the engineer with few possibilities as there are no partial safety factors developed for fatigue of composites. As a direct result, there is no way to ensure that a standardized safety level is met.

As stated earlier fiber-reinforced polymer composites are used as replacement material. Generally, reinforced concrete is reinforced with steel bars as it is effective and cost-efficient. But steel reinforcement bars are susceptible to oxidation, especially when exposed to aggressive chemicals. Typically aggressive environments are coastal areas or areas where salt is used for de-icing. Fiber-reinforced polymer composites have corrosion resistance and will not rust. Generally, fiber-

reinforced polymer composites are fatigue insensitive, but unlike steel, composites are dependent on the mean load effect. As such, fatigue can become a problem for composite reinforcement bars in concrete as concrete's high density will induce mean stresses. An example of a composite reinforcement bar is ComBAR by Schöck.

## 1.1 Statement of Intent

This report will investigate fatigue of fiber-reinforced polymers with focus on tension reinforcement bars in a representative traffic bridge system. The following points are studied in the report in order to calibrate partial safety factors according to safety levels in DK NA.

- Study of fatigue life assessment methods
- Derivation of  $S-N$  curves and constant life diagrams from experimental data for Schöck ComBAR or similar material
- Estimation of fatigue loads on a bridge system
- Uncertainty modeling of strengths and loads
- Reliability analysis of fatigue limit state for composite tension reinforcement bars
- Calibration of partial safety factors including sensitivity analysis

### 1.1.1 Delimitation

In this report, all recommendations and comments are given without considering economic aspects. For all reliability analysis', all fatigue effects will be considered to follow the behavior of high cycle fatigue. All static calculations will assume complete linear elasticity, and any second order effects are disregarded. All data and analysis will be done for a single material and lay-up combination. Therefore the fatigue data, sensitivity studies, partial coefficients and all comments hereof can only be considered representative for this exact material. For generating a load spectrum no real traffic data will be used. Generally any fatigue influence from; long load exposure, temperature or chemical interaction is neglected. Lastly no fatigue effect from accidental loads will be considered. Only reinforcement bars in tension is investigated in this report.



## A Short Introduction to Composites

A composite is generally defined as an entity comprised of multiple elements. In the field of construction, a reference to a composite material will often be to glass- or carbon fiber reinforced beams. However, the definition composite is also applicable for other construction elements. Reinforced concrete is probably the most commonly known one, but even mixing thatch and mud for the construction of mud huts is a composite. Generally, composites used in construction consist of materials that complement each other.

This report will only concern the glass fiber-reinforced polymer composite, which is comprised of a polymeric resin (the matrix) and glass fiber (the reinforcement). This report will use Schöck ComBAR as vantage point. Schöck ComBAR is a glass fiber-reinforced polymer reinforcement bar. This is of great importance as even though two composite reinforcement bars comprised of the same materials will not necessarily have the same structural properties even if their outer geometry is alike. This is because the order of the layers as well as the fiber volume that comprise a glass fiber-reinforced polymer composite beam are not irrelevant. In a glass fiber-reinforced polymer, the order of layers is referred to as a lay-up. Each layer is a mat of woven glass fiber. The weave of such a mat varies and examples of mat types are shown in figure 2.1. [Fiberline Composites A/S, 2003] As the structural properties of the composite can be altered, it is possible to design glass fiber-reinforced polymers to a specific purpose. Thus a glass fiber-reinforced polymer can be adapted to a certain load configuration [Vassilopoulos and Keller, 2011].

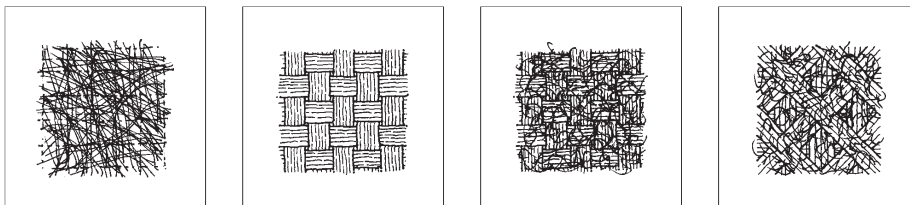


**Figure 2.1.** Examples of mat types. Left to right; continuous mat, woven mat, complex mat and bidirectional mat. [Fiberline Composites A/S, 2003]

- Continuous mat - Consists exclusively of randomly aligned fibers
- Woven mat - Half and half with  $0^\circ$  and  $90^\circ$  woven fibers
- Complex mat - As the woven mat, with some randomly aligned fibers
- Bidirectional mat - Woven with  $0^\circ$ ,  $45^\circ$  and  $90^\circ$ , and some randomly aligned fibers

As seen in figure 2.1, the layers that comprise the material, and the very fact that it is comprised by layers, yield an anisotropic material. This can result in cumbersome calculations for the design engineers but as mentioned above the gain can be significant if the material is applied correctly.

Schöck ComBAR is produced by pultrusion illustrated in figure 2.2.

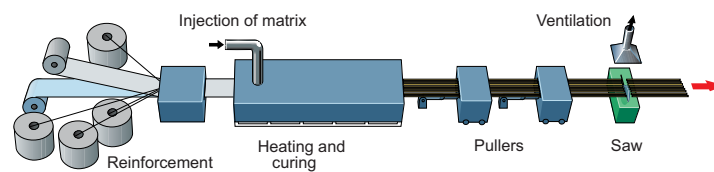


Figure 2.2. Principle of pultrusion.

Pultrusion is a continuous process which produces composite profiles with a constant cross-sectional area. The method ensures constant reproducible quality. First the fibers are positioned accurately according to the cross-sectional area. Hereafter the fibers are fed to a machine, where the fibers are impregnated with the matrix and the machine hardens the profile. The fibers fed to the machine is considered reinforcement and is either fed as layers, as shown in figure 2.1 or as roving. Roving fibers are single strands that lay in the longitudinal direction of the beam and as with the mats there are different types, shown in figure 2.3. [Fiberline Composites A/S, 2003]

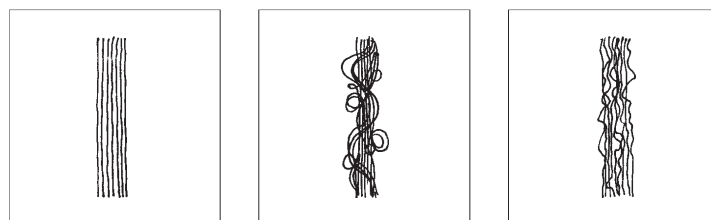


Figure 2.3. Examples of roving types. Left to right; smooth, spun, mock. [Fiberline Composites A/S, 2003]

Another manufacturing process is infusion, where the fiber mats are placed in a closed mold and infused with the liquid resin under heat and vacuum.

Furthermore additives are added to the matrix. The additives vary in function and add anything from resistance to environmental degradation to simply changing the color of the polymer.

Generally in composite materials, the reinforcement adds strength and stiffness as well as the ability to resist tension and compressive stresses. The reinforcement is typically glass fiber, carbon fiber or aramid fiber. These reinforcement

types have different advantages in comparison to each other e.g carbon fibers provide high stiffness. [Vassilopoulos and Keller, 2011]

The matrix keep the reinforcement together as well as handle shear stresses in the cross-sectional area. Additionally, the matrix type is important regarding corrosion, fire resistance and electric insulation. The types of matrices that are normally considered are; polyester, epoxy and phenolic resin. [Fiberline Composites A/S, 2003]

As composite materials are anisotropic their strengths and stiffness's vary in the different directions. Furthermore composites are prone to creep, which is why only a fragment of the strength can be utilized when calculating for example dead load. The creep is however not relevant when calculating ultimate limit state and therefore the full material strength is available for limit state [Fiberline Composites A/S, 2003]. The creep is however naturally counteracted in the sense that composites have relatively low densities.

When determining fatigue in composites, the mean stresses have effect, unlike what is assumed for steel structures. This complicates the calculations and the subject is further discussed in chapter 2.1. Although fatigue failure in composites is a complex problem, it is a fatigue resistant material. This is one of the many reasons composite materials are becoming more widely used instead of just replacing material such as steel, concrete or wood in certain parts of the structure. Their low density, high strength and adaptability makes it an appealing material for structures like foot way and light vehicle bridges. An example of this is the Fiberline bridge shown below in figure 2.4. The bridge was the first composite bridge in Scandinavia and opened in 1997. The short installation time was a clear advantage as the busy railway line restricted the installation work to only a few hours between Saturdays and Sundays. It took 18 hours to install the bridge. [Vassilopoulos and Keller, 2011] [Fiberline Composites A/S, 2003]



**Figure 2.4.** Image of the Fiberline Bridge i Kolding, Denmark [Fiberline Composites A/S, 2015].

While full composite traffic bridges may be too futuristic, the application of composite material in a traffic bridge is not. The composite reinforcement bars produced by Schöck far exceed the steel reinforcement bars currently used in components such as reinforced concrete. A comparison of some material characteristics is shown below in table 2.1.

**Table 2.1.** Comparison between steel and composite reinforcement bars [Schöck, 2014].

Properties	Steel rebar	Stainless steel rebar	Schöck ComBAR
Ultimate tensile strength $f_{u,t}$ [MPa]	550	550	>1000
Characteristic value of tensile strength $f_{y,t}$ [MPa]	500	500	No yielding
Strain at ultimate limit state	2.18 ‰	2.72 ‰	7.4 ‰
Tension modulus of elasticity [MPa]	200,000	160,000	60,000
Density [ $\frac{g}{cm^3}$ ]	7.85	7.85	2.2
Magnetism	yes	very little	no

The large tensile strength in the composite reinforcement bar is practical for ultimate limit state calculations. The interaction in-between the composite reinforcement bars and the concrete is significantly changed, due to the comparatively low Young's modulus of the Schöck ComBAR.

## 2.1 Fatigue in Composites

Engineering structures subjected to dynamic loads will experience fatigue. Fatigue is a failure mode where cracks are initiated and developed under varying load, which leads to loss of strength and stiffness and/or cracking and failure. Fatigue is progressive and localized structural damage and fracture occurs when the cross-sectional area no longer has capacity to transfer the peak loads. In structures mainly statically loaded, fatigue is rarely an issue, however in structures where a dynamic load is present and is of noticeable size compared to the total load fatigue phenomena can occur. Examples of such structures can be; bridges, offshore structures and wind turbines.

Although composite materials are characterized as fatigue-insensitive compared to metallic ones, they are subjected to fatigue load and fatigue must be considered, even in the design phase even for structures where it is not normally an issue [Vassilopoulos and Keller, 2011]. An example of this could be a concrete road bridge which is not fatigue-sensitive due to the dead loads being significantly higher than the live loads. But fatigue may become important for a light-weight composite bridge, where the dead loads are not of the same magnitude as for the concrete bridge.

Because the fatigue behavior in composite materials differ from that of metallic ones, conventional methods and fatigue life prediction cannot be applied directly to composite materials. In metals fatigue failure is assumed to be caused by a single crack that develops until the remaining cross-section is insufficient. Fatigue failure in composites does not evolve from a single crack like in metals. Instead it causes one of, or a combination of; delamination, microbuckling and translaminal crack growth. These then result in one of several failure modes. Delamination is the separation of layers along the layer planes. Microbuckling is local buckling of the fibers that reinforce the composite. Lastly translaminal crack growth is crack growth across the fiber layers. This results in a complicated failure cause.

Furthermore different material configurations such as manufacturing methods,

matrices and lamination stacking sequences makes the development of new methods that takes all these modifications into account challenging.

As composites are generally considered brittle and have no reserve load carrying capacity, an accurate prediction of failure is important. Therefore knowledge of fatigue life prediction and fatigue behavior in composites is important, especially in unidirectional composite materials. Fiber-reinforced polymer composites fatigue behavior is dependent on many factors.

- Manufacturing process
- Fiber volume
- Type of loading
- Mean stress
- Environment
- Frequency
- Interface properties
- Constituent materials

[Allah et al., 1996]

The fatigue life of a structure subjected to fatigue load is expressed by the number of load cycles to failure. The fatigue life can be determined by the use of  $S$ - $N$  curves in case of a constant amplitude load. In cases where the dynamic load will be of variable amplitude, Miners rule can be applied. The formulation of  $S$ - $N$  curves, also known as Wöhler curves, is shown in eq. (2.1). The  $S$ - $N$  curve is a simple way to represent fatigue data and it is preferred to other approaches since it requires input data that can be acquired using simple recording devices. It is an empirical formulation and assumes a linear relation in a log-log plot, as shown in figure 2.6.

$$N = K S_a^{-m} \quad \text{or} \quad \log N = \log K - m \log S_a \quad (2.1)$$

Where

$N$	Number of cycles
$S_a$	Cyclic amplitude stress
$K$	Material parameter
$m$	Material parameter

In figures 2.5 and 2.6, definition of stresses and an illustration of the  $S$ - $N$  curve is shown, where number of cycles is plotted with cyclic amplitude stress in a log-log diagram.

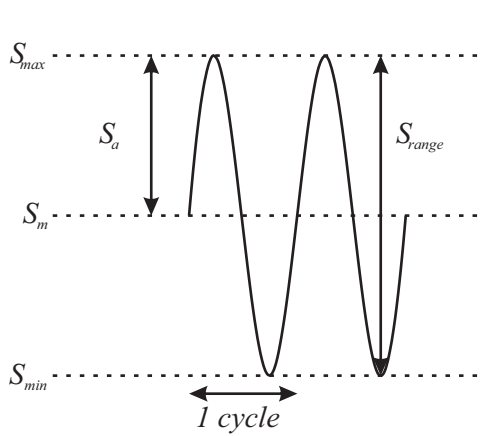
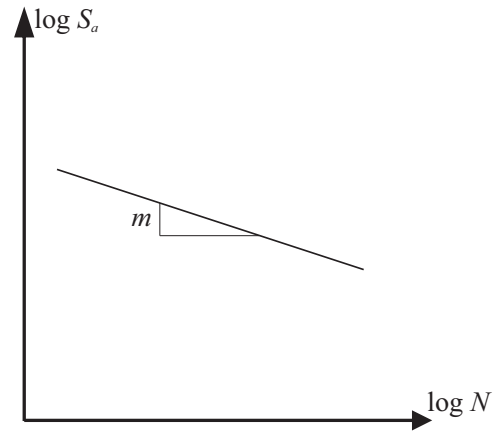


Figure 2.5. Definition of stresses.

Figure 2.6. Illustration of  $S$ - $N$  curve.

The material parameters  $m$  denotes the slope of the  $S$ - $N$  curve related to the examined material. For fiber-reinforced polymer  $m$  is typically in the range of 7 to 25, lower range for multidirectional and higher range for unidirectional composites.

The  $S$ - $N$  curves are estimated using constant amplitude fatigue data for a specific fatigue load type, where tests are conducted with different cyclic amplitude stresses and the number of cycles to failure is measured. The  $S$ - $N$  curve is fitted to the fatigue data. As seen in figure 2.6 the lower  $S_a$  stress level the longer fatigue life.

Regarding the representation of constant amplitude fatigue data for any composite material, it is accepted that a Log-Log representation is sufficiently accurate, in most cases as there is no universal theoretical model able to accurately model fatigue behavior in composite materials. [Vassilopoulos and Keller, 2011]

### 2.1.1 Damage Accumulation

When estimating the fatigue damage of a structure the empirical Palmgren-Miner damage accumulation rule is used also denoted Miner's rule. Traditionally this rule used to determine fatigue damage for metallic structures, but investigations have shown that it is also applicable to composite materials. The method is used to determine fatigue damage from loading with variable amplitude and is shown in eq. (2.2). [Vassilopoulos and Keller, 2011]

$$D = \sum_{i=1}^n \frac{n_i}{N_i} \leq 1 \quad (2.2)$$

Where

$D$	Damage
$n_i$	Number of cycles with a specific load amplitude
$N_i$	Number of cycles to failure for a specific load amplitude

A structure is considered failed if  $D \geq 1$ . Sequence effects are disregarded in Palmgren-Miner's damage rule, but can be important in composite materials if

the applied load spectrum e.g. first causes matrix cracking and subsequently the loading causes compression and thus enabling micro buckling.

The characteristic number of cycles to failure is determined by the use of the  $S$ - $N$  curve for a specific load amplitude. The number of cycles,  $n$ , and their corresponding amplitude and mean stresses  $S_a$  and  $S_m$  can be determined using different methods. In this report, the Rainflow counting method in accordance with the ASTM standard is applied, as it is suggested in engineering standards. [CEN/TC 250, 2014]

### 2.1.2 Constant Life Diagram

$S$ - $N$  curves can be obtained for different fatigue load types and plotted together in a constant life diagram. This is done in order to take the effect of the mean stress into account for the fatigue life of the material. The constant life diagram is used to derive  $S$ - $N$  curves for  $R$ -ratios different from those derived experimentally. This means that constant life diagrams offer a predictive tool to estimate the fatigue life of the material under a fatigue load type where no experimental data is available, if data from neighboring load types are available.

The constant life diagram is defined by the mean cyclic stress,  $S_m$ , the cyclic amplitude,  $S_a$ , and the  $R$ -ratio. The  $R$ -ratio is defined in eq. (2.3).

$$R = \frac{S_{min}}{S_{max}} \quad (2.3)$$

Where

$R$	Ratio between $S_{min}$ and $S_{max}$
$S_{min}$	Minimum stress
$S_{max}$	Maximum stress

In figure 2.7 an illustration of a constant life diagram is shown.

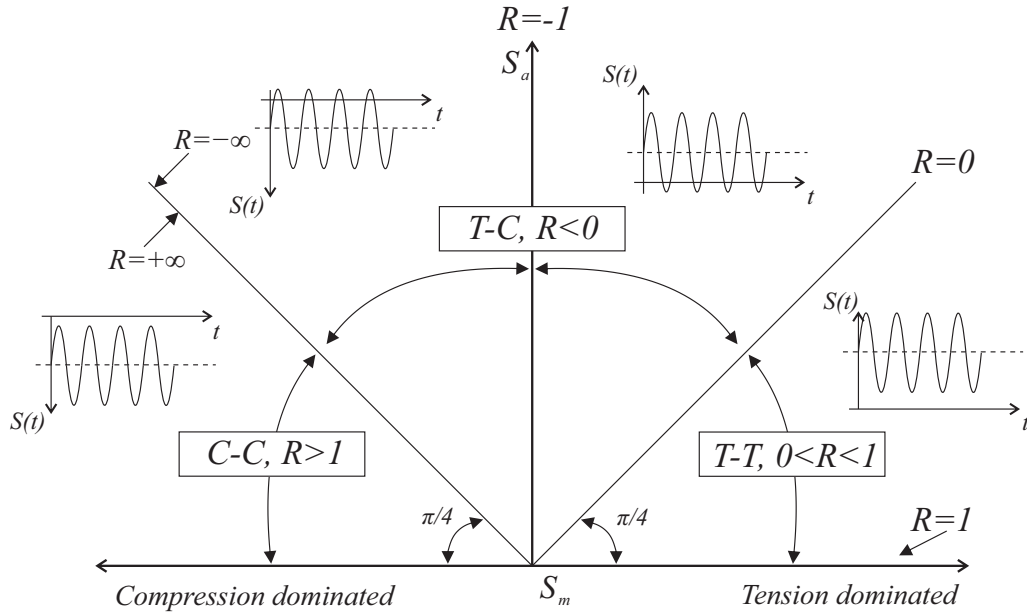


Figure 2.7. Principles in a constant life diagram.

As shown in figure 2.7, the  $(S_m - S_a)$ -half-plane is divided into three sectors. The center sector is comprised by combined tensile and compressive loading (T-C) representing  $S-N$  curves with  $R < 0$ . The tension-tension (T-T) sector is bounded by radial lines representing  $S-N$  curves at  $R = 1$  and  $R = 0$ , where  $R = 1$  corresponds to long term static loading e.g. creep and  $R = 0$  relates to tensile fatigue cycling with  $S_{min} = 0$ . The radial lines in the T-T sector has a corresponding symmetric line with respect to the  $S_a$ -axis, which is located in the compression-compression (C-C) sector whose  $R$ -ratios are the inverse of the tensile  $R$ -ratios. The radial lines shown in figure 2.7 are expressed in eq. (2.4).

$$S_a = \left( \frac{1 - R}{1 + R} \right) S_m \quad (2.4)$$

Where

$$\begin{array}{l} S_m \mid \text{Cyclic mean stress} \\ S_a \mid \text{Cyclic stress amplitude} \end{array}$$

Eq. (2.4) represent  $S-N$  curves for a specific  $R$ -ratio.

The constant life diagram is constructed by connecting  $S-N$  curves at different  $R$ -ratios, these lines are called constant life lines. The constant life lines can be linear or non-linear depending on constant life diagram formulation. Each constant life line connect data points with the same number of cycles to failure between neighboring  $S-N$  curves.

It should be noted that constant life diagrams cannot accurately model the fatigue life close to the horizontal axis which represent high mean values and very low stress amplitudes (zero stress amplitude at  $R = 1$ ).

This point cannot be considered static loading but rather creep of the material (static load over a period of time).

Several configurations of the constant life diagram have been proposed, and in the following four constant life diagrams are presented. All these constant life diagrams have different advantages and disadvantages and it is important to choose the optimal constant life diagram for the case in question.

### Shifted Goodman Diagram

The Goodman diagram is defined as symmetric and linear shown in figure 2.8.

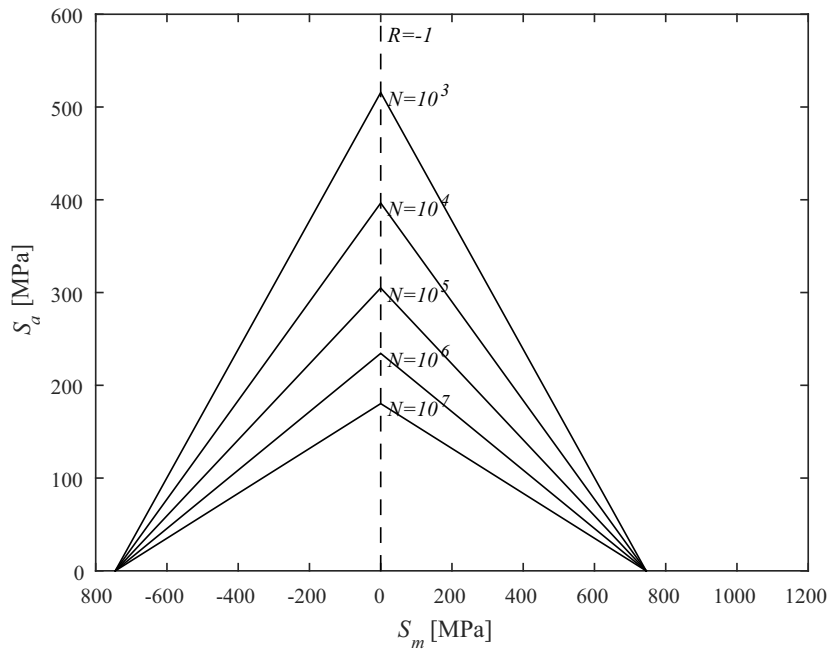


Figure 2.8. Illustration of a Goodman diagram.

As seen from figure 2.8, the Goodman diagram only uses the  $S$ - $N$  curve at  $R = -1$ . The linear Goodman diagram is not ideal for composite materials as the absolute values of the tensile and compressive strengths are not identical. A shifted Goodman diagram can be constructed based on the symmetric and linear Goodman diagram. The shifted Goodman diagram is constructed from a single  $S$ - $N$  curve and takes difference in absolute values of compressive and tension strength into consideration, as illustrated in figures 2.9 and 2.10.

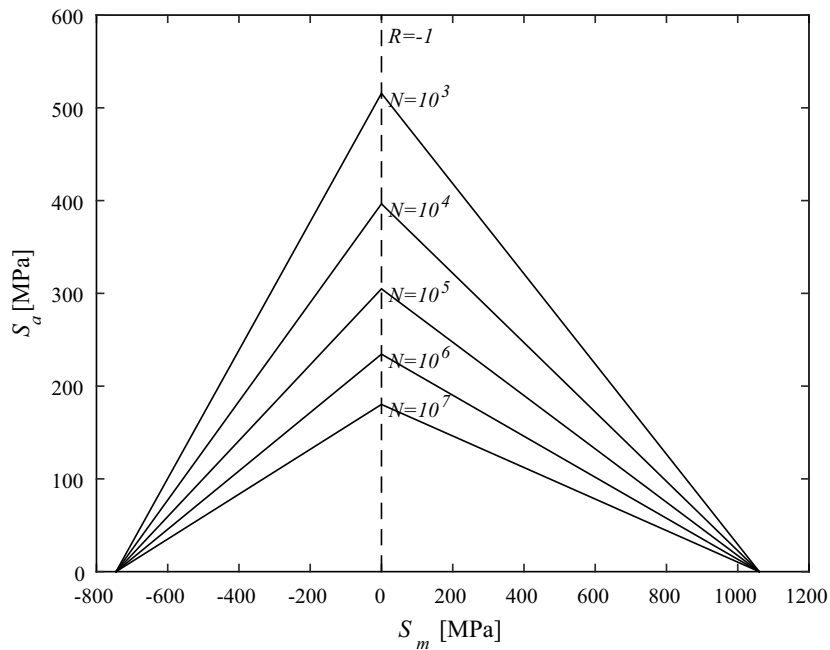


Figure 2.9. Illustration of shifted Goodman diagram based on  $S$ - $N$  curve at  $R = -1$ .

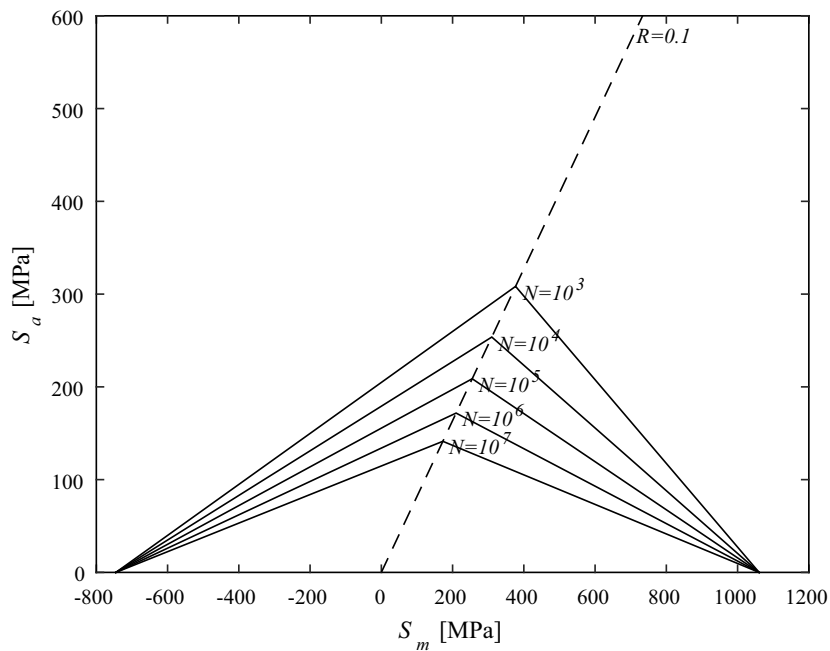


Figure 2.10. Illustration of shifted Goodman diagram based on  $S$ - $N$  curve at  $R = 0.1$ .

Where the shifted Goodman diagram based on  $S$ - $N$  curve at  $R = -1$  is denoted  $CLD_{SGM_{R=-1}}$  and the shifted Goodman diagram based on  $S$ - $N$  curve at  $R = 0.1$  is denoted  $CLD_{SGM_{R=0.1}}$ . The advantage of using a shifted Goodman diagram instead of a piecewise linear constant life diagram, is the need for fewer experimental tests, however the fatigue life predictability is reduced [Vassilopoulos and Keller, 2011]. Using a shifted Goodman diagram may prove beneficial in

cases where experimental funds or time is limited. Additional beneficiality is to be achieved if the load pattern follows the vicinity of a single  $R$ -ratio.

### Goodman Diagram by Germanischer Lloyd

Germanischer Lloyd, see section 2.2, presents in "Guideline for the Certification of Wind Turbines" a simplified method for determining a shifted Goodman diagram applicable to composites. The formulation for calculation of fatigue life requires no fatigue tests. This may prove practical in situations where limited or no fatigue tests are available or when quick calculations are needed. Fatigue life is estimated by eq. (2.5).

$$N = \left[ \frac{S_{u,t} + |S_{u,c}| - |2S_m - S_{u,t} + |S_{u,c}||}{2S_a} \right]^m \quad (2.5)$$

Where

$S_{u,c}$  | Ultimate compression strength  
 $S_{u,t}$  | Ultimate tensile strength

And with partial safety factors applied according to Germanischer Lloyd in eq. (2.6).

$$N = \left[ \frac{S_{u,t,c} + |S_{u,c,c}| - |2\gamma_{Ma} S_m - S_{u,t,c} + |S_{u,c,c}||}{2 \frac{\gamma_{Mb}}{C_{1b}} S_a} \right]^m \quad (2.6)$$

Where

$S_{u,c,c}$  | Ultimate characteristic compression strength  
 $S_{u,t,c}$  | Ultimate characteristic tensile strength

Where  $\gamma_{Ma}$  is determined as.

$$\gamma_{Ma} = \gamma_{M0}$$

$\gamma_{Mb}$  is found as.

$$\gamma_{Mb} = \gamma_{M0} \cdot \Pi C_{1b}$$

For all analysis,  $\gamma_{M0}$  is.

$$\gamma_{M0} = 1.35$$

In fatigue verification,  $\gamma_{Mb}$  is determined by multiplying with  $C_{1b}$  presented below.

$C_{1b}$	$= N^{\frac{1}{m}}$	Curve of high-cycle fatigue for the load cycle number $N$ and slope parameter $m$ . $m$ is determined by an analysis ( $S$ - $N$ curve) to be agreed with Germanischer Lloyd.
$C_{2b}$	$= 1.1$	Temperature effect
$C_{3b}$	$= 1.0$	Unidirectional reinforcement
	$= 1.1$	Non-woven fabrics and unidirectional woven rovings
	$= 1.2$	Woven fabrics and mats
$C_{4b}$	$= 1.0$	Post-cured laminate
	$= 1.1$	Non post-cured laminate
$C_{5b}$	$= 1.0$ to $1.2$	Local partial safety factor for the blade trailing edge. The exact magnitude depends on the quality of the verification (1.0 for dynamic blade test in the edgewise direction, 1.1 for FE calculation, 1.2 for calculation according to Bernoulli theory).

$m$  is defined in "Guideline for the Certification of Wind Turbines" for a number of cases defined by their resin and fiber volume. For other cases it is recommended to determine  $m$  by fatigue analysis. The guideline do not provide information of which  $R$ -ratio  $m$  is related to. In this report it is assumed to be  $R = -1$ . The Goodman diagram by Germanischer Lloyd,  $CLD_{GL}$ , is shown in figure 2.11.

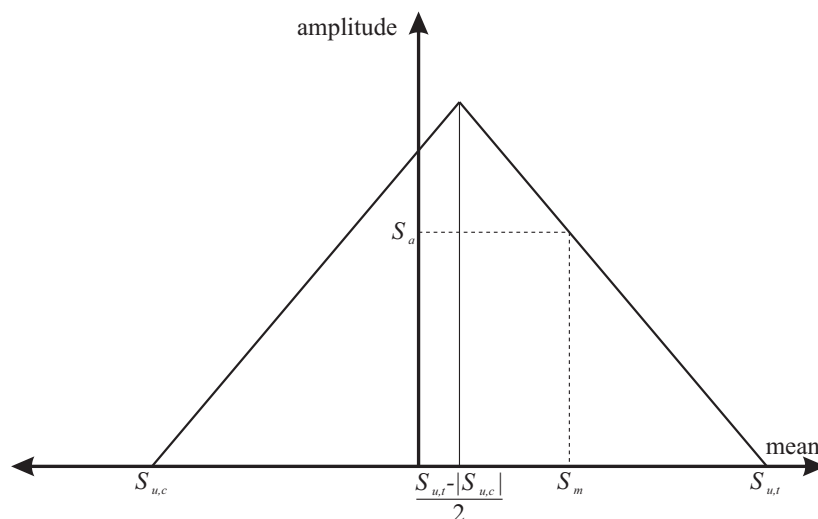


Figure 2.11. Illustration of Goodman diagram by Germanischer Lloyd.

### Piecewise Linear Constant Life Diagram

The piecewise linear constant life diagram is denoted,  $CLD_{PL}$ , and is referred to as the piecewise linear constant life diagram. and its formulation is derived

by linear interpolation between known  $S$ - $N$  curves or points in the  $(S_m - S_a)$ -plane. This formulation requires multiple experimentally determined  $S$ - $N$  curves as well as the ultimate tensile and compressive strengths of the material. Typically,  $S$ - $N$  curves with  $R$ -ratios of 10, -1 and 0.1 is chosen representing the range of possible loading patterns. A well determined piecewise linear constant life diagram is shown in figure 2.12.

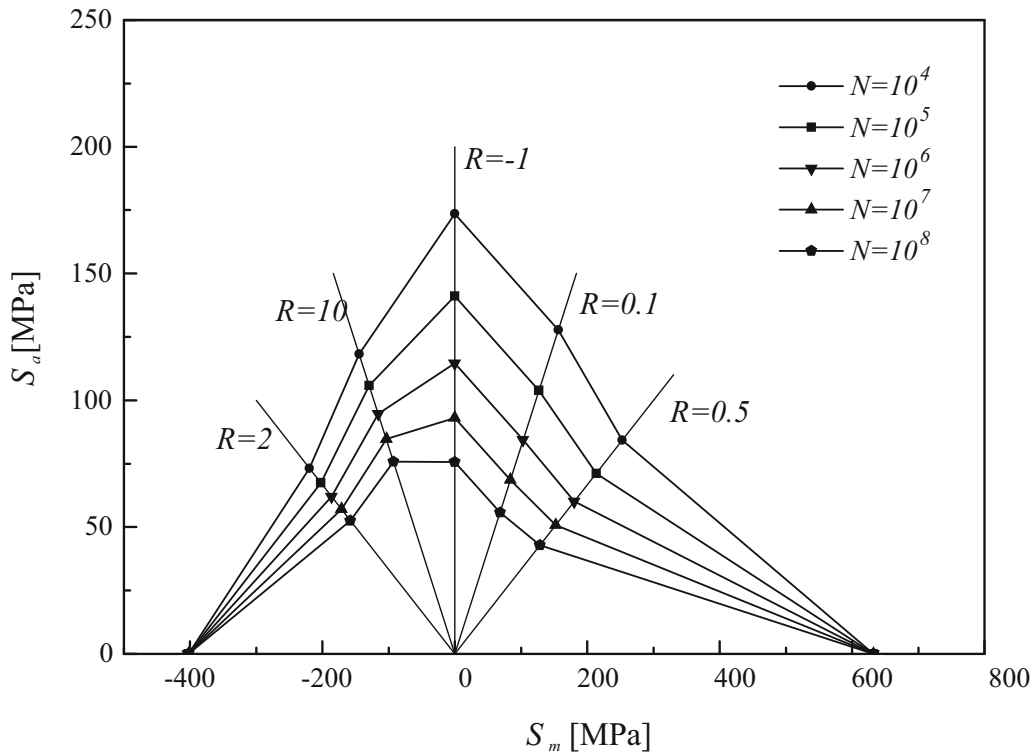


Figure 2.12. Illustration of a piecewise linear constant life diagram determined from 5  $R$ -ratios. [Vassilopoulos and Keller, 2011]

More  $S$ - $N$  curves at different  $R$ -ratios will increase the accuracy of the constant life diagram. It is however costly and time consuming to perform fatigue tests. Therefore obtaining  $S$ - $N$  curves at  $R$ -ratios in proximity of the expected loading pattern is favorable.

Of the compared constant life diagrams, the piecewise linear constant life diagram includes the most experimental data in its assessment of fatigue life. Because of this, it will be used for the reliability analysis. Previously presented constant life diagrams will still be included, and design equations using these will be presented. The calibrated partial safety factors will be applicable for the before mentioned constant life diagrams.

### 2.1.3 Det Norske Veritas Fatigue Life Prediction Method

In the following section, a fatigue life prediction method proposed by Det Norske Veritas (DNV) is presented. The method is also referred to as DNV's method. This method is needed for calculating fatigue life using a constant life diagram. It calculates the number of cycles to failure,  $N$ , corresponding to a cyclic ampli-

tude and cyclic mean stress. The method is used to predict fatigue life for all the constant life diagrams presented previously except the Goodman diagram by Germanischer Lloyd.

Det Norske Veritas' method uses a piecewise linear constant life diagram constructed from available  $S-N$  curves typically  $R = 10$ ,  $R = -1$  and  $R = 0.1$  to obtain fatigue lifetimes for cycles obtained from Rainflow counting with different mean and amplitude strains. In this report, the method is applied to stresses.

The method assumes a piecewise linear constant life diagram and constant life lines are drawn for lifetimes of 10, 100, 1000... cycles. Furthermore it assumes that all constant life lines are connected to the static tensile and compressive strains at failure as shown in figure 2.13.

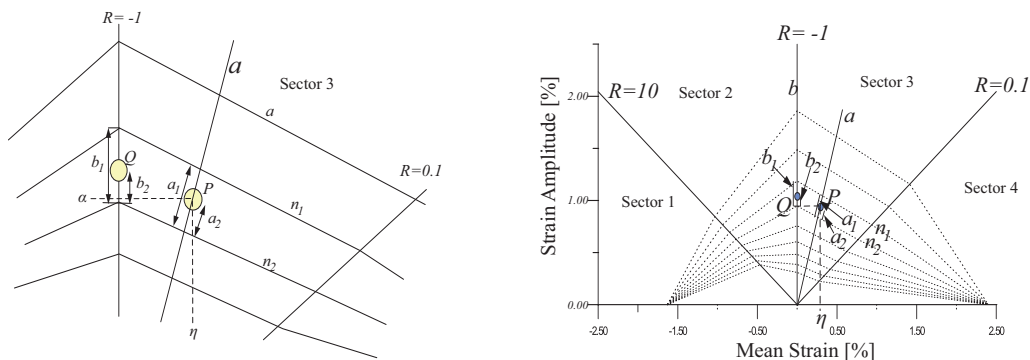


**Figure 2.13.** Principle of Det Norske Veritas' fatigue life prediction method. [Det Norske Veritas, 2006]

With the before mentioned assumptions established Det Norske Veritas presents a procedure estimating the expected lifetime to failure,  $N$ , for a given cyclic mean strain and cyclic strain amplitude presented below and shown in figure 2.13.

1. Draw the point  $P$  in the constant life diagram representing the given strain amplitude,  $\alpha$ , and mean,  $\eta$ .
2. Draw a line  $a$  from the origin of the constant life diagram (0 mean, 0 amplitude) through and beyond the point  $P$ .
3. Identify the two closest constant life lines nearest to  $P$ ,  $n_1$  and  $n_2$ , where  $n_2$  is the line with the higher number of cycles to failure.
4. Measure the length  $a_1$  on line  $a$  between the two constant life lines  $n_1$  and  $n_2$  nearest to  $P$ .
5. Measure the length  $a_2$  on line  $a$  between point  $P$  and the constant line  $n_2$  with the higher number of cycles nearest to  $P$ .
6. Find the line  $b$  nearest to  $P$  representing fatigue life of a measured  $R$ -ratio, e.g.  $R = 10$ , or  $R = -1$ , or  $R = 0.1$ .
7. Measure the length  $b_1$  on  $b$  between  $n_1$  and  $n_2$ .
8. Calculate  $b_2 = b_1 \frac{a_2}{a_1}$ .

9. Find the strain amplitude,  $\epsilon_{CLD}$ , corresponding to point  $Q$  that lies on  $b$  at a distance  $b_2$  away from the intersection of  $b$  and  $n_2$ .
10. Obtain the characteristic value of the expected number of cycles to failure  $N$  for  $\epsilon_{CLD}$  using the measured characteristic  $S-N$  curve.

[Det Norske Veritas, 2006]

The description above is programmed, the steps above are repeated for each load cycle investigated. The method is laborious compared to Germanischer Lloyds fatigue life estimation method shown in eq. (2.5). It should be noted that the method described above is an approximation of the fatigue life.

### Accuracy of Det Norske Veritas' Fatigue Life Prediction Method

As the fatigue life prediction method by DNV is an approximation, its accuracy is studied in the following section.

In order to successfully conduct reliability analysis' of fatigue in composites, an accurate fatigue life prediction is essential. In the following analysis, the fatigue life is assumed to follow a piecewise linear constant life diagram using 3  $R$ -ratios (see Appendix A). A method that iteratively achieve the fatigue life of each cycle (the spatial plane method) is compared to the approximate method proposed by DNV in DNV-OS-j102 for fatigue life prediction, see section 2.2 for further details. The full comparison and presentation of DNVs fatigue life prediction method is presented in Appendix A.

The comparison of the two methods yielded results largely dependent on the amount of computational power available. The DNV method is computationally fast, as it only approximates, by linear interpolation, the fatigue life based on the two nearest constant life lines. The spatial plane method iterates within zones of the constant life diagram. The difference in computational time is significant at only a few hundred thousand data points. Making the choice of method significant, not only in regard to accuracy. In figures 2.14 and 2.15, the convergence analysis for the two method is shown for point 2 (see Appendix A for more information).

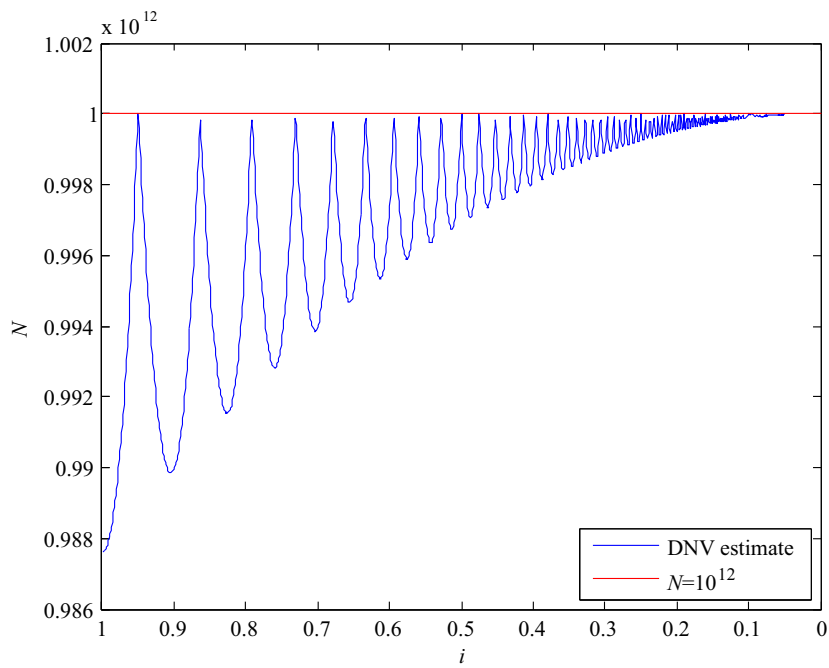


Figure 2.14. Convergence analysis of step size between constant life lines used in Det Norske Veritas' method for point 2.

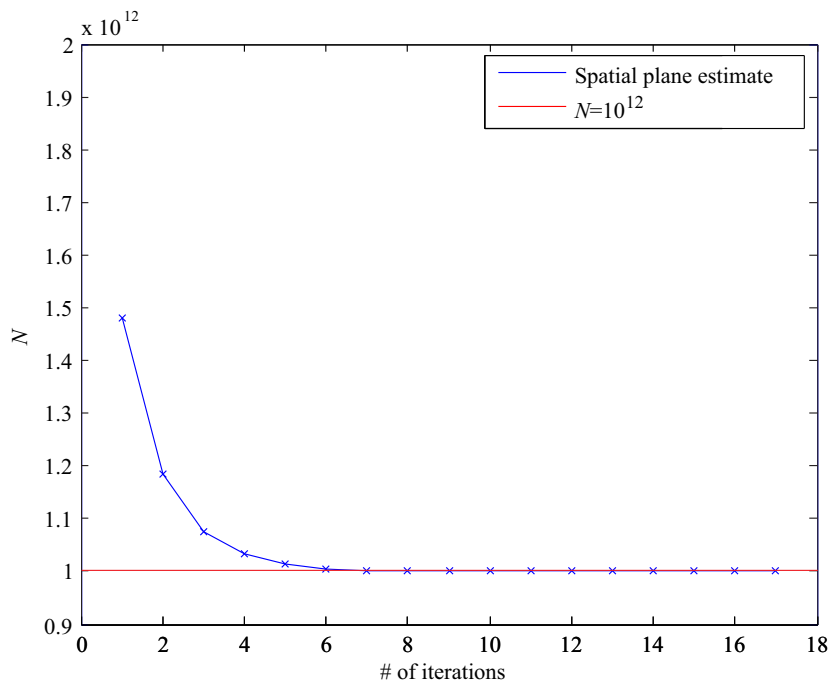


Figure 2.15. Convergence analysis for point 2 by the spatial plane method.

Where the step size,  $i_{step}$ , defined as eq. (2.7). The location of Point 2 is shown in Appendix A.

$$10^{i_{step}}, 10^{i_{step} \cdot 1}, \dots, 10^{i_{step} \cdot (n-1)}, 10^{i_{step} \cdot n_{step}} i_{step} \in \mathfrak{R} > 0 \tag{2.7}$$

Where

$i_{step}$	Step size
$n_{step}$	Number of steps

As seen in figure 2.14, the DNV method is relatively precise at its recommended constant life line distance, with a maximum deviation of 1.2 %. As the step size decrease, the constant life lines will change position and the distance to the point will therefore change with step size. Therefore the load cycles position is important in regard to the error in fatigue life.

As seen in figure 2.15, the spatial plane method converges relatively fast, however when compared to DNVs method, its computational time is more than a factor of 2 greater at a realistic amount of data points with a required relative stress precision equal to  $10^{-7}$  is chosen. A lower precision would decrease the computational time of the spatial plane method.

It is evaluated in Appendix A, that using the DNV method will be sufficient in accuracy when compared to the potential time increase required to achieve more accuracy towards the piecewise linear constant life diagram. Henceforth the DNV method with a constant life spacing of  $i_{step} = 1$  will be used.

It is noted that the accuracy of the DNV method is largely dependent of the position of the point in respect to the constant life lines. In the Appendix, two examples are shown, one where the DNV method is conservative and one where it is not. There is a clear tendency, depending on the  $m$  parameters of the two adjacent  $S-N$  lines, to whether the DNV method is conservative or not. It will however always have more conservative than non conservative areas. This does not mean that the DNV method necessarily is conservative, only that there is a tendency that it will be.

## 2.2 Fiber-Reinforced Composites in Codes

This chapter provides an overview of some standards and their approach to fatigue in fiber-reinforced polymer. Although this section treats Det Norske Veritas and Germanischer Lloyd separately, the two companies have now merged.

### 2.2.1 DS/EN

DS/EN provides a wide variety of design codes which cover the most common constructions and materials, however at the present time no design code is available for fiber-reinforced polymer structures. A working group WG4 has been established by CEN TC250 with the aim to develop a new Eurocode for "Fiber-reinforced polymer structures" [Shave, 2014]. EN 13706 is the only Eurocode which refers to fiber-reinforced polymer composites and covers testing and notification of glass fiber-reinforced polymer pultruded profiles [Potyrala, 2011].

### 2.2.2 Det Norske Veritas

Det Norske Veritas provide standards which cover composite materials. DNV-OS-C501: Composite Components is a standard developed due to lack of a good

glass fiber-reinforced polymer guideline. It is a general standard for design of load bearing structures, sandwich structures and components fabricated from fiber-reinforced polymer. However, little is mentioned about fatigue in the standard and only distribution of fatigue load effects are described. Further information about fatigue is found in DNV-OS-J102, where the fatigue limit state analysis is explained including fatigue damage of wind turbine blades. The procedure for estimating fatigue life is presented in section 2.1.3 and takes basis in Miner's rule for damage accumulation and a piecewise linear constant life diagram dependent on the number of  $R$ -ratios available.

The method proposed in DNV-OS-J102 is used for fatigue life estimation in this report.

### **2.2.3 Germanischer Lloyd**

Germanischer Lloyd (GL) provides information regarding fatigue in composites in "Guideline for the Certification of Wind Turbines". The guideline offers information regarding the characteristics of fiber-reinforced materials in general as well as information for strength analysis including fatigue. The fatigue analysis is based on a shifted Goodman diagram. A formulation for estimation of the fatigue life is given and is based on tensile and compressive strengths. There is no need for fatigue parameters from tests for the estimation. For damage accumulation Miner's rule is recommended.

### **2.2.4 Guidelines**

Manufacturers such as Fiberline Composites A/S offer design manuals intended for use with their products. Design manuals provide general information about manufacturing, product list, design concept, partial safety factors, material parameters and connections. The design manual by Fiberline Composites A/S offer no information about handling fatigue in fiber-reinforced polymer.

---

# Bridge System

The following chapter presents the traffic bridge system used in the report as basis for derivation of the partial safety factors. The traffic bridge system is a 2 lane traffic bridge that is simplified to two static systems; Along-system and Cross-system. The traffic bridge system is assumed to be representative for the majority of traffic bridges constructed.

Furthermore, the design criteria e.g. design life is listed for the bridge system and assumptions of static loading of the bridge system are presented.

## 3.1 Design Criteria

The bridge system is designed with reliability according to DS/EN 1990 for CC2 and CC3 as these are the allowable consequence classes for bridges. Furthermore a design life of 100 years is chosen according to recommended value by DS/EN 1993-2 DK NA for traffic bridges.

## 3.2 Static System

In the following section, the static systems used throughout the report are presented. The static system will represent a generic bridge system. This generic system is a simplification of reality. The bridge is sketched in 3-D in figure 3.1. Additionally, dimensions of the bridge has been chosen and are presented in figure 3.1. As seen in figure 3.1, the traffic bridge has a 30 m bridge span and 10 m wide. Dimensions are based on a typical two way traffic bridge crossing a highway in Denmark. It is assumed that any vehicle crossing have its center in the middle of the lanes e.g 3 m and 7 m along the y-axis without the inclusion of any uncertainty regarding the position of the vehicle. Furthermore, the bridge is fully paved and the dead load from guardrails is not taken into consideration. The traffic bridge system consist of two longitudinal composite reinforced concrete beam with supports a number of composite decks.

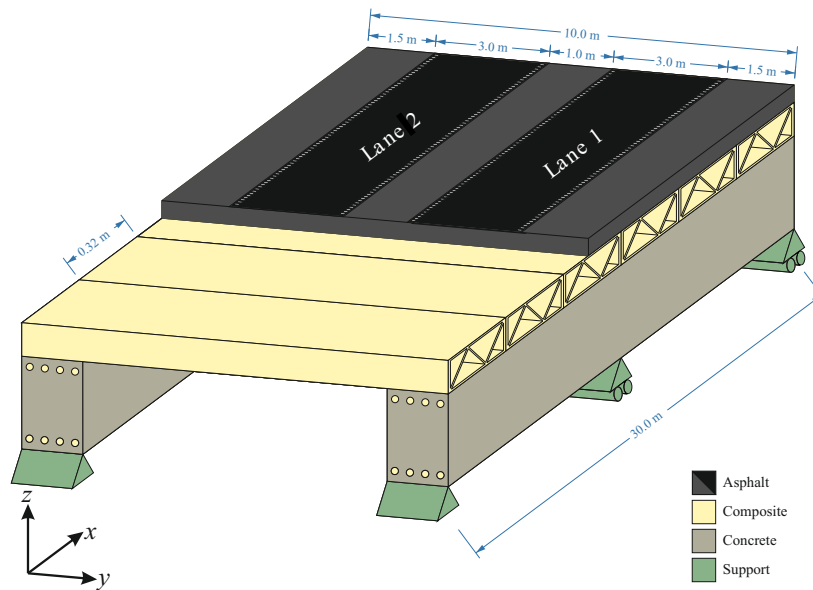


Figure 3.1. 3-D sketch of the bridge system.

In the bridge system composite materials are utilized as reinforcement bars in the concrete and as composite bridge decks. In this report only the composite bridge deck and the tension reinforcement bars are considered. Calculations are conducted for both the composite bridge deck and the tension reinforcement bars. The composite bridge deck is assumed to have the same material characterization as the reinforcement bars. Interaction between the reinforcement bars and the concrete is not investigated in this report. Furthermore it is assumed that the concrete is intact.

The composite bridge deck will distribute the vertical loads from the lorry axles and transfer it to the longitudinal beam. The longitudinal beam transfer loads to the supports. As shown in figure 3.2, the longitudinal beams are considered simply supported beam with three supports.

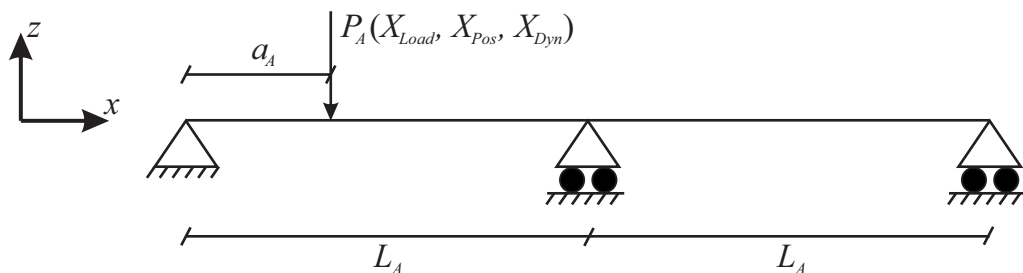


Figure 3.2. Static system of Along-system.

The static system of longitudinal beams is denoted "Along-system" and indexed with "A".  $L_A$  is equal to 15 m.

As seen on the figure 3.2, the load  $P_A$  is moving along the beam in this plane corresponding to a lorry crossing the bridge.  $P_A$  is the reaction from the bridge deck caused from a lorry axle crossing the bridge, and it is amplified or decreased by a

stochastic variables;  $X_{Load}$ ,  $X_{Pos}$  and  $X_{Dyn}$ . These stochastic variables represents the uncertainty of the load and the position of lorries in the lane, this variable is also shown in figure 3.3. This is described in further detail in chapters 4 and 5. The static system for the bridge decks are shown in figure 3.3.

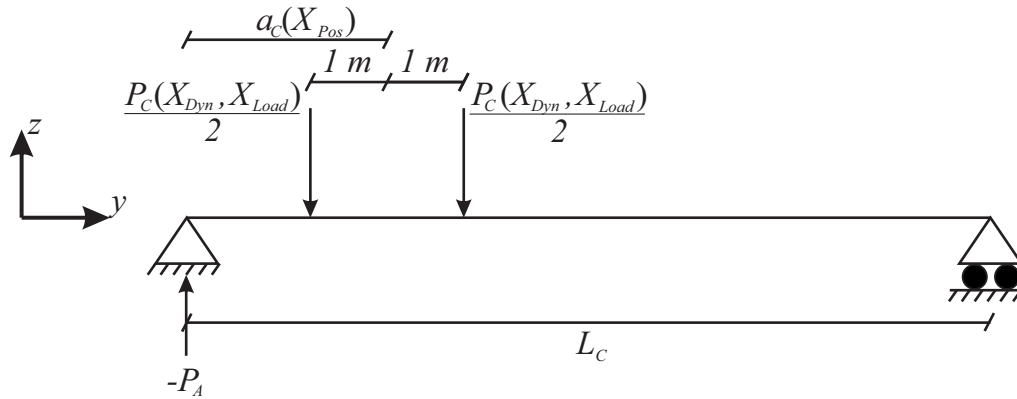


Figure 3.3. Static system of Cross-system.

The static system of the bridge decks is denoted "Cross-system" and indexed with "C".  $L_C$  is equal to 10 m.

The transverse decks are considered as simply supported beams with two supports. On each deck the loading is as presented in figure 3.3.

Regarding the width of the bridge decks shown in figure 3.1, it is assumed only one axle of a lorry is loading a single bridge deck at a time. Therefore the width of the bridge deck is 0.32 m corresponding to wheel types presented in DS/EN 1991-2. As long as the bridge decks are considered beam elements this will generate the highest stresses in the Cross-system. Plate effects and several axles on the same bridge deck is not investigated.

### 3.3 Static Loads

An estimation of the static loads acting on the Along-system and Cross-system are presented in this section. The static loads affects the mean stresses and is important in regards to the constant life diagram for composites as it changes the position of the load cycles in the constant life diagram. Static loads are based on simple assumptions and DS/EN 1992-1-1 DK NA. This estimation advances from figure 3.1 showing the parts producing a dead load that will be taken into account. Additionally, a layer of asphalt concrete with a thickness of 200 mm is assumed placed on top of the composite bridge decks [Asfaltindustrien, 2004].

#### 3.3.1 Asphalt Concrete Layer

Asphalt Concrete is assumed to have a self-weight of  $25 \text{ kN/m}^3$  [Asfaltindustrien, 2004]. As the thickness of the layer is known, the area dead load,  $G_{asphalt}$ , can be determined as.

$$G_{Asphalt} = 25 \text{ kN/m}^3 \cdot 0.2 \text{ m} = 5.0 \text{ kN/m}^2$$

### 3.3.2 Composite Bridge Decks

The bridge deck is assumed to have a height of 200 mm and [Harries and Moses, 2007] estimates a dead load presented in table 3.1 for composite decks with 200 mm heights. This is considered a slightly conservative estimate as putting composite I-profiles of the same height side by side yielded a load of  $0.7 \text{ kN/m}^2$  [Fiberline Composites A/S, 2003].

Table 3.1. Dead load of composite bridge decks.

[kN/m <sup>2</sup> ]	
$G_{Deck}$	1.0

Furthermore, it is assumed the composite bridge decks have a width allowing only one axle to load the bridge deck at a time. A width of 32 cm is assumed based on geometrical definitions of tires in DS/EN 1991-2. This assures maximum dynamic load relative to static load, as 32 cm is the smallest width a deck can have and still single-handedly carry an axle.

### 3.3.3 Reinforced Concrete Beams

The dead load from the reinforced concrete beams,  $G_{Beam}$ , is determined by a deterministic calculation in ultimate limit state in order to estimate its dimensions. Partial coefficients according to DS/EN 1990-1-1 DK NA and DS/EN 1992-1-1 is used. The calculations are presented in Appendix B. In table 3.2, the dead load of the concrete beams is presented with an assumed weight density of  $25 \text{ kN/m}^3$ . The cross-section is  $1000 \text{ mm} \times 800 \text{ mm}$  and shown in figure 3.4.

Table 3.2. Dead load of concrete beams.

[kN/m]	
$G_{Beam}$	20

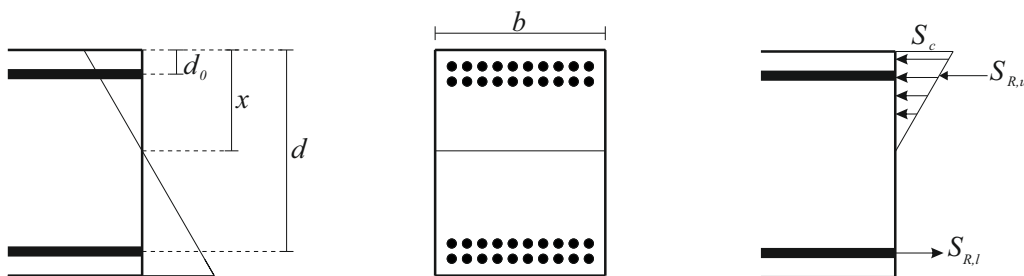


Figure 3.4. Cross-section of the longitudinal concrete beams.

The reinforced concrete beams have a first moment of area as shown in table 3.3.

**Table 3.3.** First moment of area of concrete beams.

	[mm <sup>3</sup> ]
$z_{Beam}$	$31 \cdot 10^6$

First moment of area as shown in table 3.3 is the first moment of area at the tension reinforcement bars.

### 3.3.4 Line Load on Along-system

The line load on Along-system is found by determining the reactions from the bridge decks and adding the dead load of the concrete beams. Due to symmetry and the width of the bridge decks are 10 m, the line load on Along-system can be determined by eq. (3.1)

$$\begin{aligned} q_A &= G_{Beam} + \frac{L_C}{2} \cdot (G_{Deck} + G_{Asphalt}) \\ &= 50 \text{ kN/m} \end{aligned} \quad (3.1)$$

### 3.3.5 Line Load on Cross-system

The line load on the bridge decks (Cross-system) are determined by eq. (3.2).

$$\begin{aligned} q_C &= 0.32 \text{ m} \cdot (G_{Deck} + G_{Asphalt}) \\ &= 1.92 \text{ kN/m} \end{aligned} \quad (3.2)$$

Where 0.32 m is the width of a single bridge deck.



---

# Uncertainty Modeling

In this chapter, characterization of uncertainties applied in the reliability analysis and load models are presented. How the uncertainties are introduced in reliability analysis is explained in chapters 5 and 6. An overview of the uncertainties used in this report can be found in table 4.15 on page 47.

The material properties of the composite reinforcement bars are determined based on static and fatigue tests using statistical analysis. Fatigue tests are used to determine  $S-N$  curve for the material at two  $R$ -ratios in the tension part of the constant life diagram. Additionally, the Maximum-Likelihood Method is used to determine statistical uncertainties regarding the fatigue tests.

Furthermore, uncertainties regarding the fatigue load is presented. Three stochastic variables are used to describe the uncertainty related to the fatigue load.

Uncertainties are identified by two major categories; aleatory and epistemic. Aleatory uncertainties are irreducible uncertainties associated with the physical system or the environment, which cannot be changed by the modeler. Epistemic uncertainties are due to lack of knowledge of the system or the environment. These uncertainties can be reduced by gathering more data, introducing better models etc.

Uncertainties are typically modeled as stochastic variables  $\mathbf{X} = (X_1, \dots, X_n)$  and can be divided into the following sub groups.

## Aleatory

- *Physical uncertainty*: Inherent variation associated with natural randomness of a quantity.

## Epistemic

- *Measurement uncertainty*: Related to imperfect measurements.
- *Statistical uncertainty*: Related to limited sample size of a quantity. The statistical uncertainty is reduced by increasing the sample size of the quantity.
- *Model uncertainty*: Related to inaccuracy of the mathematical models used and choice of distribution types for the stochastic variables.

These are the types of uncertainties accounted for in a reliability analysis, however another type of uncertainty which is not covered is gross errors or human

errors. This type of uncertainty is managed through quality controls. [Sørensen, 2011b]

## 4.1 Experimental Characterization of Fiber-Reinforced Composite Materials

In the following chapter, the static and fatigue data is presented. The data is used for estimation of  $S-N$  curves for use in constant life diagrams as well as determining compression and tension ultimate strengths. Least Square Method and Maximum-Likelihood Method is used to determine fatigue properties;  $\log K$  and  $m$ . Classic statistics are used to determine static failure characteristics;  $S_{u,c}$  and  $S_{u,t}$ .

An ideal scenario is to acquire data for Schöck ComBAR. Unfortunately, it has not been possible to acquire an adequate amount of tests for Schöck ComBAR. Instead, a similar material with data available is used.

The characteristics for Schöck ComBAR is listed in table 4.1.

**Table 4.1.** Characteristics for Schöck ComBAR. [Schöck, 2014]

Material	ComBAR
Fiber Type	Glass
Lay-up	-
Fiber volume, %	75
Resin Type	Polyester
Ultimate tensile strength	> 1000 MPa
Process	Pultrusion

Additionally, the fiber direction in Schöck ComBAR is only unidirectional. As the fibers are unidirectional, the axial tensile strength is high, but tensile and compressive strengths in perpendicular direction to the fibers are relatively low. Furthermore, Schöck ComBAR behaves linearly elastic to failure and yielding is not observed for the reinforcement bar as shown in figure 4.1. [Schöck, 2014]. No ultimate compression strength are mentioned in [Schöck, 2014].

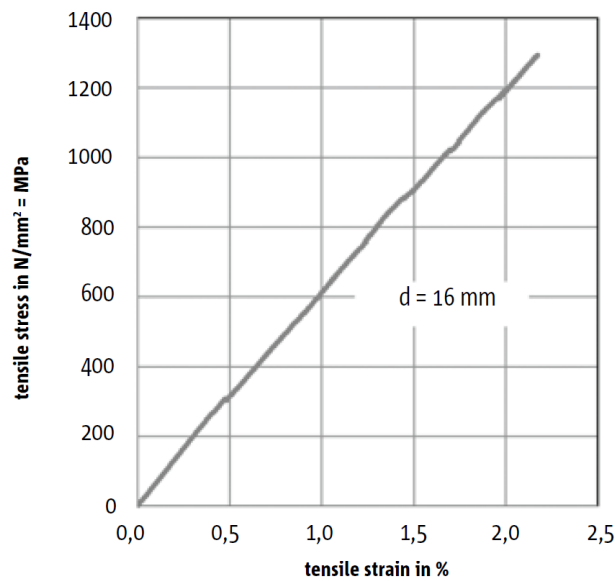


Figure 4.1. Stress-strain diagram [Schöck, 2014].

The criteria for choosing a similar material are listed below.

- Mainly or only unidirectional fibers
- Fatigue data for multiple  $R$ -ratios preferably in tension-tension
- Identical fiber and resin type, chemical composition may vary
- Similar fiber volume percentage
- Static tension and compression strength tests available
- Preferably similar tension and compression strengths

Two databases are examined for appropriate data; *OpTiDAT* and *SNL/MSU/DOE Composite Material Fatigue Database*.

*OpTiDAT* is a material database regarding *OpTiMat* blades and contains all test results by the *OpTiMat* research. The database cover various static and fatigue load type testing, as well as material characteristics. In the database only a few fatigue test are carried out using unidirectional materials and is not sufficient for a statistical analysis.

The *SNL/MSU/DOE Composite Material Fatigue Database* was established in 1989 with a goal to further increase the knowledge required to improve and understand the behavior of composite materials for structural applications. The database has more than 500 fatigue and static tests of unidirectional materials. A material with 33 tests available and characteristics alike those of a composite rebar is selected. The unidirectional material has 8 static and 25 fatigue tests available. The characteristics for the material is shown in table 4.2.

**Table 4.2.** Characteristics for suitable material.

Material	UNI-PPG1200-PU
Fiber Type	Glass
Lay-up	[0] <sub>6</sub>
Fiber volume, %	59
Resin Type	Polyester
Ultimate tensile strength	see table 4.3
Process	Infusion

Additionally, it should be noted that these fatigue tests are carried out on test coupons. A notable difference between the materials presented in tables 4.1 and 4.2, is the processing method. As the comparable material is not pultruded, it can only consist of mats and resin. Furthermore, the fiber volume is significantly lower in the suitable material compared to the ComBAR material. Generally, the fiber volume effect the mechanical properties of the material, and a high fiber volume increase the material strengths [Université libre de Bruxelles, 1996]. Additionally, it has been studied that the fiber volume has an effect on the fatigue life of composites [Allah et al., 1996].

**Table 4.3.** List of static tests on UNI-PPG1200-PU. STT: Static tension, STC: Static compression.

Static test	Test type	Failure stress [MPa]	Young's Modulus [GPa]
1	STT	1143	39.6
2	STT	1040	39.5
3	STT	1042	39.7
4	STT	1043	42.9
5	STT	1033	41.3
6	STC	-728	42.8
7	STC	-761	42.5
8	STC	-746	41.8

In table 4.3, the static tests are listed. The static load tests are carried out with constant displacement rate. Compared to the ultimate tensile strength of Schöck ComBAR presented in table 4.1, the static tension tests show similar results. In table 4.4, the fatigue tests are presented.

**Table 4.4.** List of fatigue tests on UNI-PPG1200-PU.\* indicates run-outs.

Fatigue test	$S_a$ [MPa]	$N$	$R$
1	207	1057085	-1
2	207	4000000*	-1
3	241	1680125	-1
4	310	106485	-1
5	345	20532	-1
6	345	24227	-1
7	345	27043	-1
8	345	35832	-1
9	345	42852	-1
10	379	10903	-1
11	414	7967	-1
12	414	10144	-1
13	517	219	-1
14	186	310952	0.1
15	186	678003	0.1
16	186	770361	0.1
17	202	96223	0.1
18	202	162886	0.1
19	202	173091	0.1
20	217	25643	0.1
21	217	28490	0.1
22	217	47170	0.1
23	248	9204	0.1
24	248	23966	0.1
25	248	28690	0.1

As seen from table 4.4, two  $R$ -ratios are presented. This is assumed sufficient as it is primarily the tension part of the constant life diagram that is utilized in the tension reinforcement bar. All the fatigue tests presented in table 4.4 are performed with constant load amplitude until failure occur. Failure is taken as complete separation, effects like; delamination, stable matrix cracking and fiber damage may gradually accumulate during the lifetime of the test specimen. Tests were performed at ambient laboratory air (18-24 °C) and fatigue coupons are air cooled with a fan.

It should be noted that the amount of static and fatigue tests used below the limit (25-30 tests) normally used in statistical analysis. As Fatigue test 13 is well within the limit of low-cycle fatigue (< 1000 cycles), it will be disregarded.

As the data is acquired through a renowned database and produced in a laboratory, it is assumed to be; independent, homogeneous and stationary. These prerequisites are necessary for the statistical data processing to be valid. Independence assures that no data point influences the outcome of another. Homogeneity is the assumption that the test subjects will not experience differentiating load prior to testing, that will affect the fatigue durability outcome, and thus belong to the same statistical population. Furthermore homogeneity requires for all the tests to have been performed at the same frequency. Stationarity requires

that there are no change in statistical moments as an effect of time.

#### 4.1.1 Assessment of Failure Characteristics

Tensile and compressive experiments are conducted in order to derive the examined materials strength. The experimental test results are shown in table 4.3 and are displacement controlled tests.

According to JCSS [2014], strength distributions are assumed Lognormal distributed. Both set of static tests will be fitted to Lognormal distributions, this is done with full disregard for the lacking amount of data. If this analysis and derivation of partial safety factors were to be done for a real competitive reinforcement bar material, more static tests would be needed. This would likely not be a problem as static tests are inexpensive and hasty in comparison to fatigue tests. Also it would be financially efficient as it would eliminate much of the statistical uncertainty. In this report the statistical uncertainty of the static properties is disregarded.

The statistical moments are found by equations; (4.1) and (4.2).

$$\mu_{ln} = \frac{1}{N} \sum_{i=1}^N \ln x_i \quad (4.1)$$

$$\sigma_{ln} = \sqrt{\frac{1}{N} \sum_{i=1}^N (\ln x_i - \mu_{ln})^2} \quad (4.2)$$

Where

$N$	Sample size
$x_i$	Sample no. $i$
$\mu_{ln}$	Lognormal sample mean
$\sigma_{ln}$	Logarithmic standard deviation of sample

The values calculated by equations (4.1) and (4.2) are transformed to mean and standard deviation by equations (4.4) and (4.3).

$$\sigma_{ln} = \sqrt{\ln \left( \frac{\sigma^2}{\mu^2} + 1 \right)} \quad (4.3)$$

$$\mu_{ln} = \ln \mu - \frac{1}{2} \sigma_{ln}^2 \quad (4.4)$$

where

$\mu$	Mean
$\sigma$	Standard deviation

The results are presented below in table 4.5.

Table 4.5. Statistical parameters for static properties.

	$\mu$ [MPa]	$\sigma$ [MPa]	COV	Dist.
$S_{u,c}$	745	16.5	0.02	LN
$S_{u,t}$	1060	45.2	0.04	LN

The ultimate strengths are assumed uncorrelated. It is not possible to test experimentally the correlation as it would require the break the same test specimen two times.

#### 4.1.2 Assessment of S-N curves

In this section, the S-N curves are estimated using two fitting methods; Least Square Method, which minimize the sum of the square of the error and Maximum-Likelihood Method. It maximizes the likelihood of the data belonging to the distribution, giving the most probable statistical moments. Least Square Method is used as a first estimate for the Maximum-Likelihood Method iteration. The S-N curve is shown in eq. (2.1).

##### Least Square Method

The Least Square Method determines the statistical parameters by solving the optimization problem in eq. (4.5). [Sørensen, 2011b]

$$\min_{\theta} \sum_{i=1}^n (\hat{F}_i - F_X(x_i|\theta))^2 \quad (4.5)$$

Where  $F_X$  is a given distribution function with the unknown statistical parameters  $\theta = (\theta_1, \theta_2, \dots, \theta_m)$ .  $\hat{F}$  is the empirical distribution function determined using e.g. the Weibull plotting formula shown in eq. (4.6).

$$\hat{F}_i = \frac{i}{n+1} \quad , x = \hat{x}_i \quad (4.6)$$

Where  $n$  is number of observations and  $\hat{x} = (\hat{x}_1, \hat{x}_2, \dots, \hat{x}_n)$  is data/observations sorted in size.

Least Square Method provides expected values for  $\log K$  and  $m$ .  $m$  is used in the S-N curve formulation to calculate  $\log K_i$  for each sample. Standard deviation for  $\log K$  is found using classical statistics by eq. (4.7).

$$\sigma_{\log K} = \sqrt{\frac{1}{n} \sum_{i=1}^n (\log K_i - \mu_{\log K})^2} \quad (4.7)$$

Where

$\sigma_{\log K}$	Standard deviation of $\log K$
$\mu_{\log K}$	Mean of $\log K$

$\log K_i$  is determined as

$$\log K_i = m \log S_{ai} + \log N_i$$

based on  $m$  found by Least Square Method. Where  $S_{ai}$  and  $N_i$  is found in table 4.4.

The results of the Least Square Method are shown in table 4.6.

**Table 4.6.** Results from Least Square Method for different  $R$ -ratios.

	$R = -1$	$R = 0.1$
$\mu_{\log K}$	26.3	32.4
$m$	8.6	11.8
$\sigma_{\log K}$	0.20	0.24

The results from Least Square Method are used as an initial guess for the Maximum-Likelihood Method.

#### Maximum-Likelihood Method

Statistical parameters  $(\alpha_0, \alpha_1, \dots, \alpha_m)$  are determined by maximizing the Likelihood function,  $L$ , shown in eq. (4.8) with  $x_{ij}$  being the  $j$ th coordinate of the  $i$ th observation.

$$L(\alpha_0, \alpha_1, \dots, \alpha_m) = \prod_{i=1}^n f_X(y_i = \alpha_0 + \alpha_1 x_{i1} + \dots + \alpha_m x_{im} + \epsilon) \quad (4.8)$$

Where  $f_X$  is a probability density and

$$y_i = \alpha_0 + \alpha_1 x_{i1} + \dots + \alpha_m x_{im} + \epsilon \quad (4.9)$$

is a linear regression model.  $\epsilon$  models the lack of fit of the model, the aleatory uncertainty.  $\epsilon$  has a predetermined mean value of 0 and is assumed to be normally distributed with a standard deviation  $\sigma_\epsilon$ . The statistical parameters are determined by solving the optimization problem shown in eq. (4.10).

$$\max_{\alpha_0, \alpha_1, \dots, \alpha_m, \sigma_\epsilon} \ln L(\alpha_0, \alpha_1, \dots, \alpha_m, \sigma_\epsilon) \quad (4.10)$$

If the  $S$ - $N$  curve, presented in eq. (4.11), is compared with eq. (4.9)

$$\log N = \log K - m \log S_a + \epsilon \quad \text{or} \quad N = K S_a^{-m} + 10^\epsilon \quad (4.11)$$

then

$$\begin{aligned} y &= \log N \\ \alpha_0 &= \log K \\ \alpha_1 &= -m \\ x_1 &= \log S_a \end{aligned}$$

The  $S-N$  curve is inserted in eq. (4.8), the Likelihood function becomes as shown in eq. (4.12). This formulation takes run-outs,  $n_o$ , taken into consideration.  $n$  is number of observations of failure.

$$L(\log K, m, \sigma_\epsilon) = \prod_{i=1}^n \frac{1}{\sqrt{2\pi} \sigma_\epsilon} \exp\left(-\frac{1}{2} \left(\frac{\log N_i - (\log K - m \log S_a)}{\sigma_\epsilon}\right)^2\right) \cdot \prod_{i=n+1}^{n+n_0} \Phi\left(\frac{\log N_i - (\log K - m \log S_a)}{\sigma_\epsilon}\right) \quad (4.12)$$

Where  $\Phi()$  is the standard Normal distribution function and  $n$  is number of observations of failure.  $n_o$  is number of observations of run-outs.  $\sigma_\epsilon$  is the standard deviation of  $\epsilon$ .

In table 4.7, the Maximum-Likelihood Method results is presented for  $R = -1$  with and without run-outs in order to evaluate the effect of taking run-outs into consideration.

**Table 4.7.** Results from Maximum-Likelihood Method with and without run-outs for  $R = -1$ .

	Without run-outs	With run-outs
	$\mu$	$\mu$
$\log K$	26.3	26.8
$m$	8.6	8.8
$\sigma_\epsilon$	0.20	0.21

It is seen from table 4.7, including the survival of the run-out specimen increases the expected value and the standard deviation. The increase in standard deviation is not beneficial, however the effect is counteracted by the significant increase in the expected value.

Additionally, the Maximum-Likelihood Method can give information regarding statistical uncertainty. As the Maximum-Likelihood Method parameters are determined using a limited number of data, the parameters are subject to statistical uncertainty. If the data pool is of the size 25-30 or greater the parameters  $\log K$  and  $\sigma_\epsilon$  estimated by the Maximum-Likelihood Method parameters become asymptotically normally distributed stochastic variables with expected value equal to the Maximum Likelihood estimators and a covariance matrix as shown in eq. (4.13). [Sørensen, 2011a]

As presented in table 4.4, only 12 fatigue tests are available at each  $R$ -ratio. This is well below the previously mentioned limit and the estimated Maximum-Likelihood Method parameters are by the statistical uncertainty.

$$\mathbf{C}_{\log K, m, \sigma_\epsilon} = [-\mathbf{H}_{\log K, m, \sigma_\epsilon}]^{-1} = \begin{bmatrix} \sigma_{\log K}^2 & \rho_{\log K, m} \sigma_{\log K} \sigma_m & \rho_{\log K, \sigma_\epsilon} \sigma_{\log K} \sigma_{\sigma_\epsilon} \\ \rho_{\log K, m} \sigma_{\log K} \sigma_m & \sigma_m^2 & \rho_{m, \sigma_\epsilon} \sigma_m \sigma_{\sigma_\epsilon} \\ \rho_{\log K, \sigma_\epsilon} \sigma_{\log K} \sigma_{\sigma_\epsilon} & \rho_{m, \sigma_\epsilon} \sigma_m \sigma_{\sigma_\epsilon} & \sigma_{\sigma_\epsilon}^2 \end{bmatrix} \quad (4.13)$$

Where

$\mathbf{C}_{\log K, m, \sigma_\epsilon}$	Covariance for $\log K$ , $m$ and $\sigma_\epsilon$
$\mathbf{H}_{\log K, m, \sigma_\epsilon}$	Hessian matrix with second order derivatives of the log-Likelihood function
$\sigma_{\log K}$	Standard deviation on $\log K$
$\sigma_m$	Standard deviation on $m$
$\sigma_{\sigma_\epsilon}$	Standard deviation on $\sigma_\epsilon$
$\rho_{\log K, \sigma_\epsilon}$	Correlation coefficient between $\log K$ and $\sigma_\epsilon$
$\rho_{\log K, m}$	Correlation coefficient between $\log K$ and $m$
$\rho_{m, \sigma_\epsilon}$	Correlation coefficient between $m$ and $\sigma_\epsilon$

The Hessian matrix is obtained from.

$$\mathbf{H}_{i,j} = \frac{\partial^2}{\partial \alpha_i \partial \alpha_j} \ln L(\alpha_0, \alpha_1, \dots, \alpha_m)$$

Where  $\alpha$  is the statistical parameters. The Hessian matrix is estimated from numerical differentiation. In table 4.8, the Maximum-Likelihood Method results for both  $R$ -ratios with run-outs taken into consideration.

**Table 4.8.** Results from Maximum-Likelihood Method for different  $R$ -ratios with run-outs included.

	$R = -1$	$R = 0.1$
	$\mu$	$\mu$
$\log K$	26.8	32.4
$m$	8.8	11.8
$\sigma_\epsilon$	0.21	0.24

The estimated correlation matrix for the  $S$ - $N$  curve at  $R = -1$  becomes .

$$\rho_{R=-1} = \begin{bmatrix} 1 & 0.99 & 0.63 \\ 0.99 & 1 & 0.63 \\ 0.63 & 0.63 & 1 \end{bmatrix}$$

It is seen that  $\log K$  and  $m$  are highly correlated. Therefore their statistical uncertainty can be modeled together. If  $m$  is assumed deterministic with the value estimated by Maximum-Likelihood Method and the parameters  $\log K$  and  $\sigma_\epsilon$  is determined by Maximum-Likelihood Method, the results presented in table 4.9 are achieved.

**Table 4.9.** Results from Maximum-Likelihood Method for  $R$ -ratios -1 and 0.1 with run-outs.  $m$  is assumed deterministic determined by Maximum-Likelihood Method. \*Values taken from table 4.8.

	$R = -1$		$R = 0.1$	
	$\mu$	$\sigma$	$\mu$	$\sigma$
$\log K$	26.8	0.06	32.4	0.07
$m$	8.8*	-	11.8*	-
$\sigma_\epsilon$	0.21	0.05	0.24	0.05

$\sigma_{\sigma_\epsilon}$  and  $\sigma_{\log K}$  represent the statistical uncertainty. The estimated correlation matrices becomes.

$$\rho_{R=-1} = \begin{bmatrix} 1 & 0.06 \\ 0.06 & 1 \end{bmatrix} \quad \rho_{R=0.1} = \begin{bmatrix} 1 & 0.01 \\ 0.01 & 1 \end{bmatrix}$$

From the correlation matrix above, it can be concluded that  $\log K$  and  $\sigma_\epsilon$  are almost completely uncorrelated. In all further analysis, it will be assumed that  $\log K$  and  $\sigma_\epsilon$  are completely uncorrelated.

The estimated mean  $S-N$  curves along with their 95 % confidence interval of  $\log K$  excluding and including of the statistical uncertainties as defined in equations (4.14) and (4.15) are plotted with the experimental data in figures 4.2 and 4.3 for respectively  $R = -1$  and  $R = 0.1$ .

$$\log K = N(\mu_{\log K}, \sigma_\epsilon) \tag{4.14}$$

$$\log K = N(\mu_{\log K}, \sigma_{\log K}) + N(0, N(\sigma_\epsilon, \sigma_{\sigma_\epsilon})) \tag{4.15}$$

In order to estimate the confidence interval of eq. (4.15) a small reliability analysis is conducted.

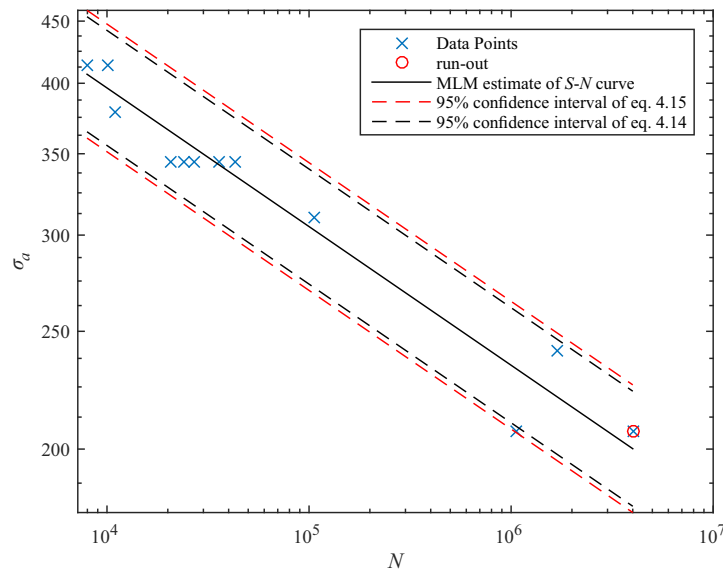
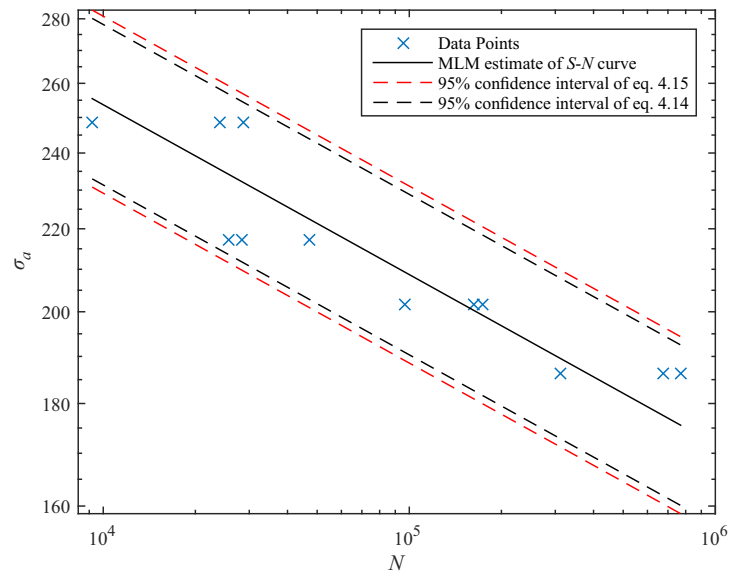
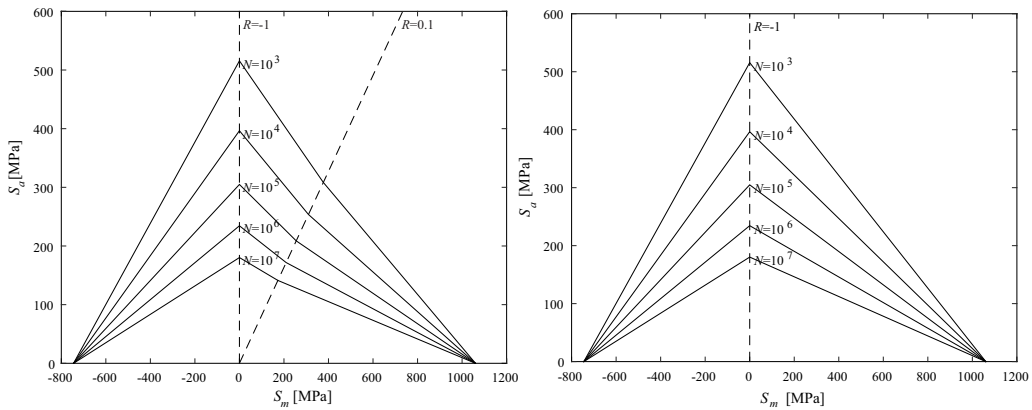


Figure 4.2. Estimated mean  $S-N$  curves and 95 % confidence interval for  $R = -1$  with and without statistical uncertainty plotted with experimental data.



**Figure 4.3.** Estimated mean  $S$ - $N$  curves and 95 % confidence interval for  $R = 0.1$  with and without statistical uncertainty plotted with experimental data.

It can be seen in figures 4.2 and 4.3 that the effect of the statistical uncertainty is of minor importance to the confidence interval. The mean  $S$ - $N$  curves are used to construct constant life diagrams as shown in figures 4.4, 4.5, 4.6 and 4.7 corresponding to the constant life diagrams presented in section 2.1.



**Figure 4.4.** Piecewise CLD constructed from **Figure 4.5**. Shifted Goodman diagram using estimated mean  $S$ - $N$  curves without statistical uncertainty.

Shifted Goodman diagram using  $S$ - $N$  curve at  $R = -1$  constructed from estimated mean  $S$ - $N$  curve without statistical uncertainty.

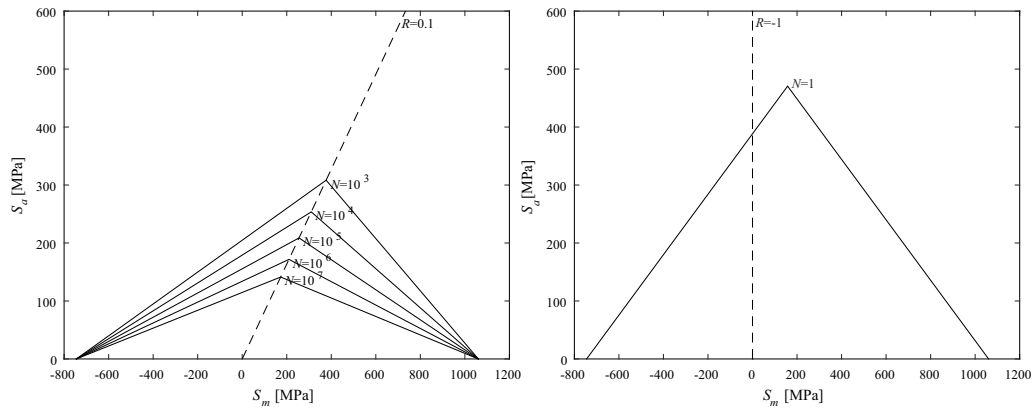


**Figure 4.6.** Shifted Goodman diagram using **Figure 4.7.** Goodman diagram by Germanischer Lloyd using  $m$ -value for  $S-N$  curve at  $R = 0.1$  constructed from estimated mean  $S-N$  curve without statistical uncertainty.  $S-N$  curve at  $R = -1$ .

The constant life diagrams presented in figures 4.4, 4.5, 4.6 and 4.7 will be used for comparison henceforth. This is done in order to account for some designs only using one  $R$ -ratio, or even a simplified constant life diagram as the one presented by Germanischer Lloyd. This will often be the economic approach as fatigue tests are expensive and fatigue rarely dictate the design of shirt traffic bridges. The constant life diagrams are named as and referred to as presented as shown below in table 4.10.

**Table 4.10.** Table of names and figures containing the used constant life diagrams.

Name	Sketched in figure
$CLD_{PL}$	4.4
$CLD_{SGM_{R=-1}}$	4.5
$CLD_{SGM_{R=0.1}}$	4.6
$CLD_{GL}$	4.7

### 4.1.3 Accuracy of Shifted Goodman Diagrams and Goodman Diagram by Germanischer Lloyd

In the following section, the accuracy in fatigue life estimation of the shifted Goodman diagrams and Goodman diagram by Germanischer Lloyd is compared with the fatigue life prediction by the piecewise linear constant life diagram using two  $R$ -ratios as it uses the most experimental data and therefore it is assumed it estimate damage most accurately.

The comparison is performed by predicting fatigue life in a grid of stress cycles (with one stress cycles at each point) located inside the constant life diagrams. The predicted fatigue life from the different constant life diagrams are compared using eq. (4.16).

$$\frac{D_{Compared}}{D_{CLD_{PL}}} \tag{4.16}$$

Where

$D_{Compared}$  | Damage of compared constant life diagram  
 $D_{CLD_{PL}}$  | Damage of piecewise linear constant life diagram

Miner’s rule is used for damage calculation. Fatigue life is estimated by DNVs method for the piecewise linear constant life diagram and the shifted Goodman diagrams. For the Goodman diagram by Germanischer Lloyd eq. (2.5) is used.  $S-N$  curves for constructing the constant life diagrams are obtained in section 4.1. The constructed constant life diagrams used for this analysis is presented in figures 4.4, 4.5, 4.6 and 4.7 on the previous page.

According to eq. (4.16),  $\frac{D_{Compared}}{D_{CLD_{PL}}} > 1$  will indicate that the shifted Goodman diagrams or Goodman diagram by Germanischer Lloyd is more conservative in its estimation of damage at the stress cycle compared to the piecewise linear constant life diagram.

The results of this is shown below in figures 4.8 through 4.10. In each of the figures the numbers position represent the placement of a cycle and the magnitude of the number represents the relative difference as shown in eq. (4.16).

In figure 4.8, the Shifted Goodman diagram using  $R = -1$  is compared with the piecewise linear constant life diagram using two  $R$ -ratios. The hatched area indicate the difference in area covered by the constant life diagrams

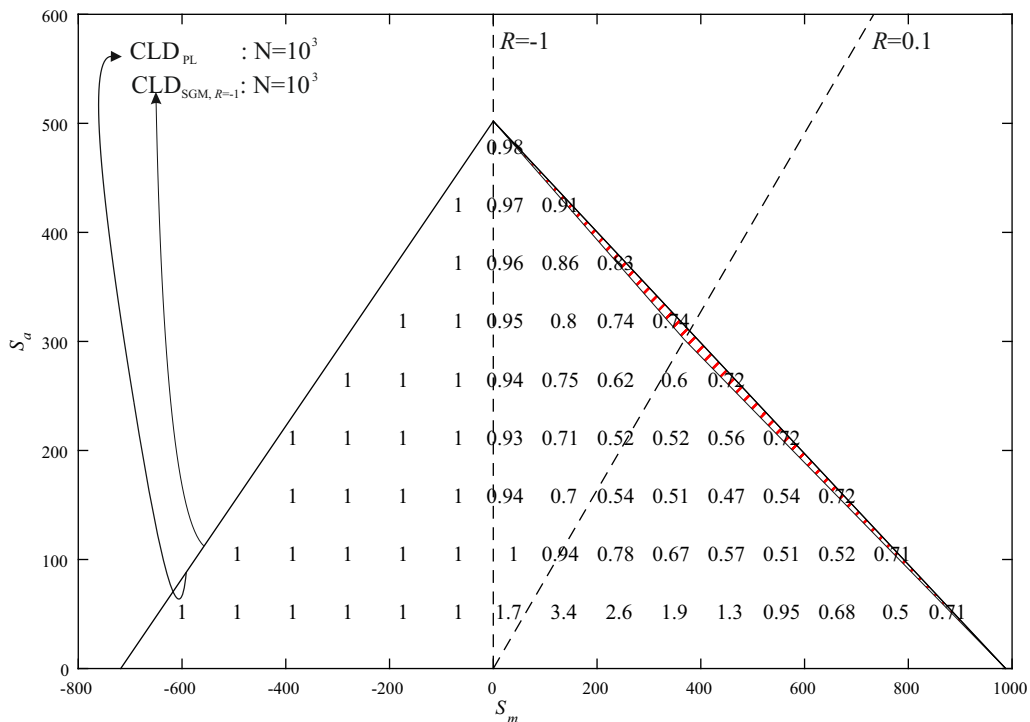


Figure 4.8. Comparison of estimated damage by Shifted Goodman diagram by  $R = -1$  line and the piecewise linear constant life diagram.

It can be seen from figure 4.8, that using a constant life diagram with  $R$ -ratio  $R = -1$  generally underestimate the damage compared to the piecewise linear constant life diagram. Additionally, the shifted Goodman diagram cover a larger

area than the piecewise linear constant life diagram. It should be noted that differences in damage estimation at low cyclic amplitudes e.g. high fatigue life, does not have as large an influence as the difference in damage at high cyclic amplitudes as these stress cycles typically contribute with the most damage. The damage in the compression side of the constant life diagram is estimated exactly as the piecewise linear constant life diagram, because of the way DNVs method estimates damage.

In figure 4.9 the shifted Goodman diagram using  $R = 0.1$  is compared with the piecewise linear constant life diagram.

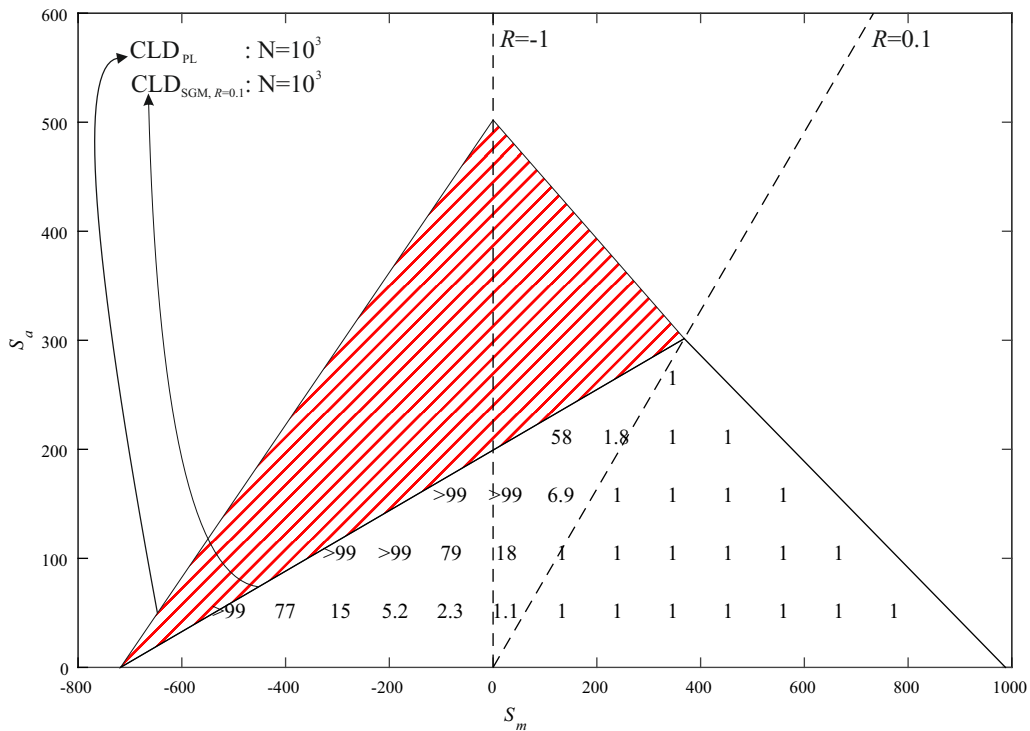


Figure 4.9. Comparison of estimated damage by Shifted Goodman diagram by  $R = 0.1$  line and the piecewise linear constant life diagram.

From figure 4.9, it can be seen that everything right of  $R = 0.1$  is estimated similarly as expected. The rest of shifted Goodman diagram generally estimate more damage compared to the piecewise linear constant life diagram. At high stress levels this can have a large influence on the damage estimation by the shifted Goodman diagram as these stress cycles contributes with most of the damage.

In figure 4.10, the Goodman diagram by Germanischer Lloyd is compared with the piecewise linear constant life diagram.



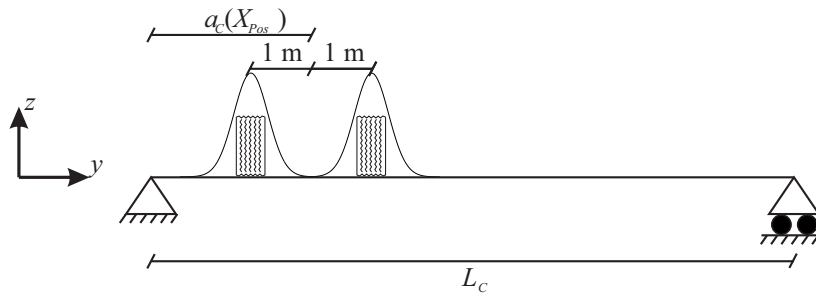


Figure 4.11. Sketch of  $X_{Pos}$  on the Cross-system.

Table 4.11. Mean and standard deviation of  $X_{Pos}$ .

	$\mu$	$\sigma$
$X_{Pos}$	0.0	0.24

### 4.3 Uncertainty for Variable Loads

These uncertainties take dynamic effects and variable load of lorries into consideration.

The uncertainty,  $X_{Dyn}$ , is modeled as a normally distributed stochastic variable with an expected value 1.0 and a standard deviation of 0.2 corresponding to high uncertainty according to [Road Directorate et al., 2004]. This uncertainty takes the dynamic effects of lorry crossings into consideration such as additional force exerted to the bridge from bumps in the road or suspension system in the lorry. The dynamic uncertainty refers to the total load, the lorry exerts upon the bridge both amplitude and mean load.

Furthermore an uncertainty, which takes varying traffic loads into account is introduced. This uncertainty,  $X_{Load}$ , is assumed normally distributed with an expected value 0.0 and a standard deviation of 49 kN (= 5t). This variable is added to the mean load of each crossing lorry. [Road Directorate et al., 2004]  $X_{Dyn}$  and  $X_{Load}$  are realized for each lorry individually.

Table 4.12. Mean and standard deviation of  $X_{Dyn}$  and  $X_{Load}$ .

	$\mu$	$\sigma$
$X_{Dyn}$	1.0	0.2
$X_{Load}$	0.0	49 kN

### 4.4 Uncertainty in Calculation of Stresses

This uncertainty is related to calculation of stress amplitude. Description the uncertainty related to the transformation from load to stresses. The uncertainty is denoted,  $X_{Model}$ , and is modeled as an independent lognormally distributed stochastic variable with an expected value 1.0 and a standard deviation of 0.1

[Sørensen, 2009].  $X_{Model}$  is applied to both cyclic stress amplitudes and cyclic mean stresses. The uncertainty is applied per lifetime. Application of  $X_{Model}$  is shown in eq. (5.5).

Table 4.13. Mean and standard deviation of  $X_{Model}$ .

	$\mu$	$\sigma$
$X_{Model}$	1.0	0.1

## 4.5 Damage Accumulation Model

Palmgren-Miner's damage accumulation rule is normally recommended to estimate damage in composite materials. Even though new models for damage accumulation have been proposed, these models do not perform much better [Toft and Sørensen, 2009]. Therefore the Miners rule is used and uncertainties related to Miner's rule can be divided into three parts.

- Model uncertainty on Miner's rule
- Physical uncertainty on the  $S-N$  curves
- Statistical uncertainty on the  $S-N$  curves

Model uncertainty related to  $S-N$  curves and constant life diagrams can be improved with better models. In the present report, the physical and statistical uncertainty related to the  $S-N$  curves are determined based a number of constant amplitude tests at different  $R$ -ratios, see section 4.1. The model uncertainty for Miner's rule,  $\Delta$ , is assumed lognormally distributed with an expected value 1.0 and a standard deviation 0.40. The standard deviation for Miner's rule is based on the assumption that it should be less certain than the standard deviation for steel (0.3 [JCSS, 2014]). If variable amplitude tests were available,  $\Delta$  could be determined.  $\Delta$  is included in the reliability analysis.  $\Delta$  is applied per lifetime.

Table 4.14. Mean and standard deviation of  $\Delta$ .

	$\mu$	$\sigma$
$\Delta$	1.0	0.4

## 4.6 Overview of Uncertainties and Stochastic Variables

In table 4.15, an overview of the uncertainties used in the present report are presented. Distribution types and characteristic values take basis in DS/EN 1990 and JCSS' "Probabilistic Model Code". Characteristic values are normally chosen as 5-% quantiles. As there is no valid Eurocode or Danish annex for fiber-reinforced polymers yet, this will be used there as well.

Table 4.15. Overview of uncertainties.

	$\mu$	$\sigma$	COV	Dist	Characteristic quantile	Characteristic value
$X_{Load}$	0	49 kN	-	N	-	-
$X_{Pos}$	0	0.24 m	-	N	-	-
$X_{Model}$	1	0.10	10 %	LN	-	-
$X_{Dyn}$	1	0.20	20 %	N	-	-
$\log K_{R=-1}$	26.8	0.06	0.2 %	N	see eq. (4.17)	26.4
$\log K_{R=0.1}$	32.4	0.07	0.2 %	N	see eq. (4.17)	32.0
$\sigma_{\epsilon,R=-1}$	0.21	0.05	24 %	N	-	-
$\sigma_{\epsilon,R=0.1}$	0.24	0.05	21 %	N	-	-
$\Delta$	1	0.40	40 %	LN	-	1
$S_{u,c}$	745	16.5	2 %	LN	5 %	718
$S_{u,t}$	1060	45.2	4 %	LN	5 %	988

$$\log K_{C,0.05} = \mu_{\log K} + \Phi^{-1}(0.05) \sigma_{\epsilon} \quad (4.17)$$

Note that eq. (4.17) does not include statistical uncertainty, it can be seen from figures 4.2 and 4.3 that this would have a minor effect on the characteristic value. The 5% quantiles of the two log K values would be 26.4 and 32.0 if the statistical uncertainty was included. All stochastic variables are assumed uncorrelated. The correlation between the log Ks is investigated further in section 6.7. As the error term,  $\epsilon$ , is assumed to be normally distributed with an expected value of 0.0. The standard deviation modeled as a Normal distribution,  $\epsilon$  is modeled as shown in eq. (4.18).

$$\begin{aligned} \epsilon_{R=-1} &= 0 + u_{R=-1} \sigma_{\epsilon,R=-1} \\ \epsilon_{R=0.1} &= 0 + u_{R=0.1} \sigma_{\epsilon,R=0.1} \end{aligned} \quad (4.18)$$

where  $u_{R=-1}$  and  $u_{R=0.1}$  are standard Normal distributions.

Figures showing the Characteristic  $S-N$  curves found from the Characteristic log K values presented above, is presented below in figures 4.12 and 4.13.

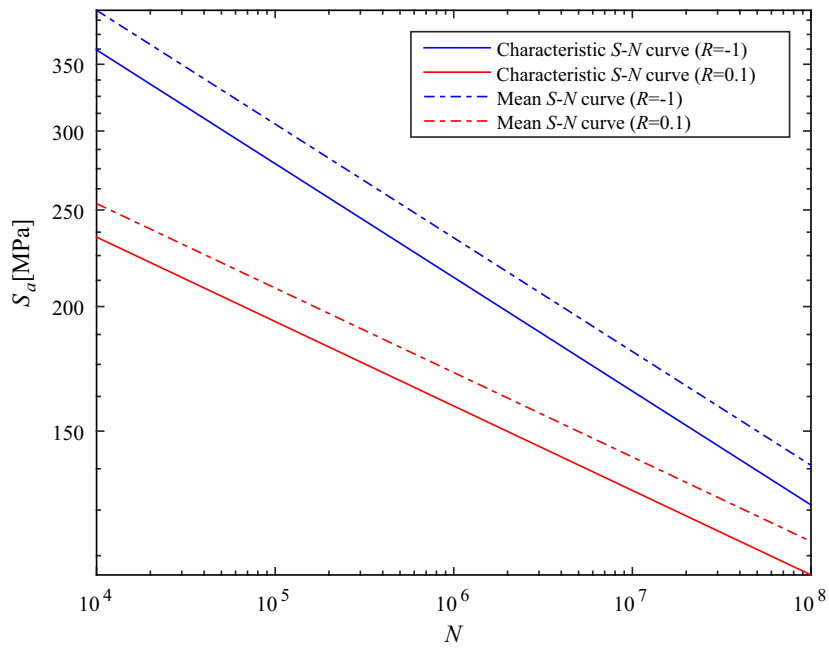


**Figure 4.12.** The Characteristic  $S$ - $N$  curves and their mean curves without statistical uncertainty.

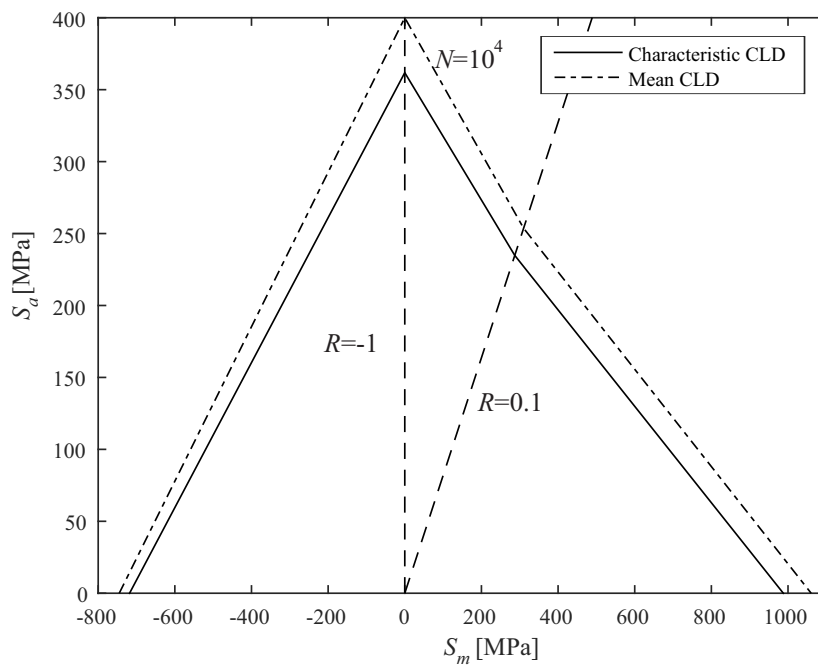


**Figure 4.13.** Characteristic constant life diagram for  $N = 10^4$  along with the constant life diagram found by the mean values.

---

## Fatigue Loads

In the following chapter, a fatigue load model is presented in order to determine the reliability level of the bridge system. It is important the fatigue load model is representative to ensure the partial safety factors are representative.

Often when designing a structure in fatigue limit state, only critical areas of the structure are designed and the design is applied for the whole structure. Therefore, critical fatigue points in the bridge system are investigated to ensure a representative load spectrum. Furthermore, the load spectrum in selected points across the bridge system is studied.

Additionally, it is investigated how many lorries needs to cross the bridge system in order to represent the uncertainties related to the fatigue load.

In order to verify fatigue resistance in structures fatigue load models can be used. This is done because a precise prediction of the actual dynamic load pattern is hard, or impossible to acquire. Therefore a load model that predicts a conservative estimate is convenient. Most of the load models presented in DS/EN 1991-2 are only intended for predicting a lack of the possibility of fatigue failure (infinite life). For the majority of the load models a characteristic property is that they do not claim to have the same traffic as the traffic on the intended site. The claim is that the fatigue damage from the models is equivalent to the fatigue damage that the traffic on the intended site would cause. All the models presented here have chosen to consider cars as negligible and only lorries are of importance. Below a summarization of the five fatigue load models presented in DS/EN 1991-2 and their characteristic properties are presented.

- Fatigue load model 1  
Intended for checking for infinite life. Used for determining fatigue from a single type of crossing. Can be modified for a specific case.
- Fatigue load model 2  
Intended for checking for infinite life. Used for determining fatigue from a single type of crossing. Load defined by a set of frequent lorries, wherein the most critical is chosen for analysis. All traffic is assumed to be of this type.
- Fatigue load model 3  
Intended for fatigue life assessment. Used for determining fatigue

from a single lorry crossing. Can not be used for assessing infinite life. Defined by a single lorry geometry, unlike the other fatigue load models it refers to a plane parallel to the road.

- Fatigue load model 4  
Intended for fatigue life assessment. Can not be used for assessing infinite life. Defines a number of lorry types and proposes several mixes of traffic. Each of the lorries are assumed to cross the bridge alone. Rainflow counting is suggested for determining stress ranges. Intended for determination of a stress range spectra.
- Fatigue load model 5  
Intended for fatigue life assessment. Prerequisites relevant traffic data.

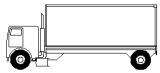
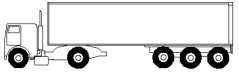
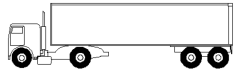
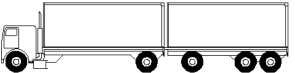
For all load models an amount of annual crossings is to be chosen. A replication of the table showing these in DS/EN 1991-2, is shown below in table 5.1. These categories are all paired with short descriptions of the traffic situation they represent.

Henceforth, load model 4 will be used. Fatigue load model 4, as the only one, presents a distribution of heavy traffic. These distributions are described as representative for traffic in Europe. This is in line with the goal of the report which is to develop partial safety factors for fatigue assessment, corresponding to the safety levels presented in Eurocode. The heavy traffic distributions are defined by table 5.2 which is as presented in DS/EN 1991-2. Traffic category 2 is used for calibrating partial safety factors in this report as traffic category 1 require 2 or more lanes per direction. Later in this chapter, it is investigated if  $5 \cdot 10^5$  lorry crossings is adequate amount to represent the uncertainties related to the fatigue load described in chapter 4. Fatigue load models defined in DS/EN 1991-2 assumes that each standard lorry is considered to cross the bridge in absence of any other lorry. Lorry crossings in both direction are simulated.

**Table 5.1.** Indicative number of heavy vehicles expected per year and per slow lane. [DS/EN 1991-2, 2003]

Traffic categories		$N_{obs}$ per year and per slow lane
1	Roads and motorways with 2 or more lanes per direction with high flow rates of lorries	$2 \cdot 10^6$
2	Roads and motorways with medium flow rates of lorries	$0.5 \cdot 10^6$
3	Main roads with low flow rates of lorries	$0.125 \cdot 10^6$
4	Local roads with low flow rates of lorries	$0.05 \cdot 10^6$

**Table 5.2.** Indicative number of heavy vehicles expected per year and per slow lane [DS/EN 1991-2, 2003]. Lorries are denoted Lorry 1, Lorry 2, Lorry 3, Lorry 4 and Lorry 5 from the top.

Vehicle Types			Traffic Type			
			Long distance	Medium distance	Local traffic	
Lorry	Axle Spacing [m]	Equivalent axle loads [kN]	Lorry %	Lorry %	Lorry %	Wheel type
	4.5	70 130	20.0	40.0	80.0	A B
	4.20 1.30	70 120 120	5.0	10.0	5.0	A B B
	3.20 5.20 1.30 1.30	70 150 90 90	50.0	30.0	5.0	A B C C
	3.40 6.00 1.80	70 140 90 90	15.0	15.0	5.0	A B B B
	4.80 3.60 4.40 1.30	70 130 90 80 80	10.0	5.0	5.0	A B C C C

As seen in the table 5.2, the standard defines different wheel types shown in table 5.3.

Table 5.3. Definition of wheel and axle types. [DS/EN 1991-2, 2003]

Wheel/ Axle type	Geometrical definition
A	
B	
C	

All the wheel types; A, B and C can be simplified to two point loads with 2 m in-between, this simplification is applied in this report.

Based on the load model 4, a time series of lorries crossing the bridge system is realized in order to assess the load cycles. The time series is based on traffic category 2 and the "Long distance" traffic distribution. All lorries have the uncertainties;  $X_{Load}$ ,  $X_{Pos}$  and  $X_{Dyn}$  applied to their load. The total load of each lorry will vary with a normally distributed variable,  $X_{Load}$ , with a mean of 0 and a standard deviation of 49 kN. The position of the lorry in the lane will vary from the enter position of the driving lane with a random outcome of a normally distributed variable,  $X_{Pos}$ , with a mean of 0 and a standard deviation of 24 cm. Each lorry crossing will maintain its transverse position for the entire length of the crossing. Lastly, bumps in the road and difference in the individual lorries' suspension systems will cause the lorries to exert an amplified or decreased force upon the bridge. For the realizations a normally distributed variable,  $X_{Dyn}$ , with an expected value of 1 and a standard deviation of 0.2 is applied to the total load of the lorry e.g. all axle have the same outcome of  $X_{Dyn}$  applied. All of these are applied to each lorry individually and their application and interaction with other stochastic variables shown in equations (5.1) to (5.4). Uncertainties not mentioned here is applied in the reliability analysis per lifetime.

When lorries crosses the bridge system, their load effect is determined using influence lines. Influence lines describe the load effect in a point as a function of a single loads position. Influence lines for Along-system and Cross-system are shown in figures 5.1 and 5.2 and their formulations in equations (5.1) and (5.2).

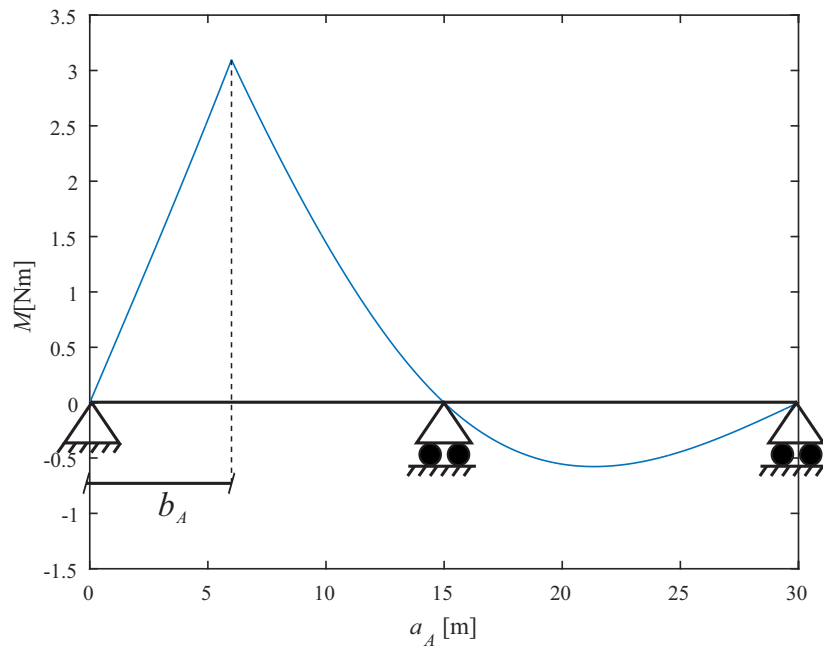


Figure 5.1. Influence line at  $b_A = 0.4L$  for a single point load in Along-system.

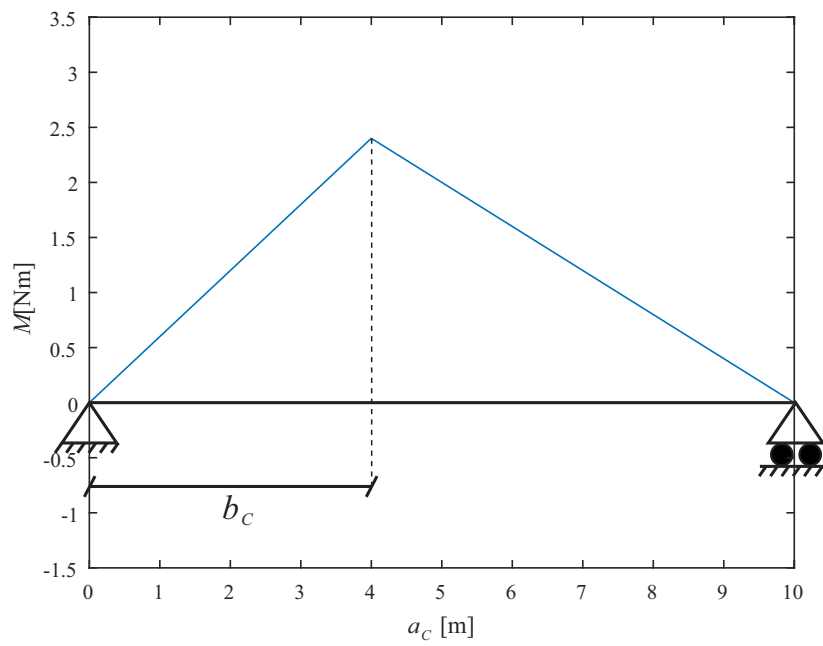


Figure 5.2. Influence line at  $b_C = 0.4L$  for a single point load in Cross-system.

The formulations yielding the influence lines are shown for respectively the Along-system and the Cross-system in equations (5.1) and (5.2).

$$\begin{aligned}
 M_A(a_A) &= P_A (b_A - a_A) - \frac{4P_A L_A^3 - 5P_A L_A^2 a_A + P_A a_A^3}{4L_A^3 b_A} & 0 \leq a_A \leq \frac{L_A}{2} \\
 M_A(a_A) &= -\frac{4P_A L_A^3 - 5P_A L_A^2 a_A + P_A a_A^3}{4L_A^3 b_A} & \frac{L_A}{2} \leq a_A \leq L_A
 \end{aligned} \tag{5.1}$$

$$M_A(a_A) = -\frac{P_A (2L_A - a_A)^3 - L_A^2 P_A (2L_A - a_A)}{4L_A^3 b_A} \quad L_A \leq a_A \leq 2L_A$$

$$\begin{aligned}
 M_C(a_C) &= P_C (L_C - (a_C + X_{Pos})) \frac{b_C}{L_C} & 0 \leq a_C \leq b_C \\
 M_C(a_C) &= P_C (a_C + X_{Pos}) \frac{L_C - b_C}{L_C} & b_C \leq a_C \leq L_C
 \end{aligned} \tag{5.2}$$

$M$	Rotational moment
$P_i$	Point load
$L_i$	Length of section
$a_i$	Distance to point load
$b_i$	Distance to point investigated by influence line

$P_i$  is the load from the tires and is defined respectively for Along-system and Cross-system as shown in equations (5.3) and (5.4).

$$P_A = P_C \frac{(a_C + X_{Pos})}{L_C} \tag{5.3}$$

$$P_C = (Q + X_{Load}) X_{Dyn} \tag{5.4}$$

Where  $Q$  is the tire force of a single tire on the lorry, which varies depending on axle and lorry type as shown in table 5.2. As seen in eq. (5.3), the load effect in Along-system is dependent on position of the lorry, as it will change the corresponding reaction force from the lorry.

As composites behaves linearly elastically with no yielding, superposition is valid up until failure. The load effect from both tires are superimposed to give the total load effect. Furthermore the reactions from each tire force in the Cross-system are superimposed to give the total load effect at a point in the Along-system.

When the loads are determined, the stresses can be obtained as shown in eq. (5.5).

$$\begin{aligned}
 S_a &= \frac{M_a}{z} X_{model} \\
 S_m &= \frac{M_m}{z} X_{model}
 \end{aligned} \tag{5.5}$$

$z$	Design parameter
$M_a$	Amplitude rotational moment
$M_m$	Mean rotational moment

$M_a$  and  $M_m$  are obtained by performing a Rainflow count on the time series generated by lorry crossings.

Where  $z$  is the design parameter representing the first moment of area. Thus by changing  $z$  the stresses changes. As defined in chapter 4,  $X_{model}$  is applied to each lifetime and not the lorries, and therefore will not be taken into consideration in this chapter. As the uncertainty and the design parameter are applied to both the amplitude and mean stress, it will not change the  $R$ -ratio of the load cycle.

By using the influence lines shown in equations (5.1) and (5.2), time series of lorry crossings can be generated. In figures 5.3 and 5.4, the "Long distance" traffic distribution presented in table 5.2 is simulated using the influence lines for both Along-system and Cross-system. 20 lorries are simulated as this is what is needed in order to represent the traffic distribution. The time series presented in figures 5.3 and 5.4 are shown only with extreme values as only these are needed for Rainflow counting in order to determine cyclic amplitude stresses and cyclic mean stresses. Furthermore the times series shown in figures 5.3 and 5.4 are generated without any stochastic uncertainties shown in equations (5.1) and (5.2). The static load from the bridge determined in section 3.3 is applied.

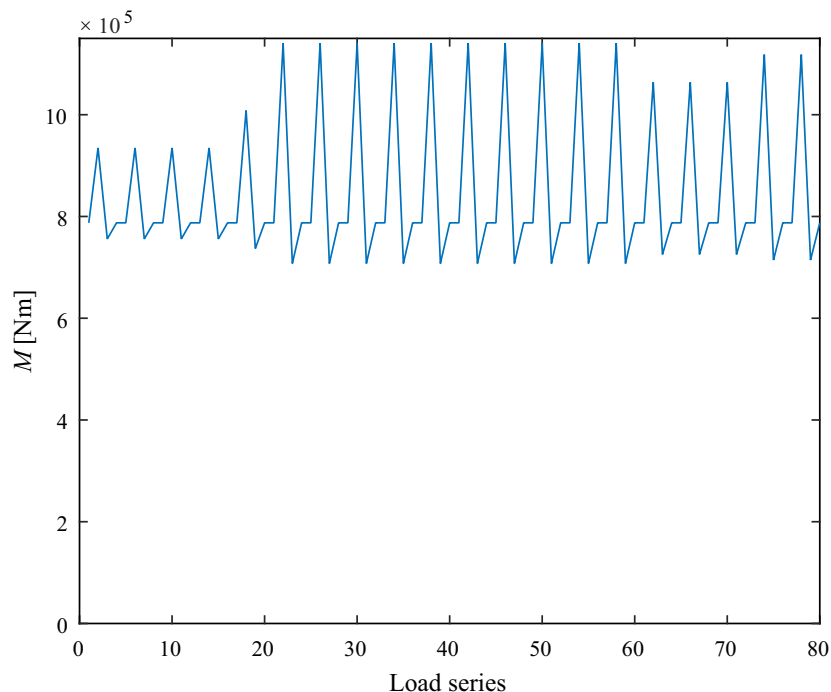


**Figure 5.3.** Traffic time series of load effect at  $b_A = 0.4L_A$  for Along-system, 20 lorry crossings are shown.

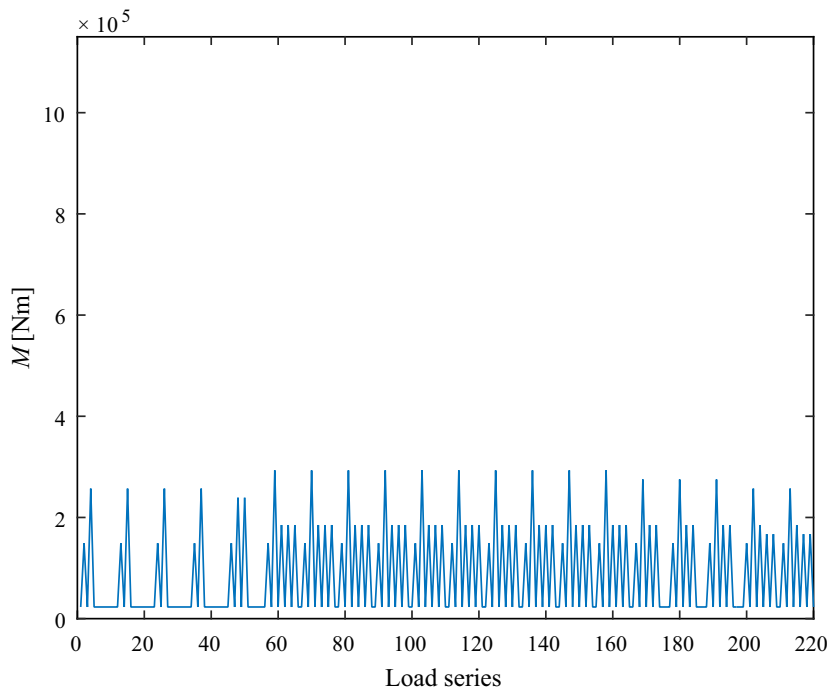


**Figure 5.4.** Traffic time series of load effect at  $b_C = 0.4 L_C$  for Cross-system, 20 lorry crossings are shown.

As seen in figures 5.3 and 5.4, Lorry 3 contributes with the largest load ranges, and therefore contributes with most damage. Thus the "Long distance" traffic distribution is used henceforth as this distribution has the highest percentage of Lorry 3. Additionally, it can be seen that the Along-system is subject to larger mean loads than Cross-system.

After the time series has been generated, Rainflow Counting is applied to determine cyclic amplitude stresses and cyclic mean stresses. In figures 5.5 and 5.6 for Along-system and figures 5.7 and 5.8 for Cross-system, the results from a Rainflow count of a time series with 500 000 lorry crossings with uncertainties (related to the load) applied are shown.

As concluded from section 2.1, appropriate stress levels are important. Therefore the design parameter  $z$  determined in Appendix C for fatigue limit state where "Long distance" traffic distribution is used in traffic category 2. Traffic is simulated for 100 years according to DS/EN 1993-2 DK NA for traffic bridges. The design parameter yielding a damage of 1 is the design parameter used for this analysis.

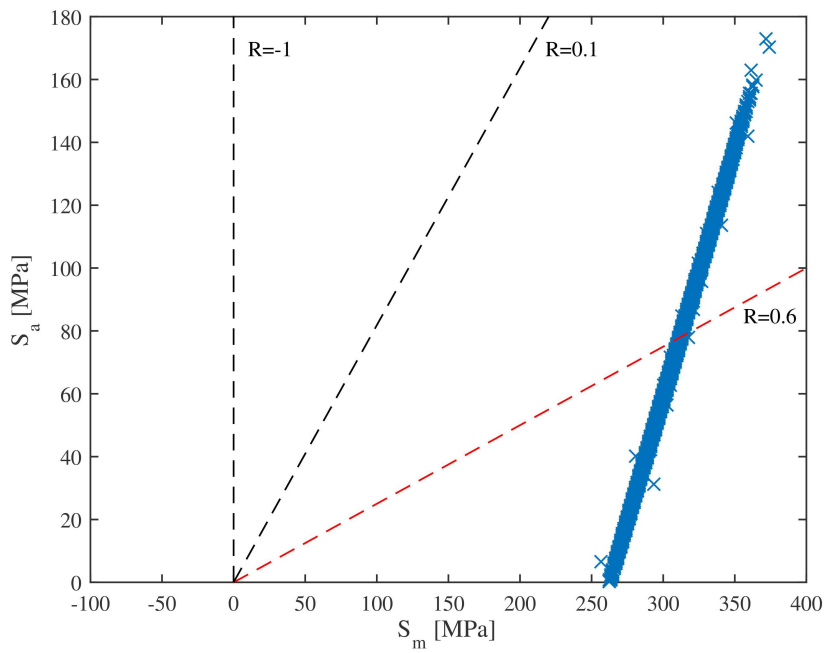


Figure 5.5. Stress cycles from 500000 lorry crossings at  $b_A = 0.4L_A$  in Along-system.

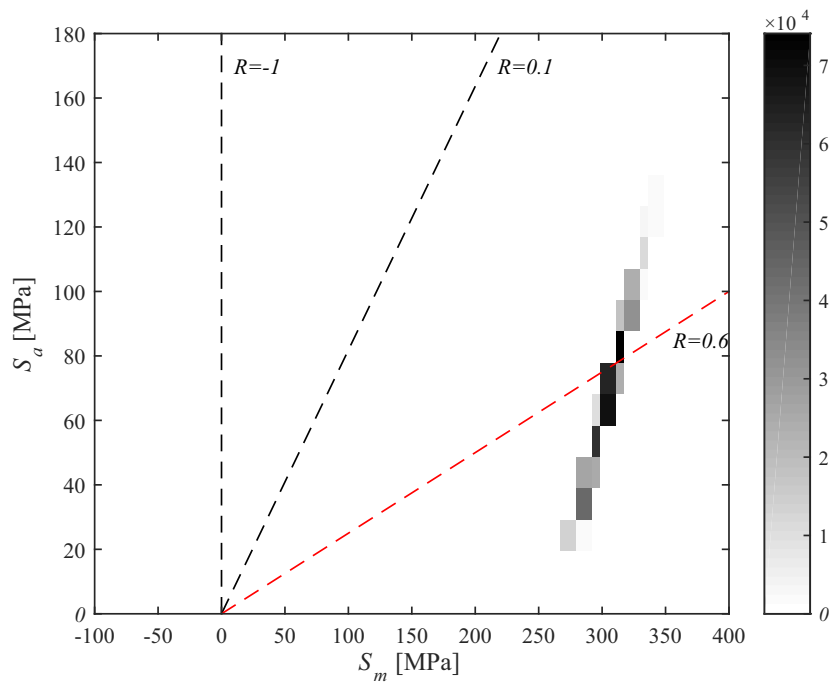


Figure 5.6. Stress cycles from 500000 lorry crossings at  $b_A = 0.4L_A$  in Along-system discretized with a step size of 10 MPa.

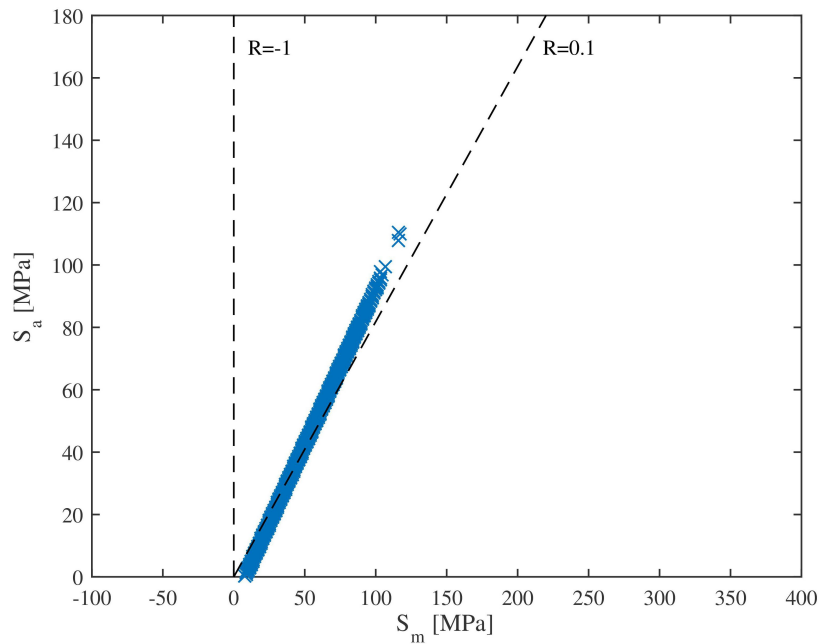


Figure 5.7. Stress cycles from 500 000 lorry crossings at  $b_C = 0.4 L_C$  in Cross-system.

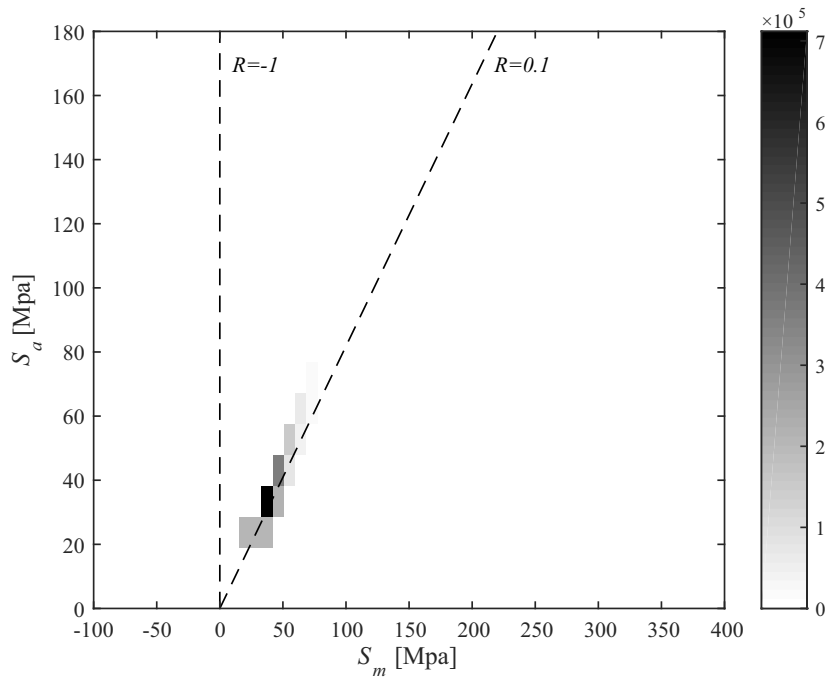


Figure 5.8. Stress cycles from 500 000 lorry crossings at  $b_C = 0.4 L_C$  in Cross-system discretized with a step size of 10 MPa.

It is important to note that the design parameter from Appendix C for fatigue limit state is for Along-system, but is also applied here to the Cross-system. Figures 5.6 and 5.8 shows the results of the Rainflow counting in a Markov matrix with step size of 10 MPa. By discretizing the load cycles the computational

time is reduced as well as the precision of the damage estimation. In figures 5.5 through 5.8 that the static load is applied which shift the load cycles to the right in the constant life diagram, but the shift is not significant in the Cross-system due to low static loads. The load cycles are mainly in the tension part of the constant life diagram. Therefore only  $S-N$  curve with  $R$ -ratios in the tension part of the constant life diagram is of interest when performing fatigue tests.

In figure 5.6, it can be seen that the  $R$ -ratios -1 and 0.1 are not the optimal  $R$ -ratios to perform fatigue tests for, with the considered load spectrum in the Along-system. A more precise estimate of damage would be achieved by performing fatigue tests at  $R = 0.6$ . For the load spectrum in the Cross-system seen in figure 5.8,  $R = 0.1$  seems appropriate.

Additionally, it can be seen that the stresses are of reasonable size.

## 5.1 Critical Fatigue Points

In this section, critical fatigue points in the Along and Cross-system are studied as performing reliability analysis on all points along each system would be impractical and time consuming. Therefore it is typical to design structures at critical points and apply this design to the rest of the structure. Therefore, it is important that the partial safety factors are calibrated to the load spectrum in the most critical point of the structure. This ensures that the partial safety factors are representative of the load spectrum the structure would be designed for. Typically, these critical fatigue points are details, but in this report only fatigue points in the Along-system and Cross-system are investigated. Therefore an analysis is conducted to determine critical fatigue points for the Along-system and Cross-system. Additionally, the appearance of the load spectrum of along the Along-system and Cross-system is investigated.

For the analysis, all the constant life diagrams presented in section 2.1 are used to study if different constant life diagrams result in different fatigue points.

As concluded in section 2.1, it is important that the stresses are of appropriate size. Stress levels are adjusted by the first moment of area (the design parameter), therefore in this analysis, the first moment of area found in Appendix C is used.

### 5.1.1 Critical Fatigue Points in the Along-system

To determine the critical fatigue point in the Along-system, the maximum load range of a point load moving across the system is considered. In a situation where mean stress did not affect the fatigue life, the largest load range would generate the most damage, and because the stress amplitude is raised to the power of  $-m$  in the  $S-N$  formulation, the single largest stress amplitude could dictate the location of the critical fatigue point.

Therefore a analysis is conducted where influence lines are formulated at different points,  $b_A$ , along the Along-system. A unit load is moved across the Along-system and the maximum load range in every point of  $b_A$  is determined. The calculation of the maximum load range in a point  $b_A$  is shown in eq. (5.6).

$$\Delta M(b_A) = \max(M_A(a_A, b_A) - \min(M_A(a_A, b_A))) \quad 0 \leq a_A \leq 2L \quad (5.6)$$

Where

$\Delta M$	Rotational moment range
$b_A$	Distance to where influence line is defined. $b_A$ is defined in figure 5.1
$a_A$	Distance to the load. Defined in figure 3.2
$M_A$	Rotational moment in Along-system

In figure 5.9, the maximum load range for influence lines is shown.

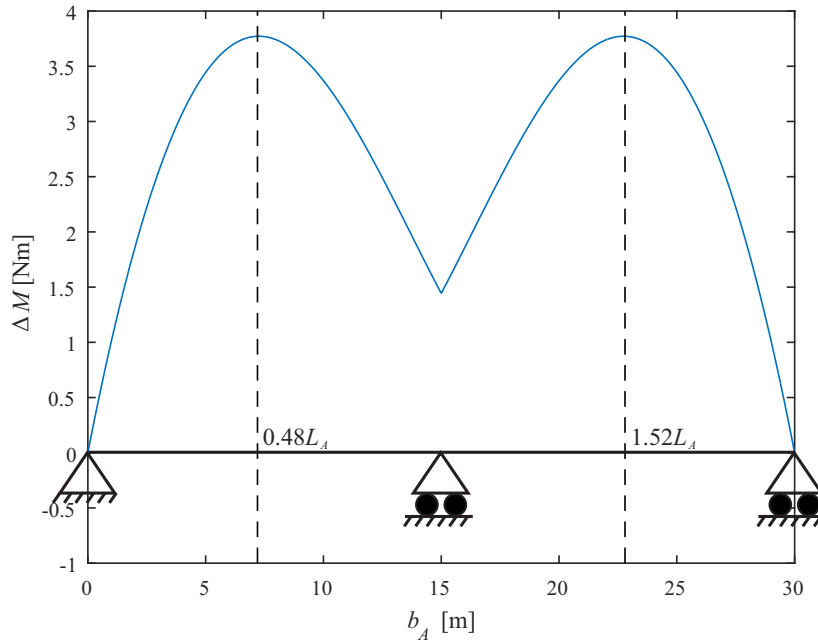


**Figure 5.9.** Load range for influence lines for a unit point load moving across the Along-system.

It can be seen from figure 5.9, that the largest load range is experienced in  $0.48L_A$  and due to symmetry in  $1.52L_A$ . As previously mentioned composites materials are sensitive to mean load effects. Therefore the effect induced by the dead load of the bridge introduces complexity. The load effect from the dead load is shown in figure 5.10.

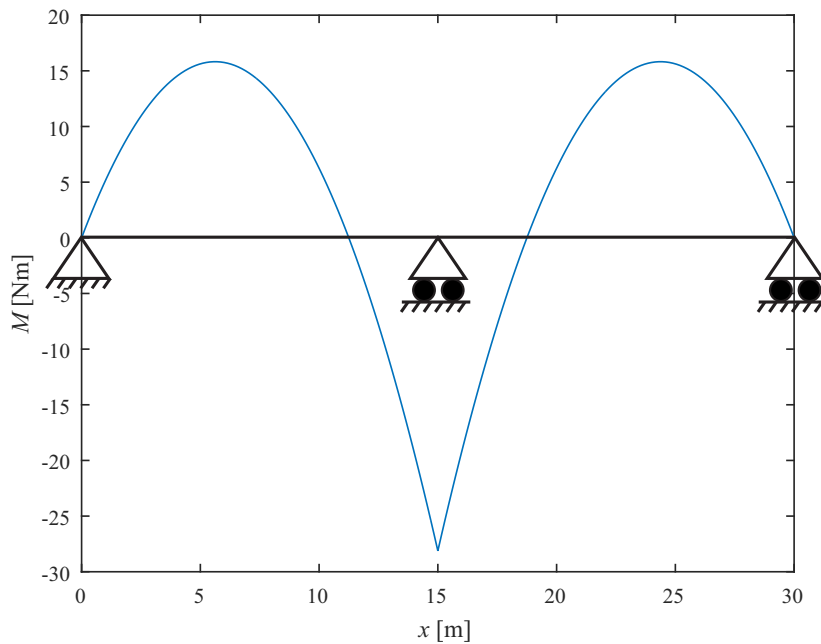


**Figure 5.10.** Rotational moment,  $M$ , of a unit line load. Positive  $M$  is tension in the bottom of the beam.  $x$  defines the position along the Along-system.

$x$  defines the position along the Along-system in figure 5.10. It can be seen in figures 5.9 and 5.10, that the extreme values are not located at the same point. Therefore, figures 5.9 and 5.10 do not provide sufficient information about the location of the critical fatigue point. Therefore the fatigue damage and the load spectrum appearance along the Along-system are determined as the mean effect changes the load cycles position in the constant life diagram and influence the fatigue life.

In figure 5.11 and figures 5.12 through 5.15, shows how the load spectrum changes along to static system. Figure 5.11 illustrates where the load spectrum is investigated and which reinforcement bars are investigated. Only the tension parts of the reinforcement bars are of interest based on the rotational moment distribution of the mean load in figure 5.10. Figures 5.12 through 5.15 are shown with piecewise linear constant life diagrams and a load spectrum corresponding to 500 000 lorry crossings of the Along-system with uncertainties included. The  $R$ -ratio that match the majority stress cycles is also shown in the constant life diagrams. This  $R$ -ratio is the recommended  $R$ -ratio to perform fatigue test for, if no fatigue data is available.

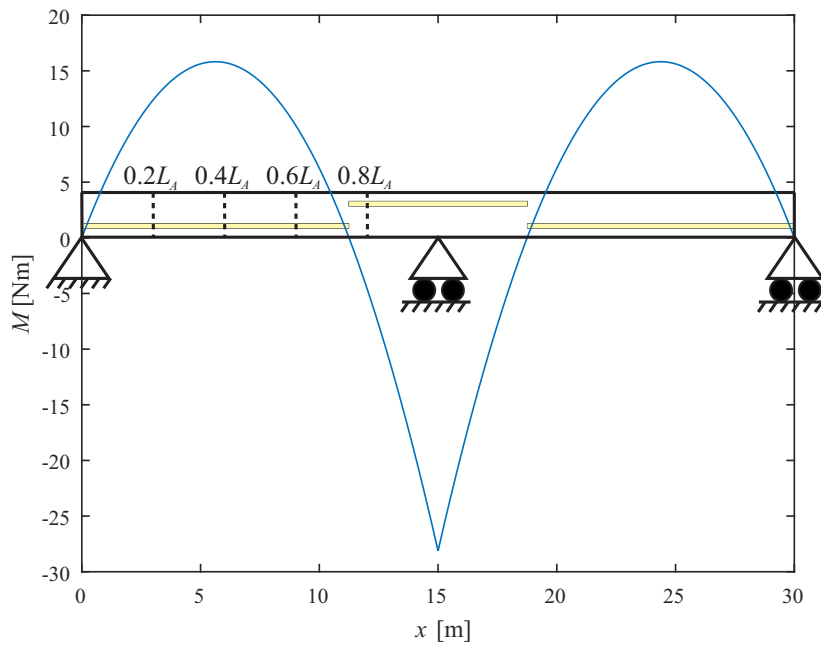


Figure 5.11. Cross-sections where the load spectrum is investigated.

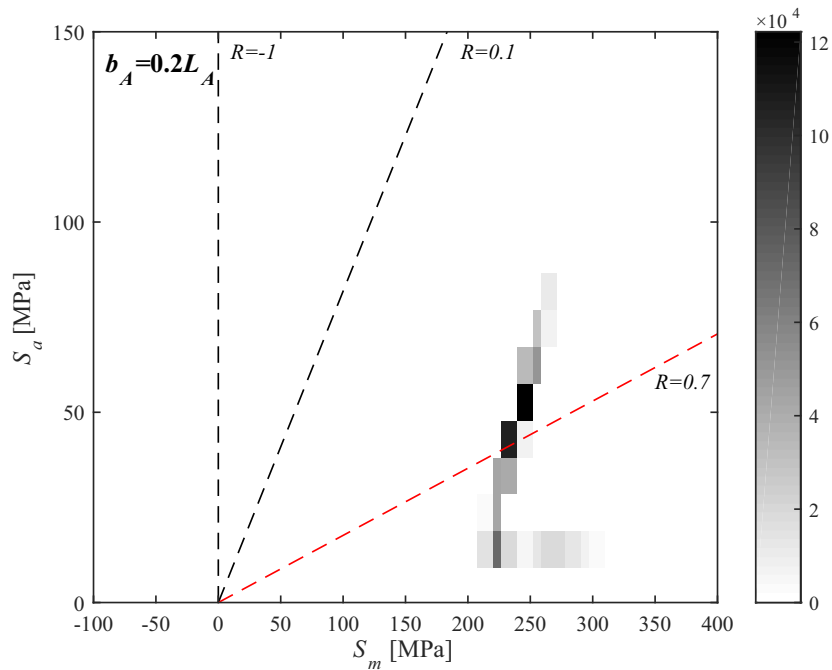


Figure 5.12. Piecewise linear constant life diagram with load spectrum at  $b_A = 0.2L_A$  in Along-system. The colorbar indicates number of cycles,  $n$ .

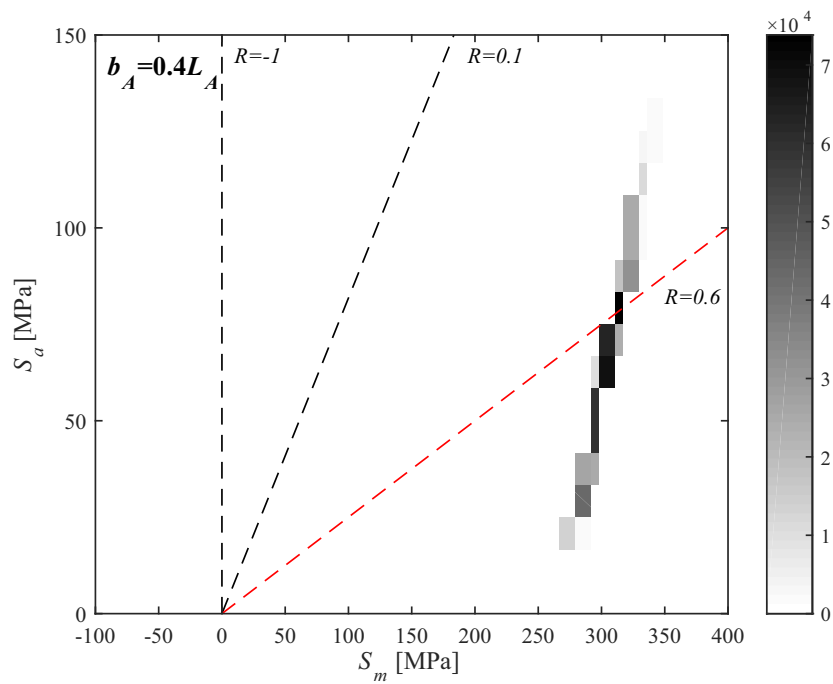


Figure 5.13. Piecewise linear constant life diagram with load spectrum at  $b_A = 0.4L_A$  in Along-system. The colorbar indicates number of cycles,  $n$ .

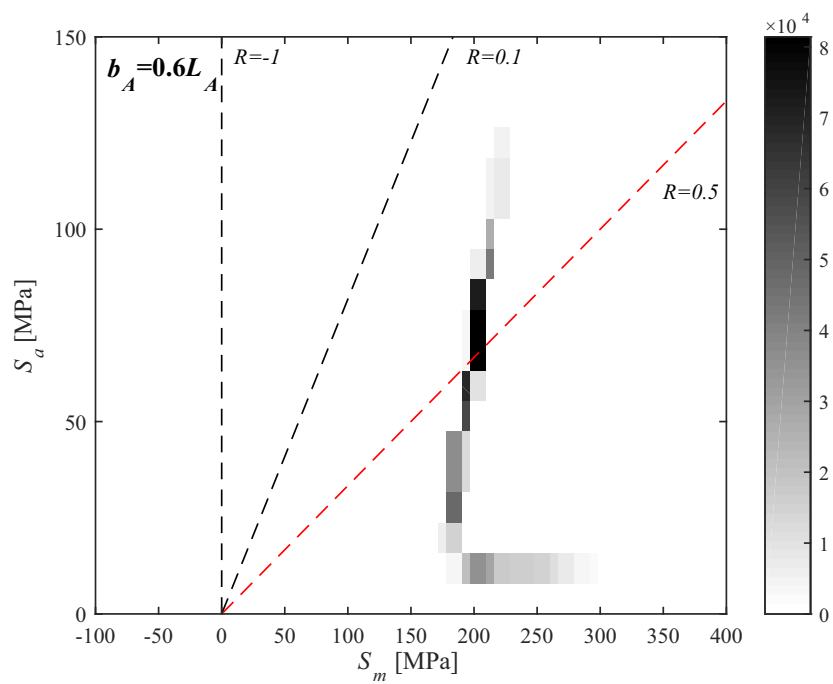
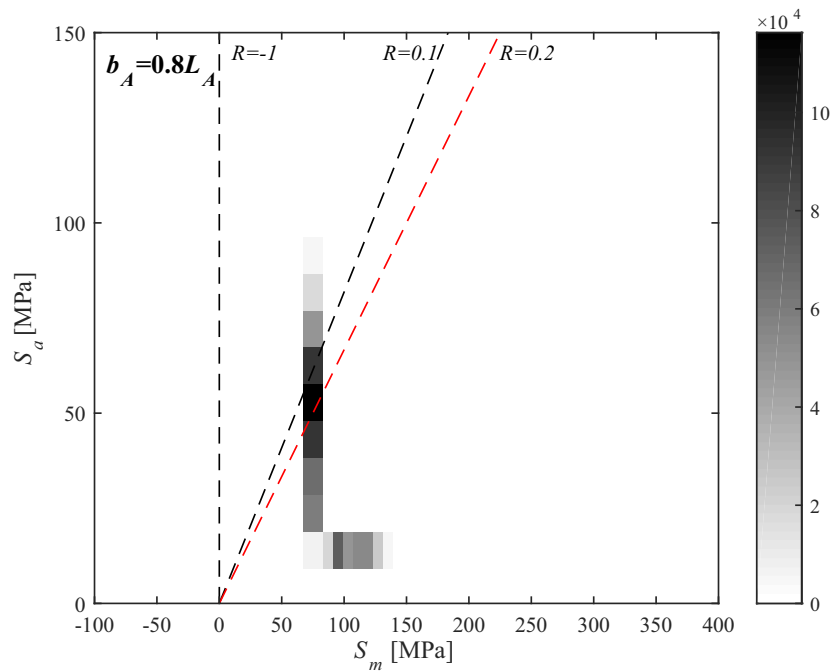


Figure 5.14. Piecewise linear constant life diagram with load spectrum at  $b_A = 0.6L_A$  in Along-system. The colorbar indicates number of cycles,  $n$ .



**Figure 5.15.** Piecewise linear constant life diagram with load spectrum at  $b_A = 0.8L_A$  in Along-system. The colorbar indicates number of cycles,  $n$ .

From figures 5.12 through 5.15, it can be seen that stress cycles changes slightly. The  $R$ -ratio that match the majority of the stress cycles are almost constant along the Along-system except close to the center of the Along-system where stress cycles have an  $R$ -ratio of 0.3.

As previously stated, the fatigue damage along the Along-system is determined in order to investigate the critical fatigue point. 20 lorry crossings are simulated to represent the lorry distribution presented earlier in chapter 5. The stochastic uncertainties shown in equations (5.1) and (5.2) are not applied in this analysis as it is assumed these will not change the location of the critical fatigue point as it will not change the shape of the load spectrum. Furthermore traffic from the opposite lane is neglected as this will not change the critical fatigue point. The fatigue damage along the Along-system using the four constant life diagrams presented in section 2.1 to estimate the damage are shown in figures 5.16, 5.18, 5.20 and 5.22. Only half of the Along-system is shown due to symmetry.

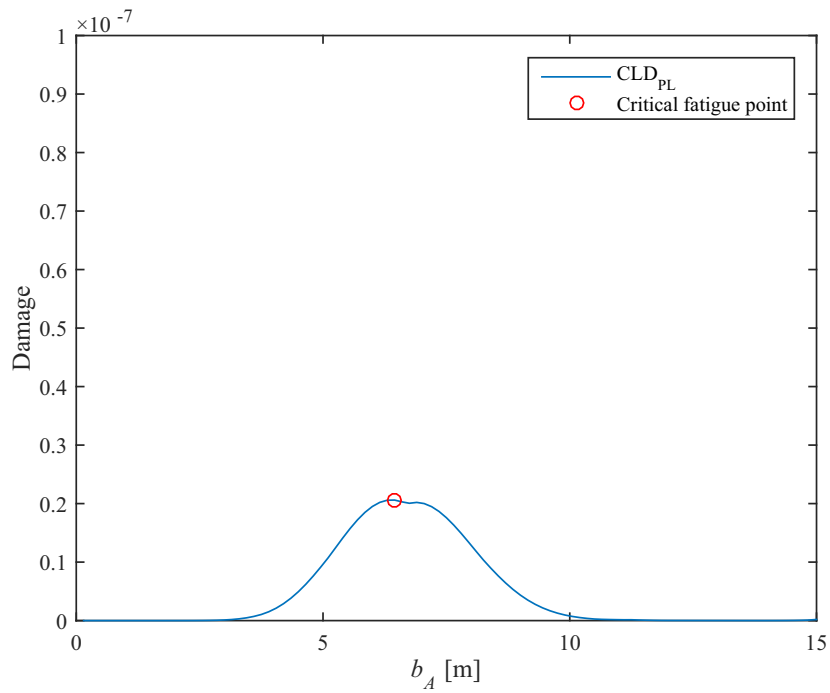


Figure 5.16. Fatigue damage along the Along-system using  $CLD_{PL}$  without stochastic uncertainties. Red circle indicate largest fatigue damage.

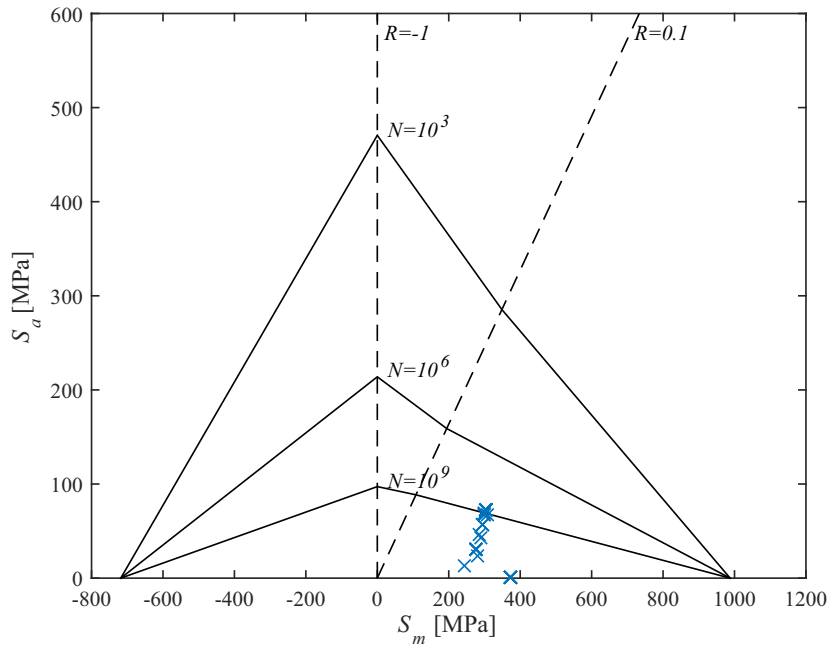


Figure 5.17. Stress cycles where the fatigue damage is maximum ( $b_A = 0.4L_A$ ) using  $CLD_{PL}$  without stochastic uncertainties.

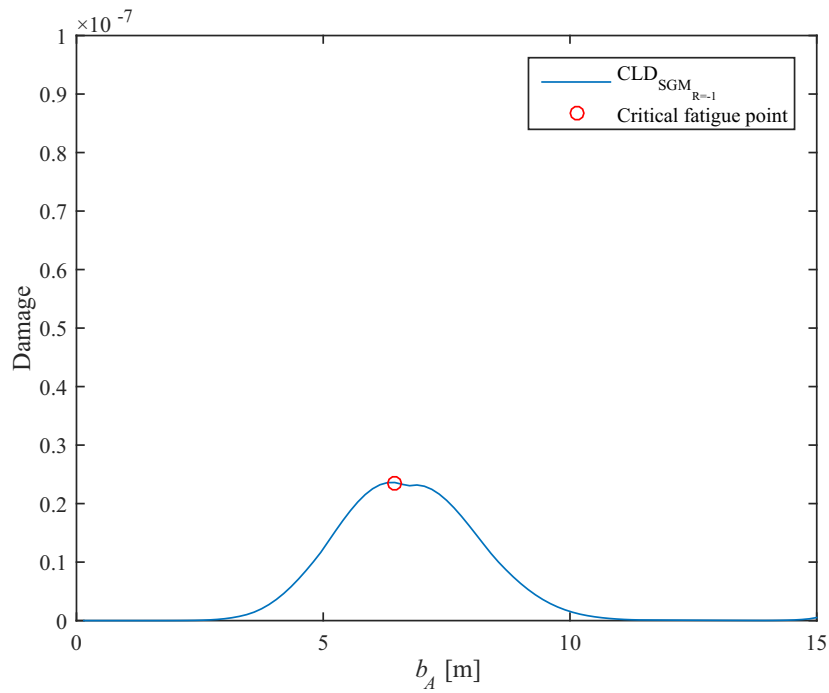


Figure 5.18. Fatigue damage along the Along-system using  $CLD_{SGM_{R=-1}}$  without stochastic uncertainties. Red circle indicate largest fatigue damage.

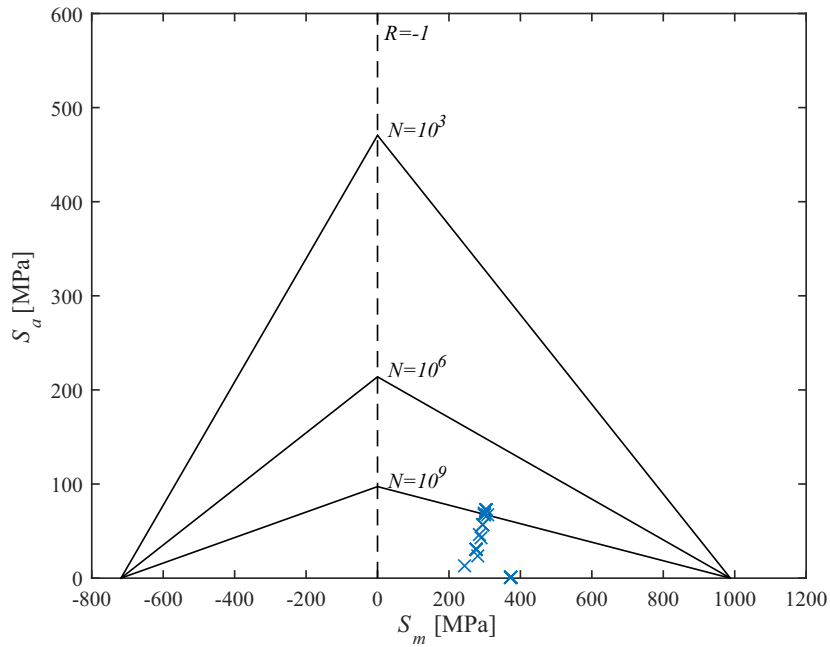


Figure 5.19. Stress cycles where the fatigue damage is maximum ( $b_A = 0.4L_A$ ) using  $CLD_{SGM_{R=-1}}$  without stochastic uncertainties.

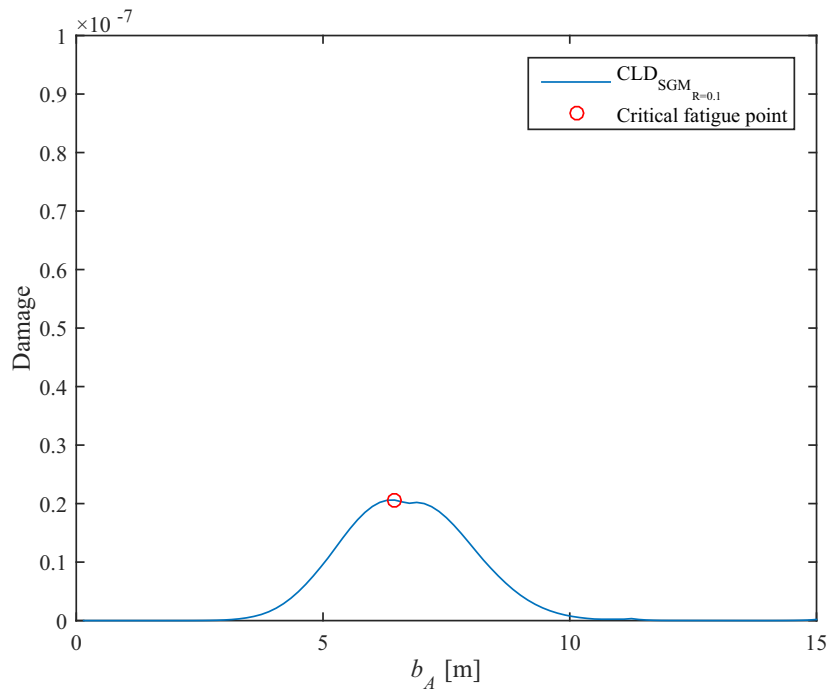


Figure 5.20. Fatigue damage along the Along-system using  $CLD_{SGM_{R=0.1}}$  without stochastic uncertainties. Red circle indicate largest fatigue damage.

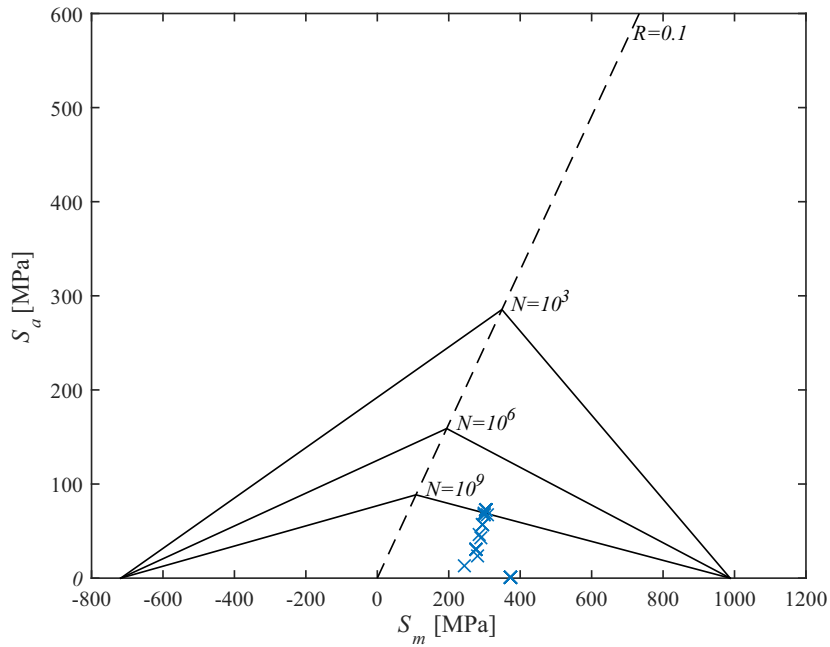
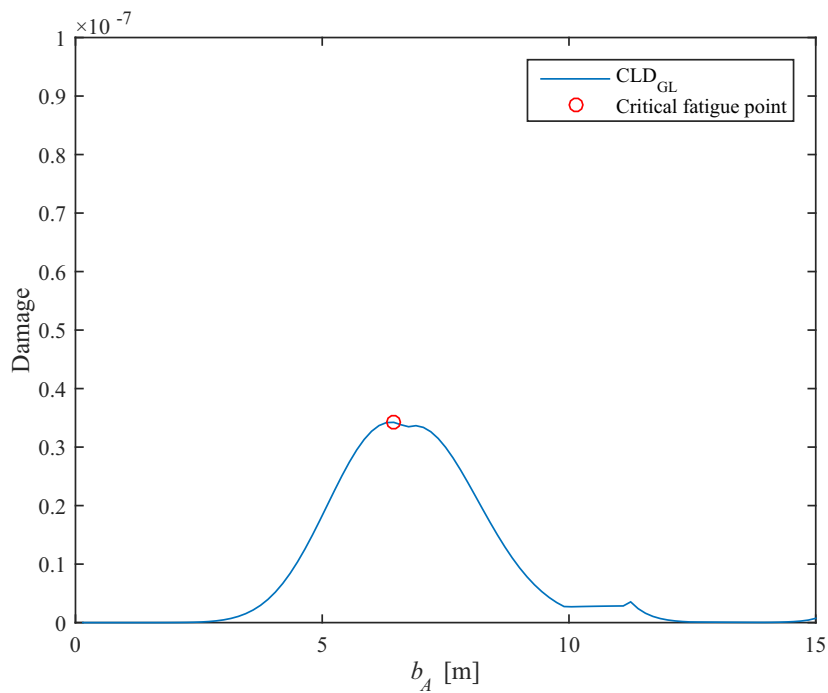
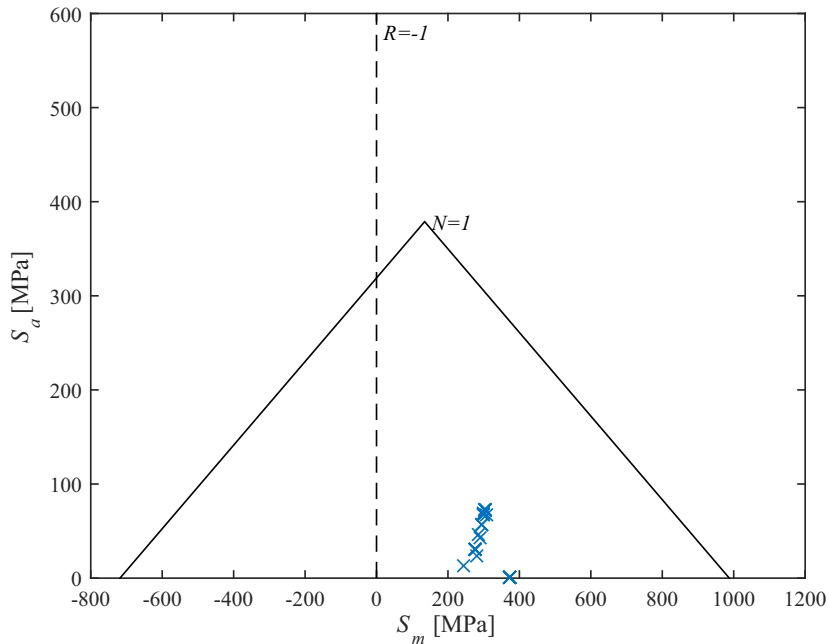


Figure 5.21. Stress cycles where the fatigue damage is maximum ( $b_A = 0.4L_A$ ) using  $CLD_{SGM_{R=0.1}}$  without stochastic uncertainties.



**Figure 5.22.** Fatigue damage along the Along-system using  $CLD_{GL}$  without stochastic uncertainties. Red circle indicate largest fatigue damage.



**Figure 5.23.** Stress cycles where the fatigue damage is maximum ( $b_A = 0.4L_A$ ) using  $CLD_{GL}$  without stochastic uncertainties.

From figures 5.16, 5.18, 5.20 and 5.22 and table 5.4, it can be seen that all constant life diagrams tested estimate approximately  $0.4L_A$  (6 m) as the critical fatigue point. The fatigue point changes slightly with adjustment of  $z$ . It is assumed

that this point,  $0.4L_A$ , is representative for similar load spectra and henceforth used to calibrate partial safety factors.

**Table 5.4.** Comparison of critical fatigue points using different constant life diagrams in the Along-system.

	Damage in Critical point	Critical point [m]
$CLD_{PL}$	$2.06 \cdot 10^{-18}$	$0.4L_A$
$CLD_{SGM_{R=-1}}$	$2.36 \cdot 10^{-18}$	$0.4L_A$
$CLD_{SGM_{R=0.1}}$	$2.06 \cdot 10^{-18}$	$0.4L_A$
$CLD_{GL}$	$3.42 \cdot 10^{-18}$	$0.4L_A$

Compared to figure 5.9, the point where the largest load range is observed is where the critical fatigue point is located.

### 5.1.2 Critical Fatigue Points in the Cross-system

In the Cross-system, the lorries are crossing the Cross-system perpendicular with only one axle loading the Cross-system a time. Therefore the Cross-system is either loaded or not (when investigating only one bridge deck). Based on this and conducting the same investigation as for the Along-system, the critical fatigue point in Cross-system is expected to be directly under the tire closest to the center of the bridge as it is where the load range is largest as shown in figure 5.24. Figure 5.24 assumed the transverse position of all lorries are constant.

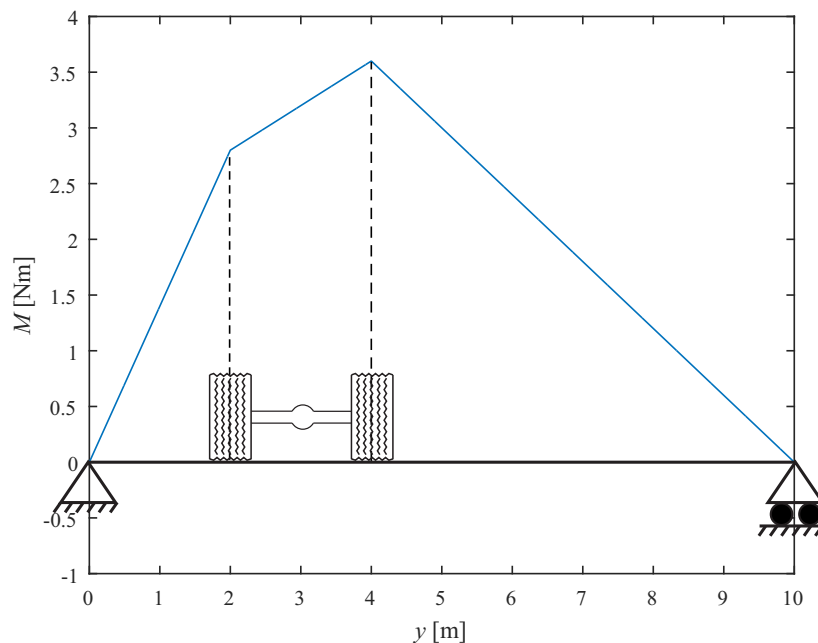


**Figure 5.24.** Rotational moment,  $M$ , as a function of  $y$  where Cross-system is loaded with two unit loads with positions corresponding to that of a lorry axle.

Although the dead load of the bridge deck is minor in comparison to the line load the along-system experiences, its effect can only be included through calculation of fatigue damage. The rotational moment,  $M$ , exerted by the dead load is shown in figure 5.25.

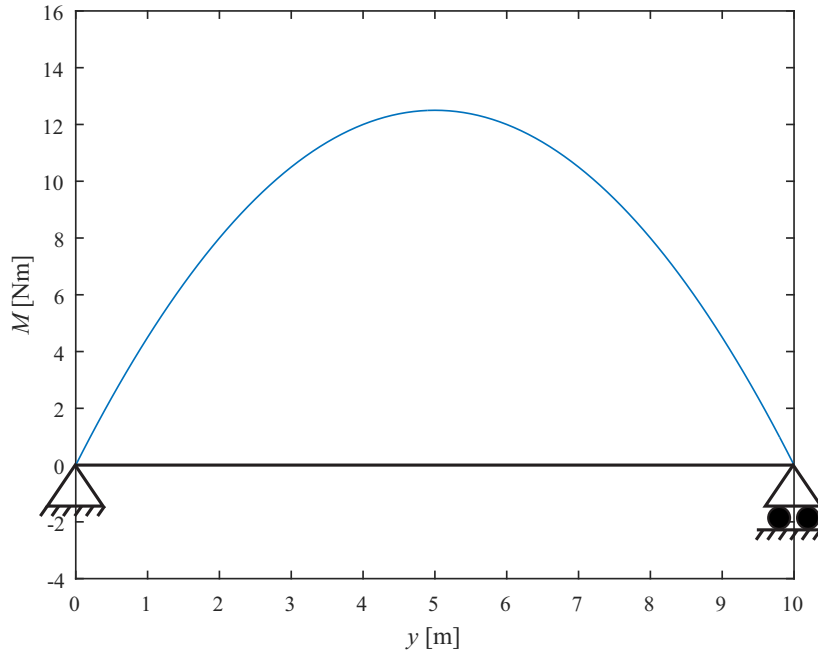


Figure 5.25. Rotational moment,  $M$ , of the static load in the Cross-system.

Along with the introduction of mean load effect, the stochastic uncertainty,  $X_{Pos}$ , is introduced. This will vary the position of the lorries center when crossing the bridge. In figure 5.26, it is shown different points in the Cross-system where the load spectrum is investigated. In figures 5.27 through 5.30, the load spectrum is shown at different points in the Cross-system with the static load applied.

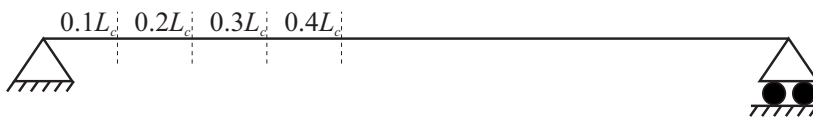


Figure 5.26. Cross-sections where the load spectrum is investigated in the Cross-system.

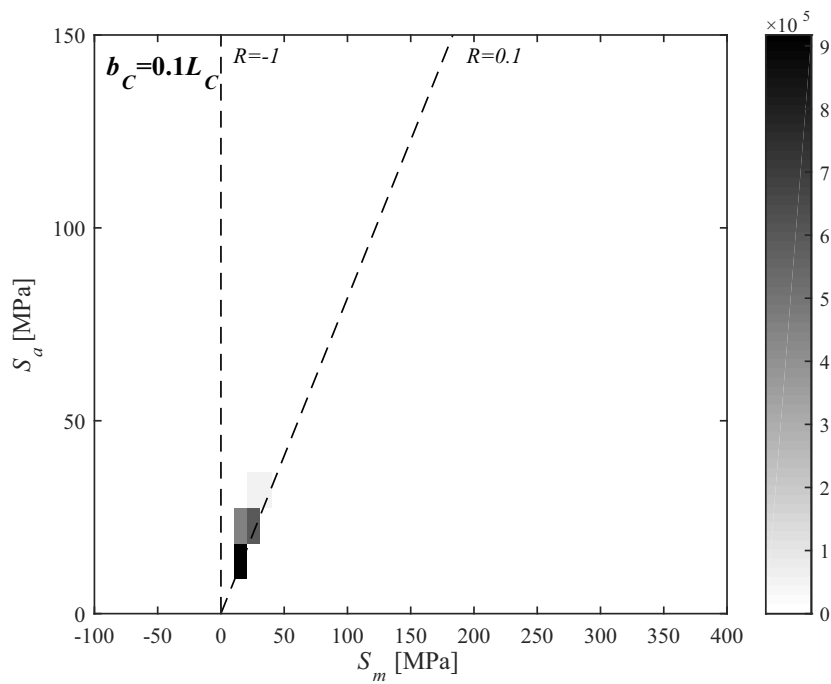


Figure 5.27. Piecewise linear constant life diagram with load spectrum at  $b_C = 0.1L_C$  in Cross-system. The colorbar indicates number of stress cycles,  $n$ .

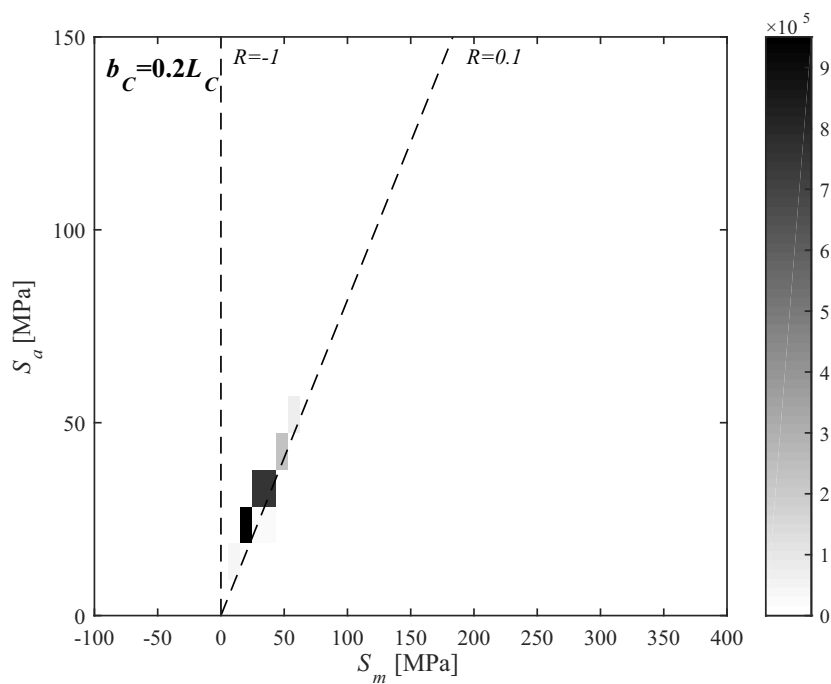
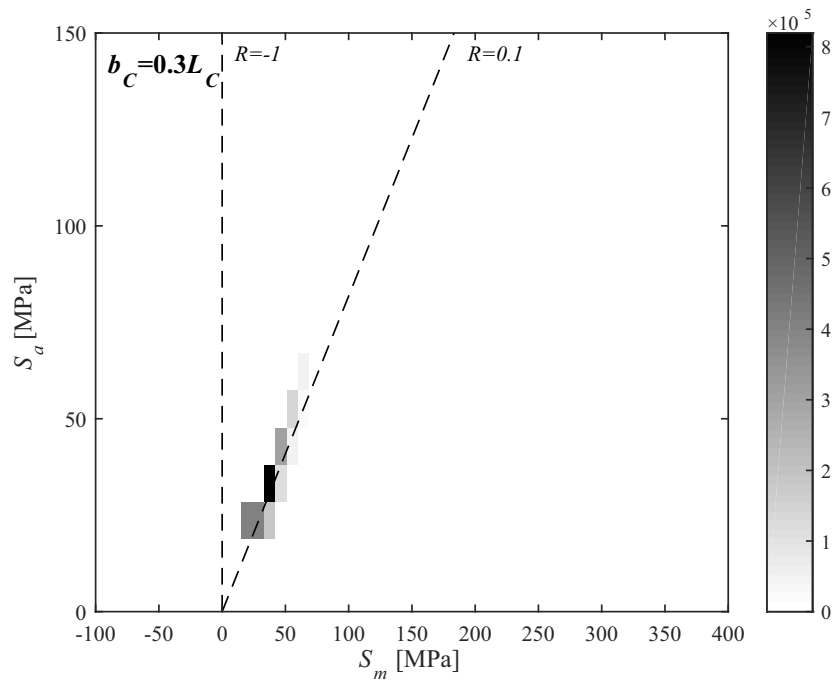
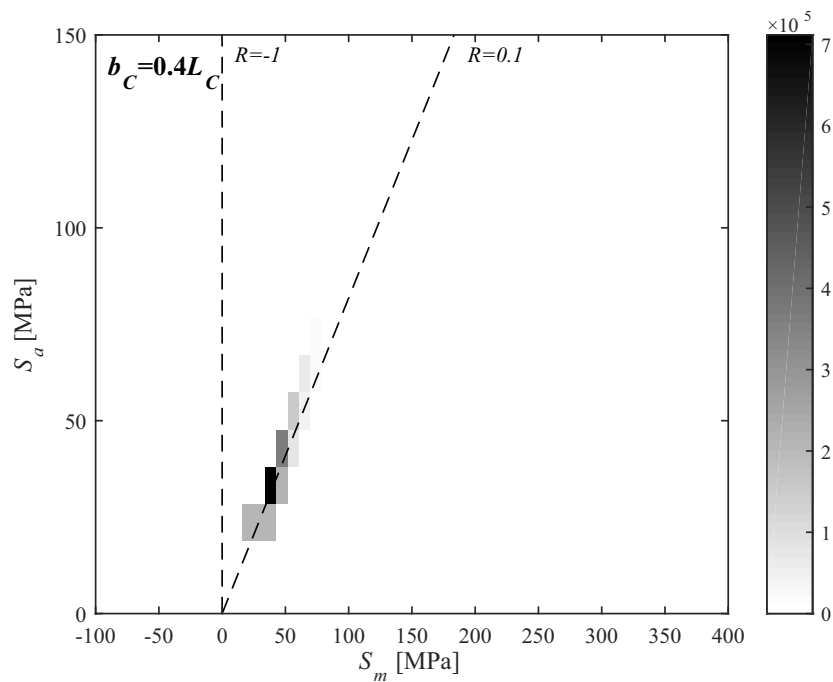


Figure 5.28. Piecewise linear constant life diagram with load spectrum at  $b_C = 0.2L_C$  in Cross-system. The colorbar indicates number of stress cycles,  $n$ .



**Figure 5.29.** Piecewise linear constant life diagram with load spectrum at  $b_C = 0.3L_C$  in Cross-system. The colorbar indicates number of stress cycles,  $n$ .



**Figure 5.30.** Piecewise linear constant life diagram with load spectrum at  $b_C = 0.4L_C$  in Cross-system. The colorbar indicates number of stress cycles,  $n$ .

In figures 5.27, 5.28, 5.29 and 5.30, it is seen that the  $R$ -ratio that match the majority of the stress cycles does not along the length of the Cross-system due to

the low static load.

As the load spectrum changes along the Cross-system, the fatigue damage is estimated. The damage from 10000 lorries is simulated and shown in figure 5.31. The only stochastic uncertainty taken into consideration is  $X_{Pos}$ , as this is the only uncertainty that affects the shape of the load spectrum is  $X_{Pos}$ . 10000 realizations of lorry crossings is assumed sufficient to model a single stochastic variable.  $CLD_{PL}$  is used for damage estimation.

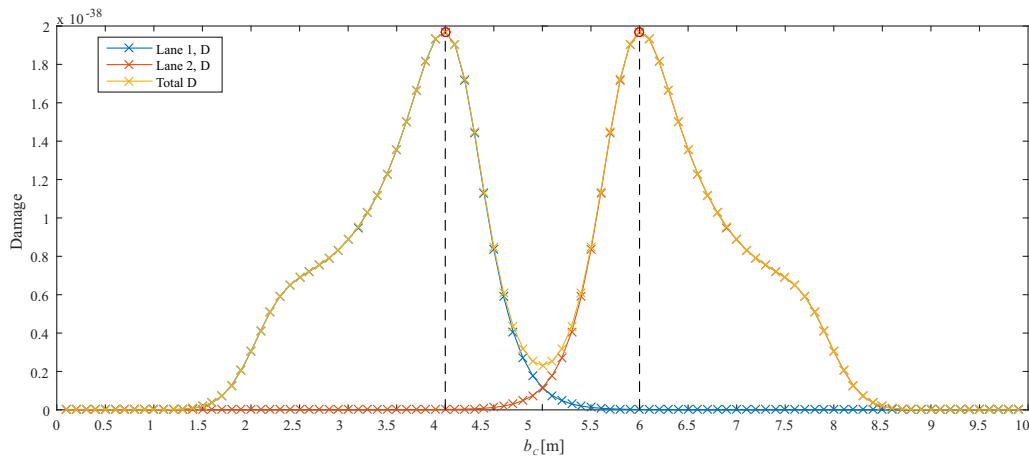


**Figure 5.31.** Damage of Cross-system after the lorry distribution crossed with the stochastic variable  $X_{Pos}$  taken into account, 10000 lorries simulated.

As seen in figure 5.31 the critical fatigue point is  $b_C = 0.4L_C$  (4 m). This point will be used for calibration of partial safety factors in the Cross-system. Lastly, it can be seen that the opposite lane traffic contribute insignificantly to the fatigue in the critical point. Therefore, in order to save computational power, ongoing traffic will not be simulated and henceforth neglected. It is however only insignificant because of the chosen load model. If the load model included multiple lorries on the bridge, this assumption may not be valid.

In table 5.5 and figures 5.32 and 5.33, a comparison of critical fatigue points using the piecewise linear constant life diagram, shifted Goodman diagrams and the Germanischer Lloyd proposed constant life diagram as presented in section 2.1 to ensure that the critical fatigue point is  $b_C = 0.4L_C$  for all constant life diagrams.

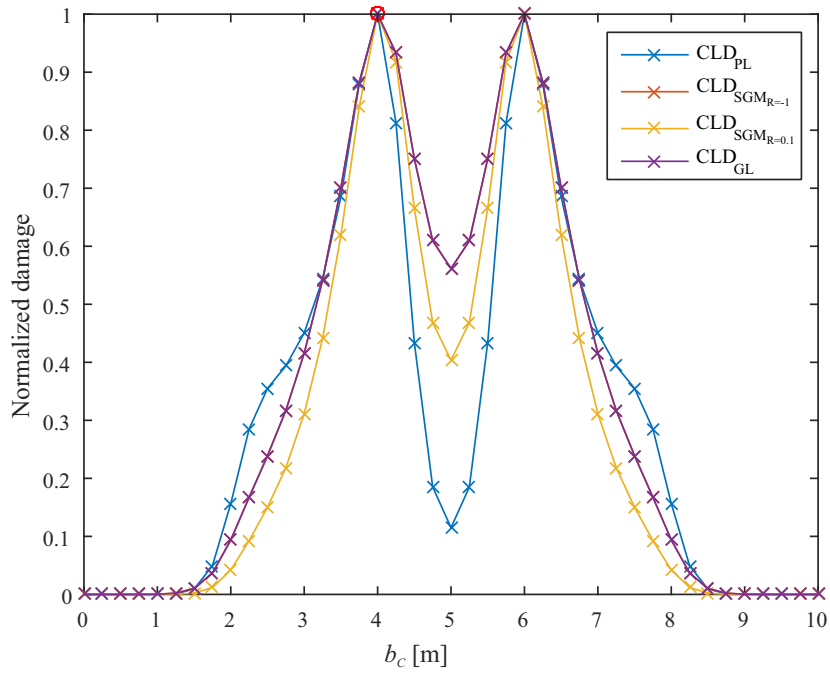


Figure 5.32. Comparison of critical fatigue points using different constant life diagrams.

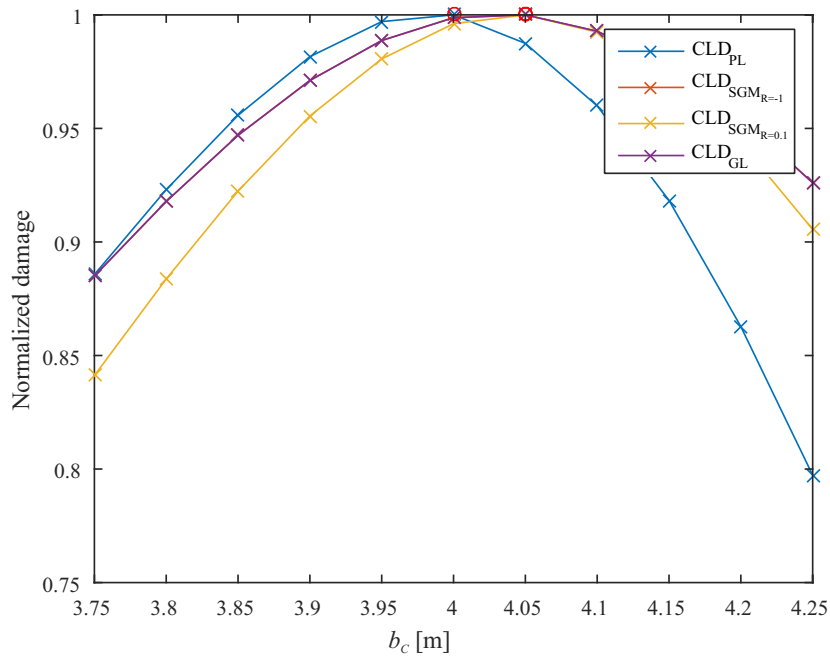


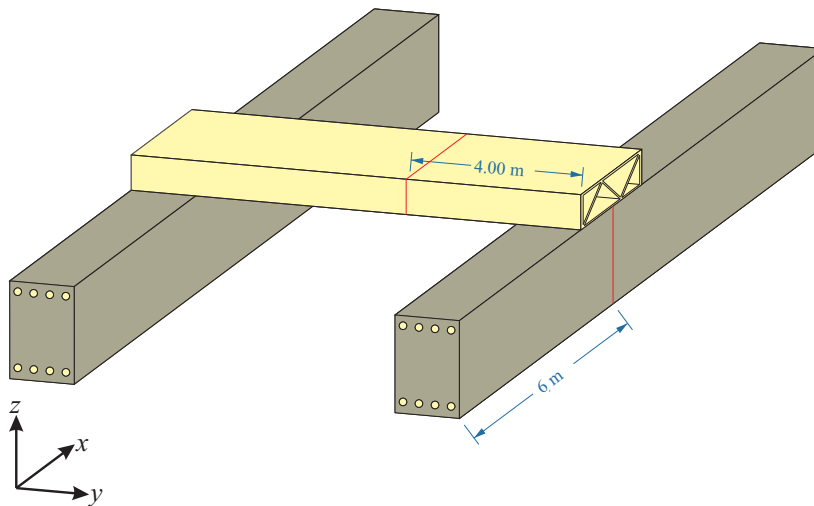
Figure 5.33. Zoom of figure 5.32.

**Table 5.5.** Comparison of critical fatigue points using different constant life diagrams.

	Damage in Critical point	Critical point [m]
$CLD_{PL}$	$2.14 \cdot 10^{-38}$	4.00
$CLD_{SGM_{R=-1}}$	$2.54 \cdot 10^{-31}$	4.05
$CLD_{SGM_{R=0.1}}$	$1.21 \cdot 10^{-39}$	4.05
$CLD_{GL}$	$1.01 \cdot 10^{-29}$	4.05

From table 5.5 and figures 5.32 and 5.33, it can be seen that the critical fatigue point is approximately the same regarding the use of different constant life diagrams.

The critical fatigue points found previously are marked on figure 5.34 for both Along-system and Cross-system and presented in table 5.6.

**Figure 5.34.** Illustration of the critical fatigue points.**Table 5.6.** Comparison of critical fatigue points using different constant life diagrams.

	Critical point
$b_A$	$0.4L_A$ (6 m)
$b_C$	$0.4L_C$ (4 m)

These are the two points that will be considered in the reliability analysis. The distance from start of each static system to the critical fatigue point will be denoted as  $b_A$  and  $b_C$  for respectively Along-system and Cross-system.

## 5.2 Estimation of Adequate Amount of Lorry Crossings

In the realization of the load signal each lorry crossing is affected by three stochastic variables, as shown in equations (5.1) and (5.2). To ensure that each of these stochastic variables has been represented properly e.i. the stochastic variables mean and standard deviation have converged, a convergence analysis is conducted. As previously mentioned traffic category 2 is used, and it is investigated in this section if  $5 \cdot 10^5$  lorry crossings is an adequate amount of lorry crossings in order to ensure the stochastic variables are represented properly.

In figures 5.35 and 5.36, the convergence analysis is illustrated. The blue crosses indicate the deviation,  $\Delta_{D_{avg}}$ , from the total average damage per lorry from all simulations,  $D_{tot,avg}$ , both defined in equations (5.7) and (5.8). 40 simulations are performed at different amounts of lorry crossings e.g. 100000 lorry crossings are simulated 40 times.

$$\Delta_{D_{avg,ij}} = \frac{D_{avg,ij}}{D_{tot,avg}} - 1 \quad (5.7)$$

$$\begin{aligned} D_{tot,avg} &= \frac{D_{tot}}{n_{tot}} & D_{avg,ij} &= \frac{D_{sim,ij}}{n_{rel,ij}} \\ n_{tot} &= \sum_{j=1}^{n_{set}} \sum_{i=1}^{n_{sim}} n_{rel,ij} & D_{tot} &= \sum_{j=1}^{n_{set}} \sum_{i=1}^{n_{sim}} D_{sim,ij} \end{aligned} \quad (5.8)$$

Where

$\Delta_{D_{avg}}$	Deviation from the total average damage per lorry from all simulations, $D_{tot,avg}$
$D_{avg,ij}$	Average damage per lorry for a simulation in a set
$D_{tot}$	Total damage from all simulations
$D_{sim,ij}$	Damage from a simulation in a set
$n_{tot}$	Total number of realizations from all simulations
$n_{rel,ij}$	Number of realizations in given simulation
$n_{sim}$	Number of simulations in a set
$n_{set}$	Number of sets

Outcomes of  $\Delta_{D_{avg}}$  are assumed to be normally distributed with an expected value of zero and a standard deviation given as.

$$\sigma_j = \sqrt{\frac{1}{n_{sim}} \sum_{i=1}^{n_{sim}} (\Delta_{D_{avg,ij}})^2}$$

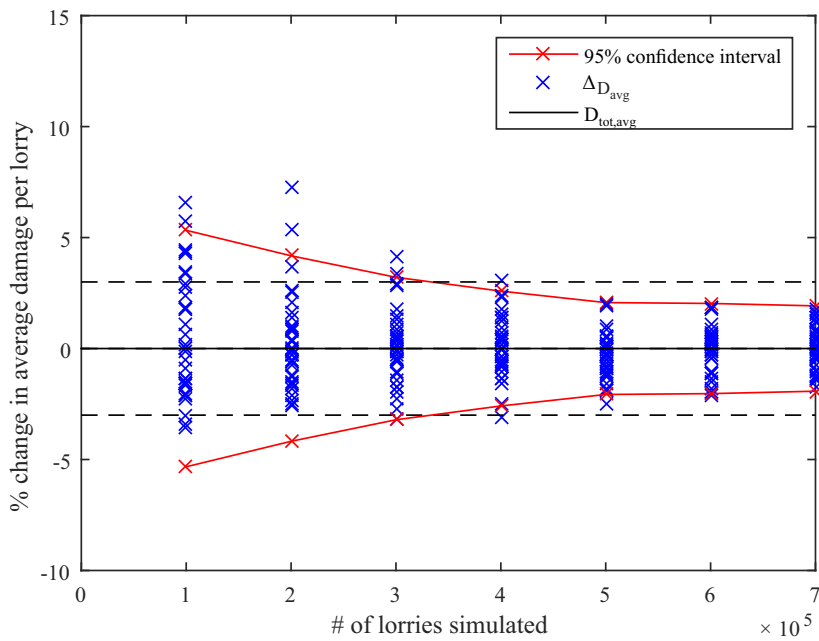


Figure 5.35. Convergence analysis of amount of lorries needed for Along-system.

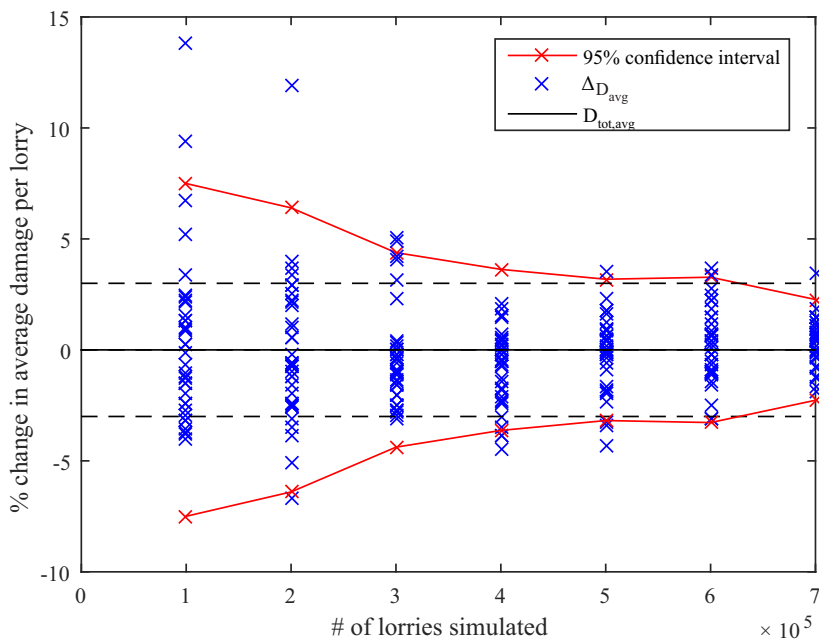


Figure 5.36. Convergence analysis of amount of lorries needed for Cross-system.

In figures 5.35 and 5.36, the dashed line indicate 3 % variation from the total average damage per lorry from all simulations,  $D_{tot,avg}$ . A criteria for a suitable amount of lorry crossings could be that the 95 % confidence interval is within this 3 % change of total average damage per lorry from all simulations,  $D_{tot,avg}$ . The Along-system is already within this limit at  $4 \cdot 10^5$  lorry crossings per year, however the Cross-system would need  $7 \cdot 10^5$  lorry crossings per year to comply with the criteria. A reasonable compromise is made to keep to the computa-

tional time down for the reliability analysis. At  $5 \cdot 10^5$  lorry crossings per year, the Along-system is within this limit and the Cross-system is close. This amount of lorry crossing will be used for the reliability analysis and derivation of partial safety factors. Furthermore  $5 \cdot 10^5$  lorry crossings per year corresponds traffic category 2 in table 5.1.

As the largest load cycles typically contribute with the largest amount of damage, figures 5.35 and 5.36 are strongly dependent on the largest load cycles. Therefore it is an extreme value problem, dependent on few large realizations in the time series. This can be seen by evaluating the damage contribution from the most critical 5 % of the cycles. If  $5 \cdot 10^5$  lorry crossings are simulated and the total damage of the lorry crossings is estimated using the piecewise linear constant life diagram, the 5 % largest load cycles contribute with 94% of the total damage.

### 5.3 Precision of Discretization

In the following section, the effect of discretizing the data is studied. The discretization changes the estimated fatigue, but the advantage is reduction in computational time. The piecewise linear constant life diagram is used for damage calculation and 500000 lorry crossings are simulated in this analysis corresponding to traffic category 2. The design parameter used is determined in Appendix C.

After a time series have been generated, Rainflow counting is applied, with the added feature of recording the mean value of the registered cycles. The result of the Rainflow counting is plotted along with the  $R$ -ratios with  $S$ - $N$  curves below in figures 5.37 and 5.38 where the mean effect of the static loads are taken into account.  $S_a$  is cyclic load amplitude and  $S_m$  is cyclic mean load.

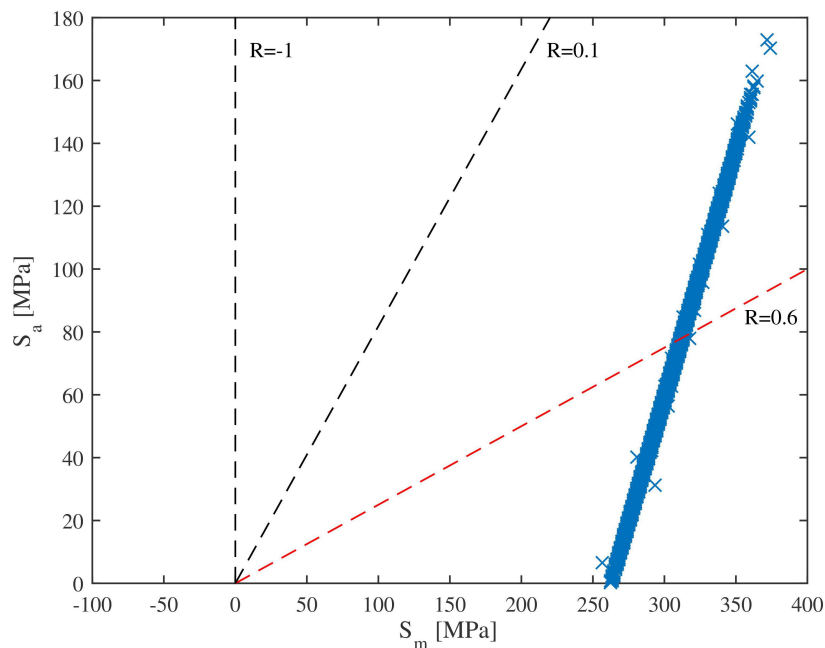


Figure 5.37. Stress cycles from one year of traffic at  $b_A = 0.4L_A$  (6 m) in Along-system.

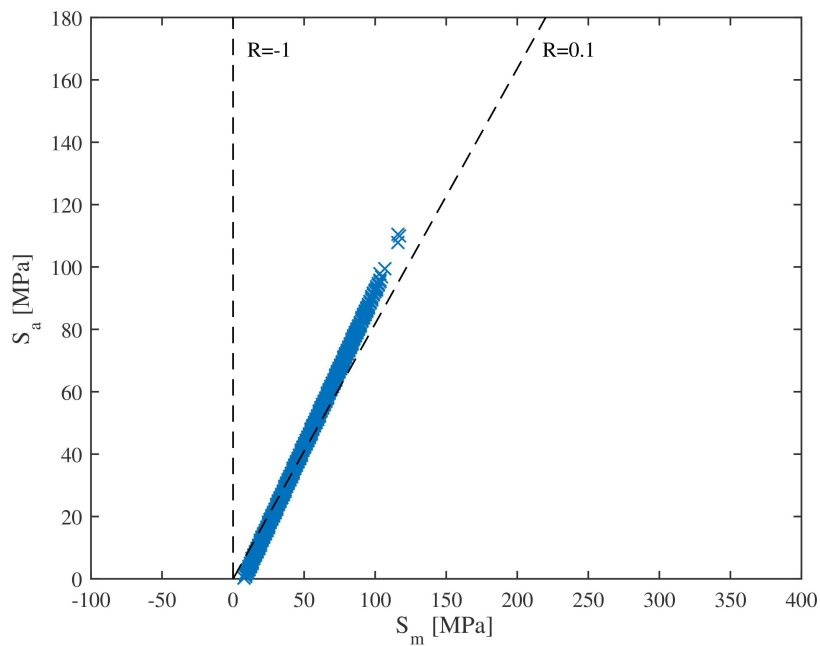


Figure 5.38. Stress cycles from one year of traffic at  $b_C = 0.4L_C$  (6 m) in Cross-system.

Figures 5.37 and 5.38 are discretized in order to keep calculations manageable in the reliability analysis and calibration of partial safety factors. Below in figures 5.39 and 5.40, a discretization load effect is shown with a step size of 10 MPa.

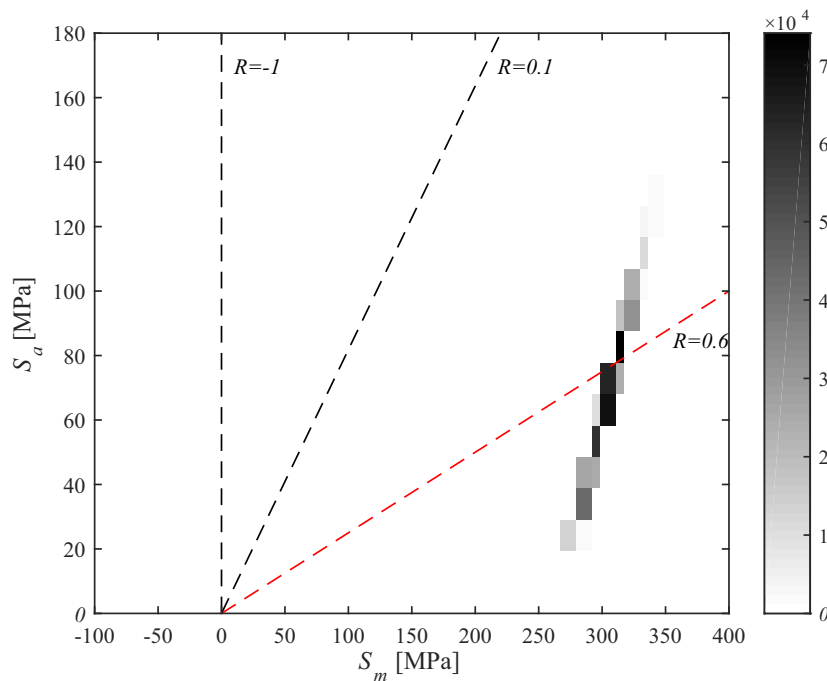
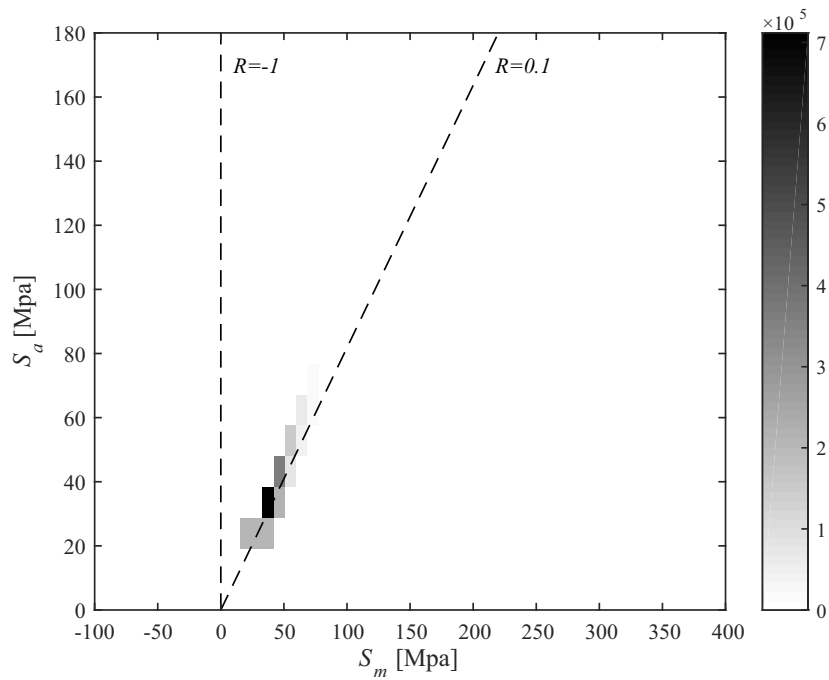


Figure 5.39. Stress cycles from one year of traffic, discretized with a step size of 10 MPa.



**Figure 5.40.** Stress cycles from one year of traffic, discretized with a step size of 10 MPa.

In the above figures, a design parameter is applied. However when conducting the reliability analysis, the results from the Rainflow count is discretized with a step size of  $1 \cdot 10^3$  Nm before the design parameter is applied.

With the chosen discretization the amount of unique cycles that will need individual damage calculations is decreased by respectively 99.7 % and 99.9 % for the Along-system and Cross-system. This reduction is at the cost of some accuracy, this is tested below in tables 5.7 and 5.8.

**Table 5.7.** Precision loss after discretization for Along-system measured by change in calculated damage in year 100 with a first moment of area of  $3 \cdot 10^6$  mm<sup>3</sup>, as found in Appendix C.

	Discretization None	Discretization $= 1 \cdot 10^3$ Nm	Discretization $= 1 \cdot 10^4$ Nm	Discretization $= 1 \cdot 10^5$ Nm
# of unique cycles	500037	1574	99	8
Damage in year 100	0.199	0.201	0.202	0.280
Relative change	0.00 %	+1.39 %	+1.81 %	+40.73 %

**Table 5.8.** Precision loss after discretization for Cross-system measured by change in calculated damage in year 100 with a first moment of area of  $3 \cdot 10^6 \text{ mm}^3$ , as found in Appendix C.

	Discretization None	Discretization $= 1 \cdot 10^3 \text{ Nm}$	Discretization $= 1 \cdot 10^4 \text{ Nm}$	Discretization $= 1 \cdot 10^5 \text{ Nm}$
# of unique cycles	2075006	575	65	7
Damage in year 100	$6.05 \cdot 10^{-5}$	$6.12 \cdot 10^{-5}$	$6.21 \cdot 10^{-5}$	$15.70 \cdot 10^{-5}$
Relative change	0.00 %	+1.10 %	+2.56 %	+158.97 %

From tables 5.7 and 5.8, the loss of accuracy is deemed acceptable as it only induces conservatism.

## 5.4 Concluding Remarks

In the following section, chapter 5 and the conclusions derived from it are presented.

In table 5.9, the assumptions for the load model is shown.

**Table 5.9.** Choices made in chapter 5.

Load model	4
Traffic category	2
Traffic type	Long distance
Lorry crossings	500 000
$b_A$	$0.4L_A$
$b_C$	$0.4L_C$
Discretization	$1 \cdot 10^3 \text{ Nm}$

In figures 5.41 and 5.42, the Markov matrices used for reliability analysis and calibration of partial safety factors for the Along-system and Cross-system is shown. The Markov matrices is presented, uses the design parameter found in Appendix C. However the Markov matrix used in reliability analysis is without the application of the design parameter,  $z$ , but is applied here for illustrative purposes. Therefore in the reliability analysis, the Markov matrix contains the cyclic amplitude loads,  $M_a$ , and the cyclic mean loads,  $M_m$ .

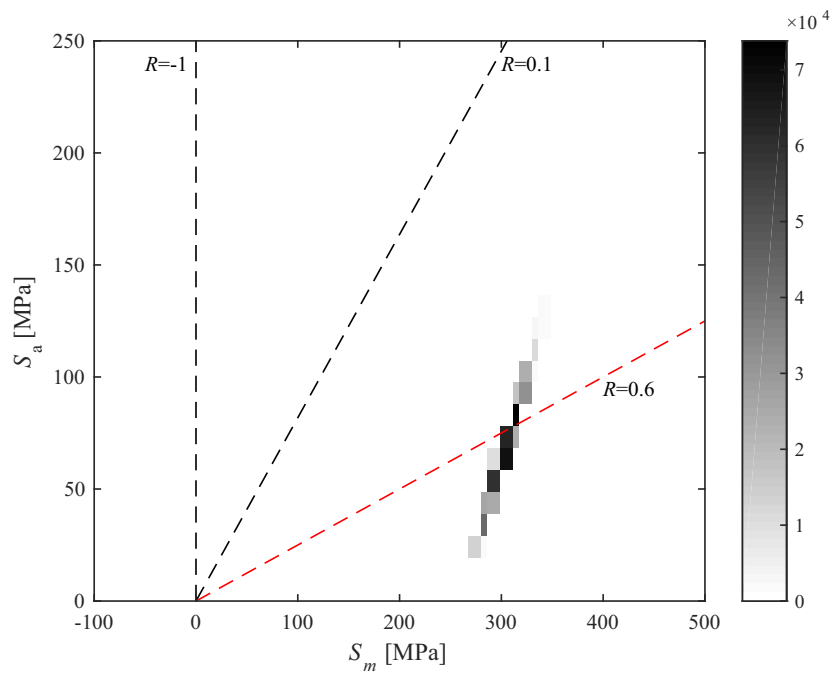


Figure 5.41. Load spectrum from one year of traffic, discretized with a step size of 10 MPa for Along-system. The colorbar indicates number of cycles,  $n$

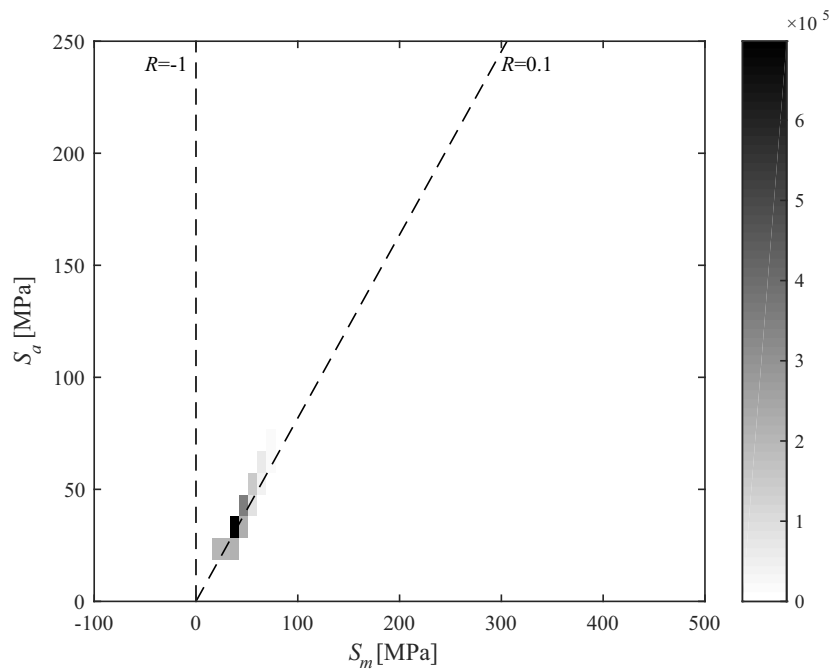


Figure 5.42. Load spectrum from one year of traffic, discretized with a step size of 10 MPa for Cross-system. The colorbar indicates number of cycles,  $n$

Figures 5.41 and 5.42 indicates that the optimal  $R$ -ratio to perform fatigue tests at are respectively  $R = 0.6$  and  $R = 0.1$  for the Along-system and Cross-system for this load spectrum. However, this is when the  $R$ -ratio is to fit well to the

majority of the stress cycles. Instead, a calculation of damage from the load spectrum can be performed. In figures 5.43 and 5.44, the damage from the load spectrum is shown.

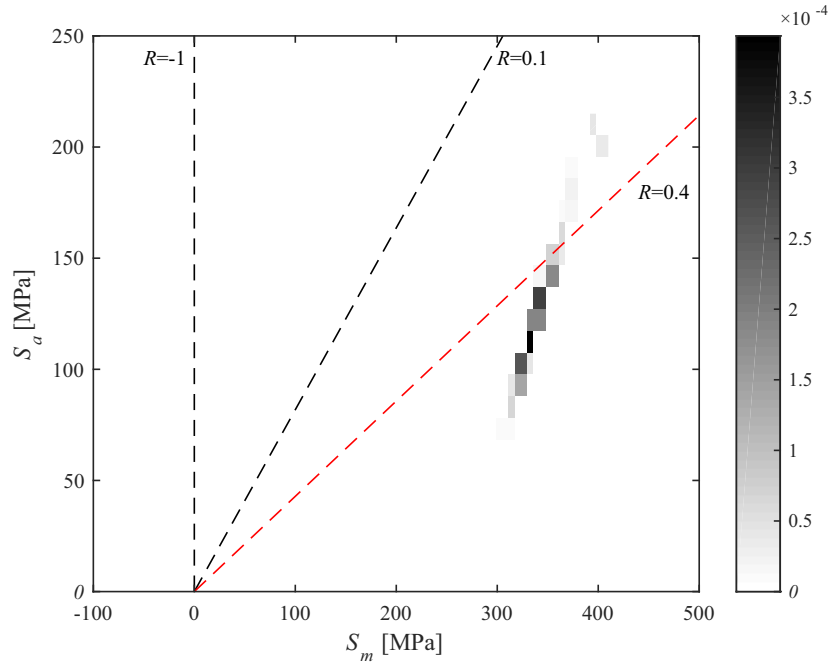


Figure 5.43. Load spectrum from one year of traffic showing damage, discretized with a step size of 10 MPa for Along-system. The colorbar indicates damage.

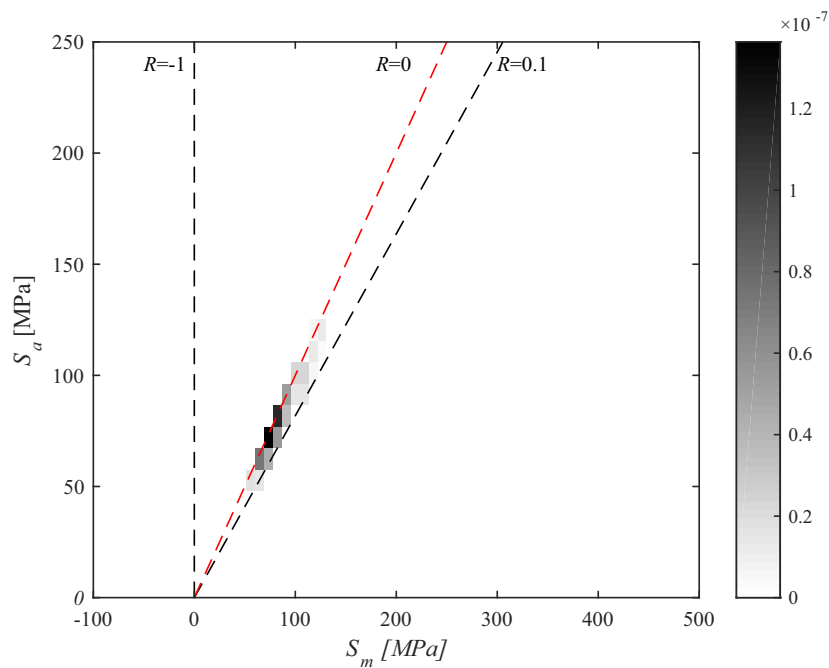


Figure 5.44. Load spectrum from one year of traffic showing damage, discretized with a step size of 10 MPa for Cross-system. The colorbar indicates damage.

From figures 5.43 and 5.44, it can be seen that the optimal  $R$ -ratio to perform fatigue tests at are respectively  $R = 0.4$  and  $R = 0$  for the Along-system and Cross-system for this load spectrum. These  $R$ -ratios correspond well with the stress cycles with the largest stress amplitudes of the load spectrum. Choosing the optimal  $R$ -ratio for performing fatigue tests requires knowledge of the load spectrum, the composite material will experience. Additionally, composites are complex materials with a large variation on capabilities. Therefore the best fatigue test plan is based on the location of the load spectrum and previous knowledge of the material.

---

# Reliability Analysis

In the following chapter, a reliability analysis is carried out in order to estimate the safety level of the bridge system. The fatigue limit state presented in this chapter is the only failure mode considered for the reliability analysis. The structural system in chapter 3 is decomposed into two systems and a fatigue limit state equation is formulated for each system. The reliability analysis is used to calibrate partial safety factors for target reliability levels presented in DK NA for DS/EN 1990. Furthermore, the reliability is evaluated by performing sensitivity analysis where both mean and standard deviation as well as correlation between parameters are investigated. Three measures of sensitivity are used to characterize the sensitivity of the reliability index with respect to stochastic variables. Additionally, the general theory used for calculating the structural reliability in this report is outlined.

## 6.1 Basic Concept of Probabilities in Civil Engineering

In civil engineering, the general objective of any structural design is to ensure the safety of the structure. This is achieved by ensuring that the resistance,  $R$ , is greater than or equal to the expected load effect,  $Q$ , as shown in eq. (6.1)

$$R \geq Q \quad (6.1)$$

Generally in civil engineering the resistance and load are deterministic quantities but are accompanied with uncertainties e.g. difference in nominal and actual resistance of an element, nature's phenomena being unpredictable or uncertainty related to idealizations of the mathematical models applied. Due to these uncertainties, eq. (6.1) can not be solved deterministically with an absolute safety. Therefore a probability of failure,  $P_f$ , for the system is introduced, describing the probability for the load to exceed the resistance during a given time period e.g. one year. As the goal in structural design is to ensure safety, a measure of the safety of the structure can be expressed as shown in eq. (6.2).

$$P_{nf} = 1 - P_f \quad (6.2)$$

Where  $P_{nf}$  is the probability of non-failure which is a measure of the safety thus expressing the structural reliability and the structural design becoming a matter of decision as to when a system is safe enough.

The structural reliability can be estimated by different methods, which can be divided into four levels.

Level I methods:	The uncertain parameters are modeled by one characteristic value, as for example in codes based on partial safety factor concept.
Level II methods:	The uncertain parameters are modeled by the mean values and the standard deviations, and by the correlation coefficients between the stochastic variables. The stochastic variables are implicitly assumed to be normally distributed. The reliability index method is an example of a level II method.
Level III methods:	The uncertain quantities are modeled by their joint distribution functions. The probability of failure is estimated as a measure of reliability.
Level IV methods:	In these methods the consequence (cost) of failure are also taken into account and the risk (consequence multiplied by the probability of failure) is used as a measure of the reliability. In this way different designs can be compared on an economic basis taking into account uncertainty, costs and benefits.

**Table 6.1.** Methods to measure the reliability of the structure. All methods can be calibrated with a method that is of higher level [Sørensen, 2011b].

The complexity of the methods increases with higher level. In this report level II and III reliability methods are considered and used to calibrate level I methods e.g. partial safety factors. Using level II and III reliability methods several techniques can be used to estimate the system reliability.

- FORM techniques: In First Order Reliability Methods the limit state function (see section below) is linearized in the design point.
- SORM techniques: In Second Order Reliability Methods a quadratic approximation of the failure function is applied in the design point and the probability of failure is estimated.
- Simulation techniques: Realizations of the stochastic variables are generated for each sample and the failure function is calculated for each realization. An example of a simulation technique is crude Monte Carlo simulation.

### 6.1.1 Basic Variables and Failure Surfaces

An important part of reliability analysis is to decide whether the quantities are modeled as stochastic variables or deterministic parameters. The stochastic variables models uncertainties related to the parameter in question. The stochastic

variables are denoted  $\mathbf{X} = (X_1, \dots, X_n)$ , where  $n$  is the number of stochastic variables. The stochastic variables in  $\mathbf{X}$  are also known as basic variables. Realizations of the basic variables are denoted  $\mathbf{x} = (x_1, \dots, x_n)$ .

In order for the mentioned reliability techniques to be applied, it is important that the realizations  $\mathbf{x}$  of the basic variables can determine whether the structure is in a safe region or a failure region. For this, a limit state function,  $g(\mathbf{x})$ , is formulated, which divide the basic variable space,  $\omega$ , into a safe region,  $\omega_S$ , and a failure region,  $\omega_F$ . The two regions are separated by the limit state function defined as eq. (6.3) and depicted in figure 6.1.

$$g(\mathbf{x}) = \begin{cases} > 0 & , \mathbf{x} \in \omega_S \\ \leq 0 & , \mathbf{x} \in \omega_F \end{cases} \quad (6.3)$$

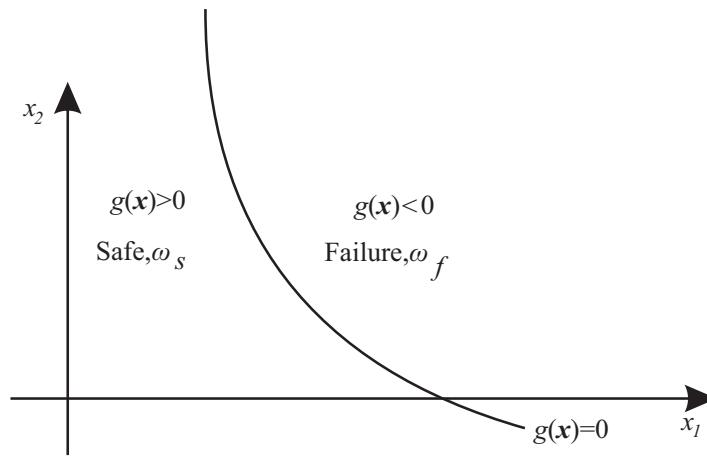


Figure 6.1. Failure function  $g(x) = 0$  in physical space.

It should be noted that the failure surface is not defined by a unique failure function in the physical space. This is however the case in the  $u$ -space.

If the realizations  $\mathbf{x}$  are replaced by the stochastic variables  $\mathbf{X}$ , the safety margin  $M$  or limit state equation (LSE) is obtained.

$$M = g(\mathbf{X})$$

Where  $M$  is a stochastic variable and the probability of failure,  $P_f$ , is.

$$P_f = P(M \leq 0) = P(g(\mathbf{X}) \leq 0)$$

The reliability index,  $\beta$ , can be obtained by eq. (6.4).

$$P_f = P(g(\mathbf{X}) \leq 0) = \Phi(-\beta) \quad (6.4)$$

If the safety margin is non linear the approximation shown in eq. (6.5) is used.

$$P_f = P(g(\mathbf{X}) \leq 0) \approx P(\beta - \boldsymbol{\alpha}^T \mathbf{U}) = \Phi(-\beta) \quad (6.5)$$

where  $\beta - \boldsymbol{\alpha}^T \mathbf{U}$  is the linearized safety margin.

The reliability index can be defined in different ways and the definition presented in eq. (6.4) is by Hasofer & Lind. In order to obtain the reliability index,

- $\beta$  Reliability index  
 $n$  Number of stochastic variables  
 $u_i$  Value of stochastic variable in design point in  $u$ -space

the limit state function is transformed using the Rosenblatt transformation from the physical domain into a normalized domain denoted  $u$ -space by eq. (6.6) to make the stochastic variables Normal distributed. Furthermore Hasofer & Lind's reliability index requires a linear safety margin.

$$\Phi(U_i) = F_{X_i}(X_i) \quad (6.6)$$

where

- |          |  |  |
|----------|--|--|
| $\Phi()$ |  | Standard normal distribution                         |
| $X_i$    |  | Stochastic variable no. $i$                          |
| $U_i$    |  | Normalized stochastic variable no. $i$ in $u$ -space |

Hasofer & Lind defines the reliability index as the shortest distance from origin to where  $g(\mathbf{u}) = 0$  in the  $u$ -space as depicted in figure 6.2.

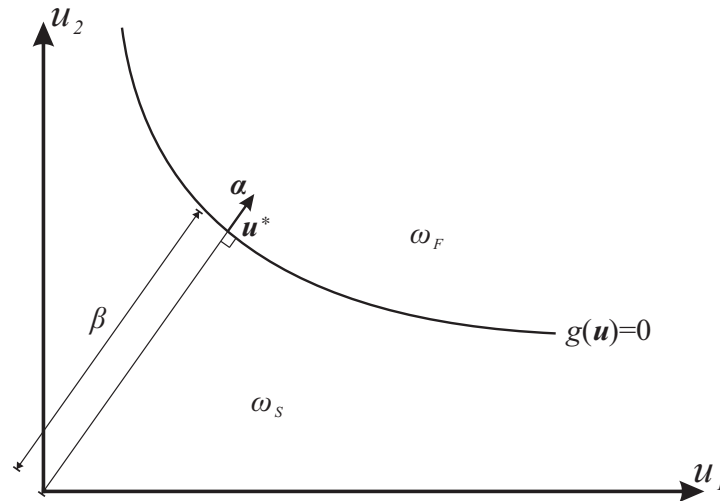


Figure 6.2. Geometrical illustration of the reliability index in  $u$ -space.

The shortest distance to the limit state function in  $u$ -space will be the most likely failure and is found the optimization problem by eq. (6.7)

$$\beta = \min_{g_u(\mathbf{u})} \sqrt{\sum_{i=1}^n u_i^2} \quad (6.7)$$

where It should be noted that the reliability index presented in eq. (6.7) is the design reliability index,  $\beta$ , and not the annual reliability,  $\beta_a$ , index which is normally presented in this report.

The annual reliability index can be found by performing two time dependent reliability analysis' on the same problem, with the time input varied by one year.

A reliability index can refer to other time periods as well, usually a reliability index will refer to the lifespan or a year.

$$\beta_a = -\Phi^{-1}(\Phi(-\beta_j) - \Phi(-\beta_{j-1}))$$

Where

$\beta_a$		Annual reliability index
$j$		Refers to the year in which $\beta_a$ is sought

Normally a structure will be build with a target safety level, that refers to a target annual reliability index. The annual reliability index of the structure should not be lower than the target annual reliability index during its design life.

## 6.2 Reliability Assessment Methods

When assessing the Hasofer & Lind reliability index  $\beta$ , a number of methods can be used, these methods are listed below in smaller sections. From all methods, a probability of failure can be found, however depending on the limit state equation this result may vary. If FORM is not considered accurate for the case, it will still be used as a starting point for the reliability assessment. In these cases SORM or simulation may be used to yield an accurate probability of failure. While SORM can be more accurate than FORM, it may still be inappropriate for some cases, as only simulation perfectly replicates all limit state functions presented.

### 6.2.1 First Order Reliability Method

FORM is the simplest approach. FORM uses a linear approximation of the limit state function at the design point (see eq. (6.8)), and estimates the probability of failure by eq. (6.6). As an effect thereof it will have the least accuracy in predicting the probability of failure and thereby the reliability index. The degree of accuracy is largely dependent on the linearity of the limit state function.

When assessing the probability of failure a transformation to u-space is needed in order to normalize the stochastic variables as standard normal distributions. This allows the probability of failure to be considered as a product of likely or unlikely outcomes, instead of physical parameters as resistance and load.

The reliability index defined in eq. (6.7) is found through numerical calculations by solving the optimization problem by iteration. In figure 6.3, a geometrical illustration of the reliability index as well as the linearized safety margin is shown.

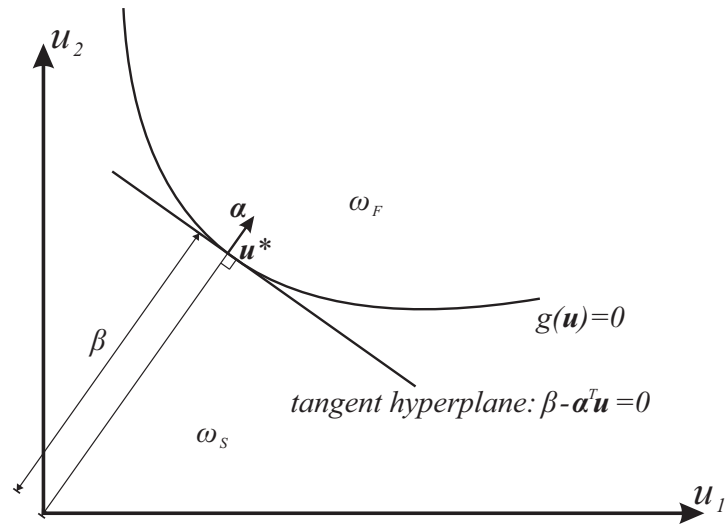


Figure 6.3. Geometrical illustration of the linear safety margin in  $u$ -space.

The linearized safety margin is defined as.

$$0 = \beta - \alpha^T \mathbf{u} \tag{6.8}$$

Lastly, any cross-section through origin in  $u$ -space will be a standard normal distribution, as it only consists of axis' with these.

### 6.2.2 Second Order Reliability Method

In contrast to FORM, SORM is obtained by approximating the failure surface in  $u$ -space with a second order surface as shown in figure 6.4.

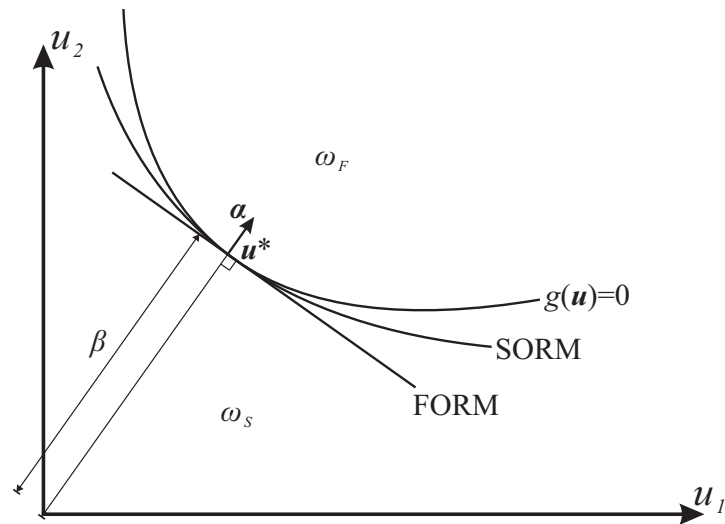


Figure 6.4. Illustration of FORM and SORM approximation of the failure function in  $u$ -space.

As the failure surface become more non-linear, SORM can be expected to yield a better estimate of the probability of failure in comparison to FORM.

### 6.2.3 Crude Monte Carlo Simulation

In simulations, the stochastic variables,  $\mathbf{X}$ , are realized with outcomes,  $\mathbf{x}$ . The probability of failure is then estimated by calculating the limit state equation for each realization. If the realization is within the failure region,  $\omega_F$ , a contribution to the probability of failure is obtained. Crude Monte Carlo (CMC) is a simulation technique which estimate the probability of failure from eq. (6.9).

$$P_f = \frac{1}{N} \sum_{j=1}^N I[g(\mathbf{x}_j)] \quad (6.9)$$

$N$		Number of realizations
$\mathbf{x}$		Realization of standard normally distributed stochastic vector, $\mathbf{X}$
$I[g(\mathbf{x}_j)]$		Indicator function

The indicator function is shown in eq. (6.10).

$$I[g(\mathbf{x})] = \begin{cases} 0 & \text{if } g(\mathbf{x}) > 0 \quad (\text{safe}) \\ 1 & \text{if } g(\mathbf{x}) \leq 0 \quad (\text{failure}) \end{cases} \quad (6.10)$$

As this report evaluates annual probabilities of failure and not the total probability of failure in a lifetime. A rewriting of the results extracted from the CMC is performed. The limit state function is as presented below in eq. (6.11), this formulation is valid as the damage caused from one year of traffic is assumed representative for each simulation.

$$g(\mathbf{x}_j) = \Delta - tD(\mathbf{x}_j) \quad (6.11)$$

In the year of failure, the limit state function will then be:

$$0 = \Delta - t_F D(\mathbf{x}_j)$$

Where  $t_F$  is the year in which failure will occur. This can be rewritten as;

$$t_F = \frac{\Delta}{D(\mathbf{x}_j)}$$

The result from a simulation will then be a year of failure, instead of an indicator of failure or not. An illustration of the annual probability of failure is seen below in figure 6.5. The annual probability of failure in a certain year can then be found by eq. (6.12).

$$P_{fa,i} = \frac{n_{fa,i}}{N_{sim}} \quad (6.12)$$

Where

$n_{fa,i}$		Number of failures in year $i$
$P_{fa,i}$		Annual probability for year $i$
$N_{sim}$		Number of lifetimes simulated

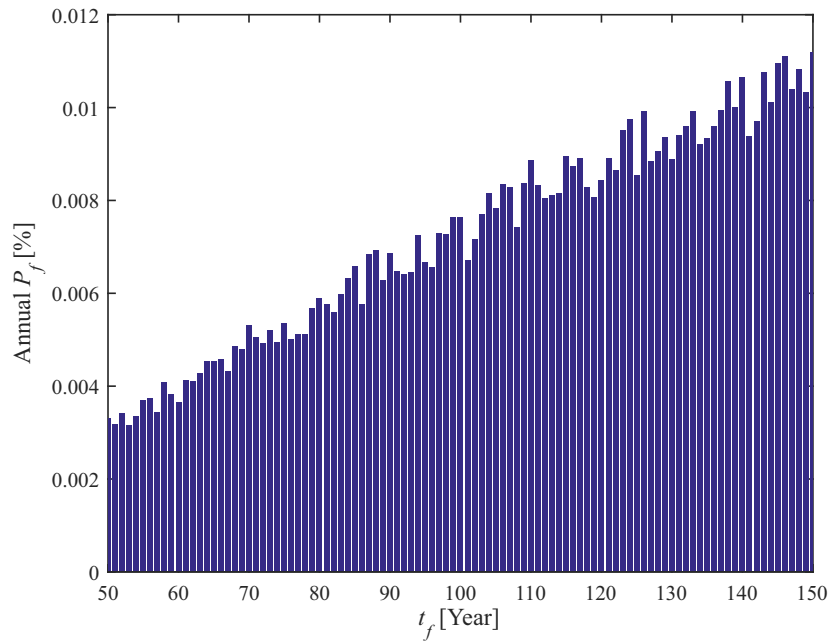


Figure 6.5. Number of failures per year from a CMC after  $7 \cdot 10^6$  simulations.

### 6.3 Target Reliability

In DS/EN, the partial safety factor method is proposed. Herein deterministic values are multiplied with factors in order to reach a predetermined safety level. This method is easily applicable and widely used in engineering practice. The safety levels are enforced by target reliability indices. The target reliability index is not to be exceeded in every case, it is merely the average of the applicable cases that is intended to have a reliability index as such. The partial safety factors that enforce the safety levels are derived from one of three methods, a, b and c, shown in figure 6.6.

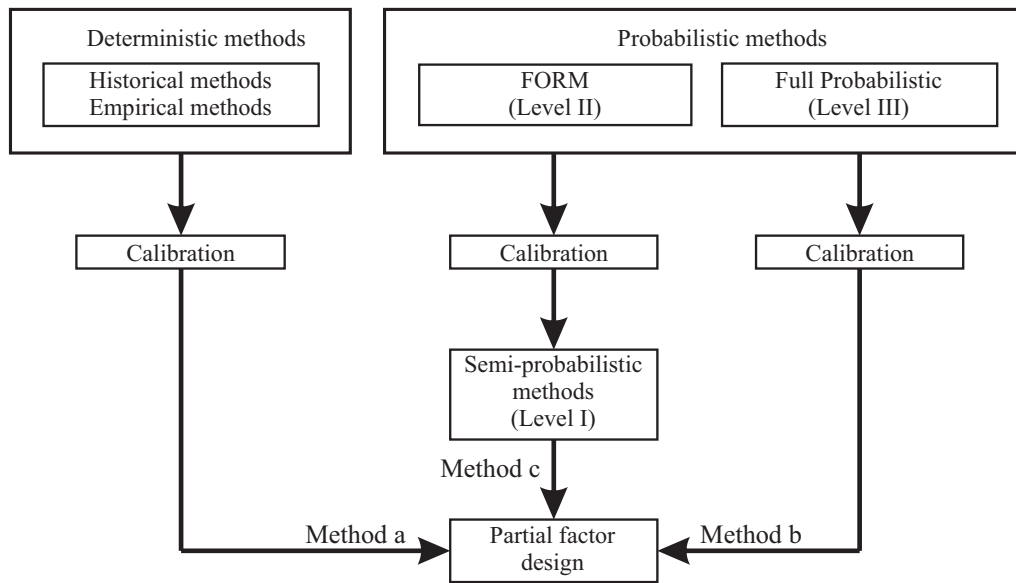


Figure 6.6. Overview of reliability methods [DS/EN 1990, 2007].

While Eurocode recommended partial safety factors are primarily derived by method a and design value format, the partial safety factors found in this report will be derived by probabilistic methods. These are both based on probabilistic analysis. Depending on the degree of approximation found in section 6.5, FORM will be used to determine the partial safety factors. This is an approximation investigated further in section 6.5.

DS/EN defines three levels of reliability and consequence. The reliability levels are shown below in table 6.2. These are rated from one to three and correspond within each level. This means that a structure evaluated to be in consequence class 3 (CC3) will also require reliability class 3 (RC3). The reliability classes have been adjusted by DK/NA to the values shown below in table 6.3.

Table 6.2. Annual target reliability classes for buildings according to DS/EN 1990. Table 6.3. Annual target reliability classes for buildings according to DS/EN 1990 DK NA.

Table 6.2		Table 6.3	
	$\beta_a$		$\beta_a$
RC3	5.2	RC3	4.7
RC2	4.7	RC2	4.3
RC1	4.2	RC1	3.8

According to [Sørensen, 2009], bridges are to be designed with the safety levels as shown below in table 6.4. These reliability levels are higher than those suggested for structures in DK NA. Bridges are only to be designed in consequence class 2 and 3, as no bridges are designed with a low consequence of failure.

Table 6.4. Annual target reliability levels for bridges. [Sørensen, 2009]

	$\beta_a$
CC3	5.2
CC2	4.8

It is in accordance with the reliability levels shown in table 6.4 that partial coefficients for the bridge system are derived.

### 6.4 Overview of Reliability Analysis

In figure 6.7, an overview of the procedure for the reliability analysis is presented.

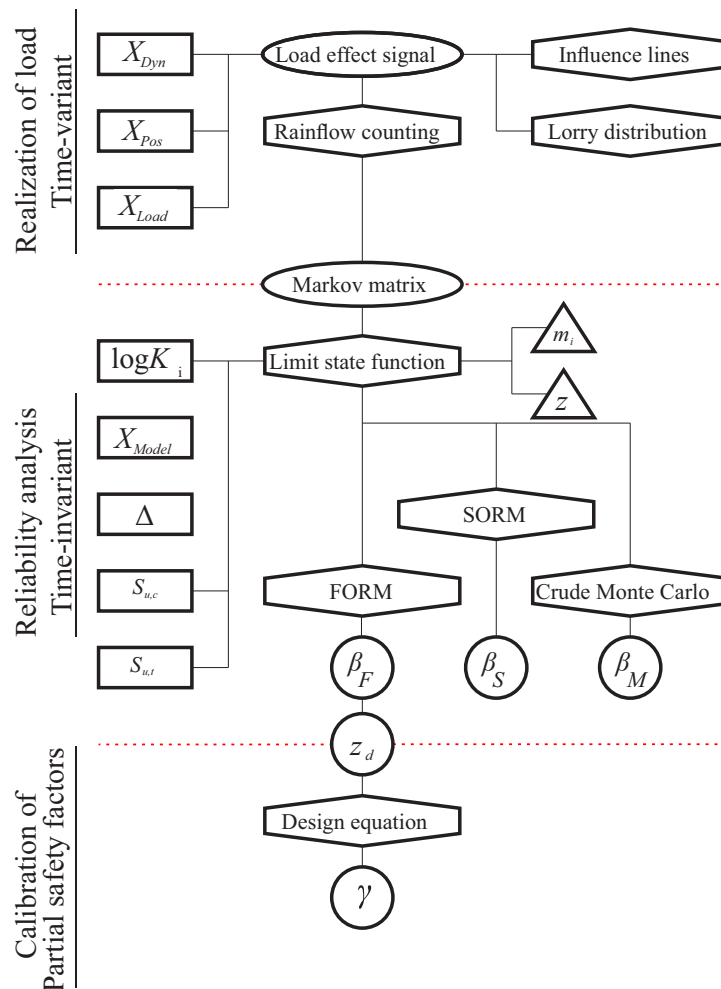


Figure 6.7. Overview of reliability analysis. Triangles: deterministic values. Squares: basic stochastic variables. Hexagon: Calculations. Circles: Results.

As illustrated in figure 6.7, the basic variables related to the load are realized and a lorry distribution is simulated before conducting the reliability analysis as the limit state equation needs the cyclic load amplitude and cyclic mean loads

as input. Rainflow counting is performed to obtain a Markov matrix containing cyclic load amplitudes and their related mean loads. In the limit state equation the rest of the basic variables are defined as well as deterministic values. The deterministic design parameter,  $z$ , is used to adjust the reliability index. The reliability index is estimated using three different methods; FORM, SORM and CMC and a  $z_d$  corresponding to the reliability index is obtained used to calibrate partial safety factors.

## 6.5 Fatigue Limit State

In the following section, a fatigue limit state equation is derived to estimate the reliability for the components in the bridge system presented in chapter 3. The fatigue limit state estimates the probability of failure due to fatigue loading and is used to derive partial safety factors for annual reliability indices described section 6.3. The fatigue limit state uses DNVs method for fatigue life prediction presented in section 2.1.3 as well as Palmgren-Miner's damage accumulation rule to estimate fatigue damage on the components. The piecewise linear constant life diagram with two  $R$ -ratios is used, under the assumption that it predicts damage accurately. Therefore no model uncertainty is related to the constant life diagram itself. Stochastic variables and uncertainties used in the fatigue limit state are presented in chapter 4. All stochastic variables are assumed uncorrelated.

The design parameter,  $z$ , is used to control the annual reliability of the system and is defined in eq. (6.13). By defining the design parameter as shown in eq. (6.13), the entire load spectrum will be scaled when  $z$  is adjusted, meaning that all points will maintain their  $R$ -ratio during all calculations.

$$\begin{aligned} S_a &= \frac{M_a}{z} X_{Model} \\ S_m &= \frac{M_m}{z} X_{Model} \end{aligned} \quad (6.13)$$

Where  $M_a$  is cyclic load amplitude and  $M_m$  is cyclic mean value obtained from Rainflow counting of the load series obtained by realization.  $M_a$  and  $M_m$  contain data from one years traffic according to traffic class 2, the derivation of  $M_a$  and  $M_m$  is covered in chapter 5. The fatigue limit state equation is presented in eq. (6.14).

$$g(\mathbf{X}) = \Delta - tD(n, S_a, S_m, K_i, m_i, \epsilon_i, S_{u,c}, S_{u,t}) \quad (6.14)$$

Where  $t$  is time in years and index  $i$  refers to properties belonging to S-N curves at  $R$ -ratio -1 and 0.1. The annual damage,  $D$ , can be expanded as shown in eq. (6.15) and illustrated in figure 6.8.

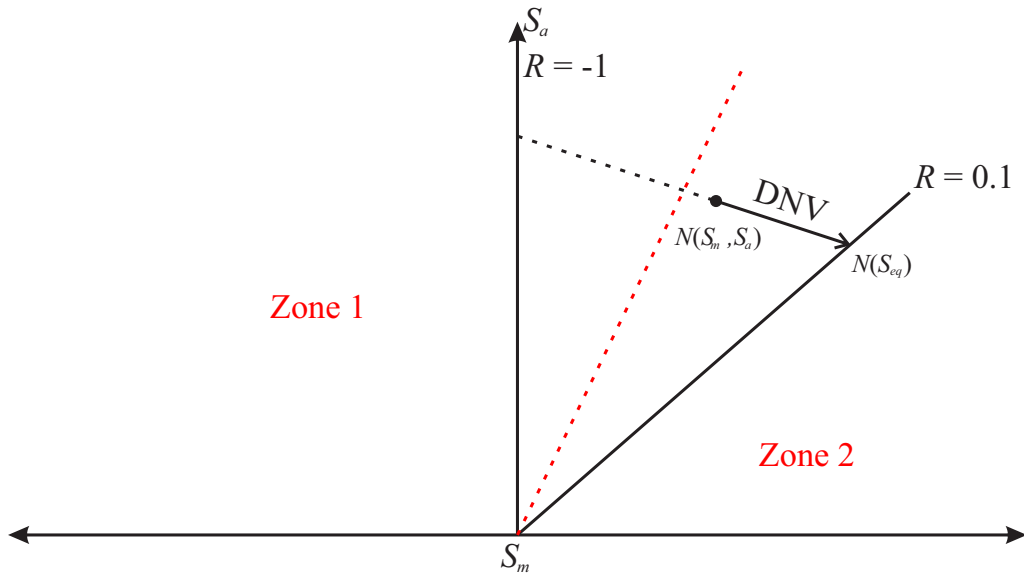


Figure 6.8. Illustration of constant life diagram and zone subdivision.

According to DNV's method for predicting fatigue life presented in section 2.1.3, an equivalent amplitude stress is obtained and belongs to a specific  $R$ -ratio. As shown in figure 6.8, two  $R$ -ratio are available for constructing the constant life diagram. Load cycles in Zone 2 are transformed into a equivalent cyclic stress amplitude on the line equal to  $R = 0.1$ . This procedure is done for all load cycles, and the load cycles are divided into to a number of zones depending on the number of  $R$ -ratios. From this observation,  $D$  can be expanded as shown in eq. (6.15).

$$\begin{aligned}
 D &= \sum_{i=1}^k \sum_{j=1}^{n_i} \frac{n_{ij}}{N_{ij}(S_{eq,ij})} \\
 &= \sum_{i=1}^k \sum_{j=1}^{n_i} \frac{n_{ij}}{K_i \cdot S_{eq,ij} (S_{a,ij}, S_{m,ij}, S_{u,c}, S_{u,t}, K_i, \epsilon_i, m_i)^{-m_i} \cdot 10^{\epsilon_i}} \\
 &= \sum_{i=1}^k \frac{1}{10^{\log K_i + \epsilon_i}} \sum_{j=1}^{n_i} \frac{n_{ij}}{S_{eq,ij} (S_{a,ij}, S_{m,ij}, S_{u,c}, S_{u,t}, K_i, \epsilon_i, m_i)^{-m_i}} \quad (6.15)
 \end{aligned}$$

Where  $k$  is equal to two (number of  $R$ -ratios) and  $n$  is equal to the amount of load cycles in the zone.

A design parameter,  $z$ , is sought, which provide an annual reliability index equal to the annual reliability index of CC2 and CC3 in year 100. The  $z$  that yields the sought annual reliability index is denoted  $z_d$ . In figure 6.9, the annual reliability index as function of time is shown for CC3 for Along-system and Cross-system.

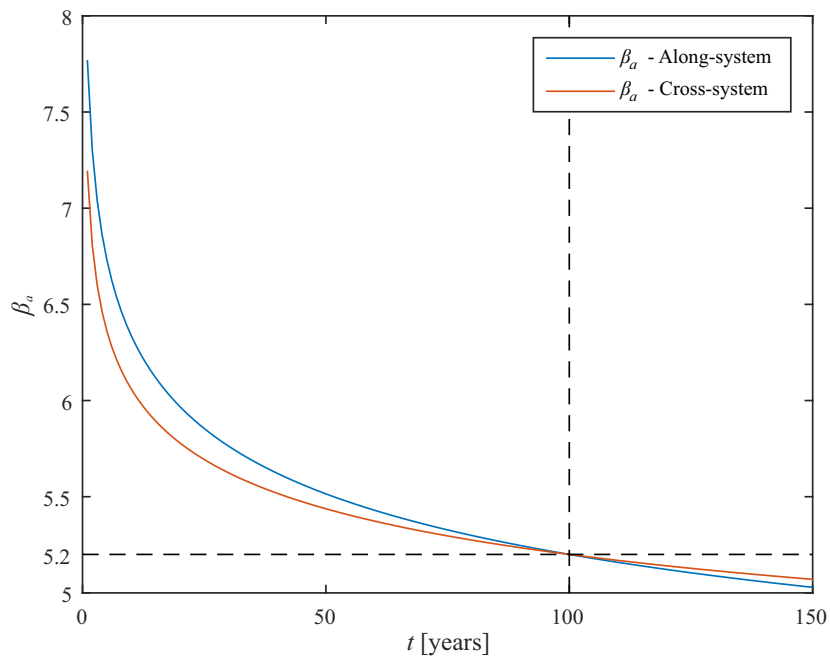


Figure 6.9. Annual reliability index as function of time for Along-system and Cross-system.

As shown in figure 6.9, the annual reliability index in year 100 is in accordance with the annual reliability indices stated for CC3 in section 6.4 for both Along-system and Cross-system.

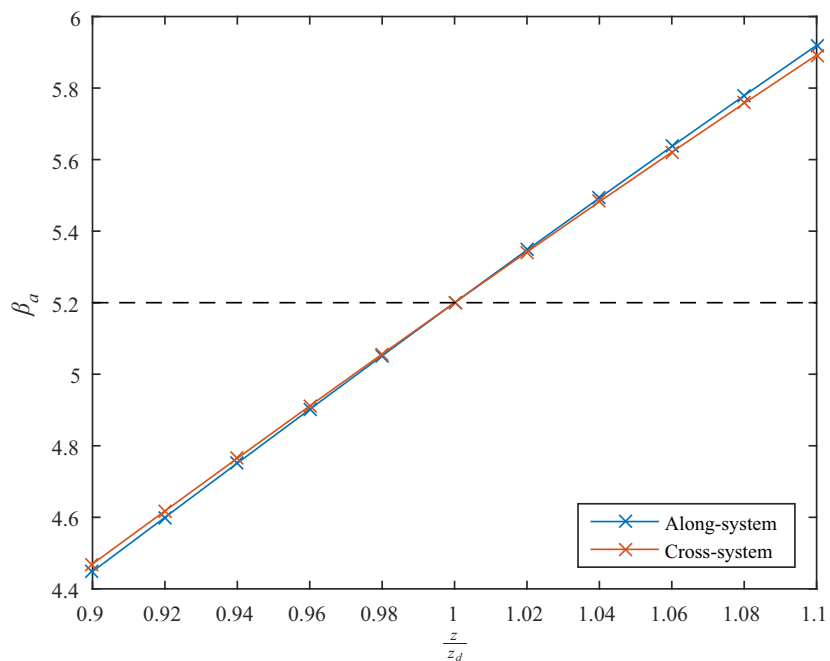


Figure 6.10. Annual reliability index as function of  $z$  for Along-system and Cross-system in year 100.  $z_d$  corresponds to  $\beta_a = 5.2$ .

Figure 6.10 illustrates how the annual reliability index changes as function of  $z$  for Along-system and Cross-system using FORM.

The design parameter,  $z_d$ , found using FORM is shown in table 6.5 for Along-system and Cross-system.

**Table 6.5.** Design parameter,  $z_d$ , estimated using FORM for Along-system and Cross-system.

$z_d$	Along-system [mm <sup>3</sup> ]	Cross-system [mm <sup>3</sup> ]
$\beta_a = 5.2$	$4.5 \cdot 10^6$	$2.2 \cdot 10^6$
$\beta_a = 4.8$	$4.2 \cdot 10^6$	$2.1 \cdot 10^6$
$\beta_a = 3.8$	$3.6 \cdot 10^6$	$1.8 \cdot 10^6$

Comparing the design parameters,  $z_d$ , estimated by FORM for fatigue limit state and the design parameter determined for ultimate limit state for the along system in Appendix B equal to  $31 \cdot 10^6$  mm<sup>3</sup>, it is seen that the design parameter for fatigue limit state is approximately 8 times smaller than the design parameter for ultimate limit state. The bridge design in Appendix B is done in consequence class 2 for structures. This means that the partial safety factors applied should give it an annual reliability index of  $\beta = 3.8$ . Therefore fatigue limit state will not dictate the size of the design parameter for the bridge system.

The design point in the physical space,  $x^*$ , and the design point in  $u$ -space,  $u^*$ , estimated using finite element reliability and shown in tables 6.6 and 6.7 for respectively Along-system and Cross-system.  $x^*$  is determined using the transformation given in eq. (6.6) and the design point,  $u^*$ .

**Table 6.6.** Design point in physical space,  $x^*$ , and  $u$ -space,  $u^*$ , estimated using FORM at  $\beta_a = 5.2$  for Along-system.

	$x^*$	$u^*$
$\Delta$	0.62	-1.05
$\log K_{R=-1}$	26.8	0
$\log K_{R=0.1}$	32.3	-0.44
$\sigma_{\epsilon_{R=-1}}$	0.21	0
$\sigma_{\epsilon_{R=0.1}}$	0.27	0.52
$u_{R=-1}$	0	0
$u_{R=0.1}$	-1.68	-1.68
$X_{model}$	1.48	3.96
$S_{u,c}$	745 MPa	0
$S_{u,t}$	1045 MPa	-0.31

**Table 6.7.** Design point in physical space,  $x^*$ , and  $u$ -space,  $u^*$ , estimated using FORM at  $\beta_a = 5.2$  for Cross-system.

	$x^*$	$u^*$
$\Delta$	0.57	-1.27
$\log K_{R=-1}$	26.8	-0.04
$\log K_{R=0.1}$	32.3	-0.49
$\sigma_{\epsilon_{R=-1}}$	0.21	0
$\sigma_{\epsilon_{R=0.1}}$	0.27	0.66
$u_{R=-1}$	-0.13	-0.13
$u_{R=0.1}$	-1.91	-1.91
$X_{model}$	1.46	3.82
$S_{u,c}$	745 MPa	0
$S_{u,t}$	1059 MPa	0

where  $u_{R=-1}$  and  $u_{R=0.1}$  is related to the physical uncertainty,  $\epsilon$ , defined in eq. (4.18). As  $u_{R=-1}$  and  $u_{R=0.1}$  are standard Normal distributions in the physical space, they will have the same design point in  $u$ -space.

It can be seen from table 6.6 and 6.7, that the uncertainty applied to the stress is the most effectful uncertainty. The design point in the  $X_{model}$ -distribution is at its 99.993 % quantile.

The  $\alpha$ -vector in the design point for Along-system and Cross-system for CC3 is shown in tables 6.8 and 6.9.

$\alpha^2$		$\alpha^2$	
$\Delta$	5.51% (24.7 %)	$\Delta$	7.92% (27.2 %)
$\log K_{R=-1}$	0.00% (0.00 %)	$\log K_{R=-1}$	0.01% (0.03 %)
$\log K_{R=0.1}$	0.95% (4.28 %)	$\log K_{R=0.1}$	1.54% (3.97 %)
$\sigma_{\epsilon_{R=-1}}$	0.00% (0.00 %)	$\sigma_{\epsilon_{R=-1}}$	0.00 % (0.00 %)
$\sigma_{\epsilon_{R=0.1}}$	1.35% (6.06 %)	$\sigma_{\epsilon_{R=0.1}}$	2.12% (7.28 %)
$u_{R=-1}$	0.00% (0.00 %)	$u_{R=-1}$	0.09% (0.29 %)
$u_{R=0.1}$	14.0% (62.8 %)	$u_{R=0.1}$	17.8% (61.2%)
$X_{model}$	77.7% (- %)	$X_{model}$	70.90% (- %)
$S_{u,c}$	0.00% (0.00 %)	$S_{u,c}$	0.00% (0.00 %)
$S_{u,t}$	0.49% (2.19 %)	$S_{u,t}$	0.00% (0.00 %)

**Table 6.8.** Sensitivities for the stochastic variables for Along-system in year 100 for  $\beta_a = 5.2$ . (..) represents sensitivities when the  $\alpha$ -vector is normalized after removing  $X_{model}$ .

**Table 6.9.** Sensitivities for the stochastic variables for Cross-system in year 100 for  $\beta_a = 5.2$ . (..) represents sensitivities when the  $\alpha$ -vector is normalized after removing  $X_{model}$ .

In order to investigate the results from FORM, SORM and CMC are used to estimate the annual reliability index as well. This is done using the design parameter,  $z_d$ , obtained from FORM. A lower  $\beta_a (= 3.8)$  corresponding to CC1 according to DS/EN 1990 DK NA for structures is chosen to decrease the amount of simulations needed for a reasonable estimate of  $P_f$  for the CMC. In figures 6.11 and 6.12, the comparison between the methods is presented. This is done in order to evaluate the approximation by FORM. If FORM yields an accurate result the tendency is assumed to be continued at other annual reliability levels and in similar analysis'.

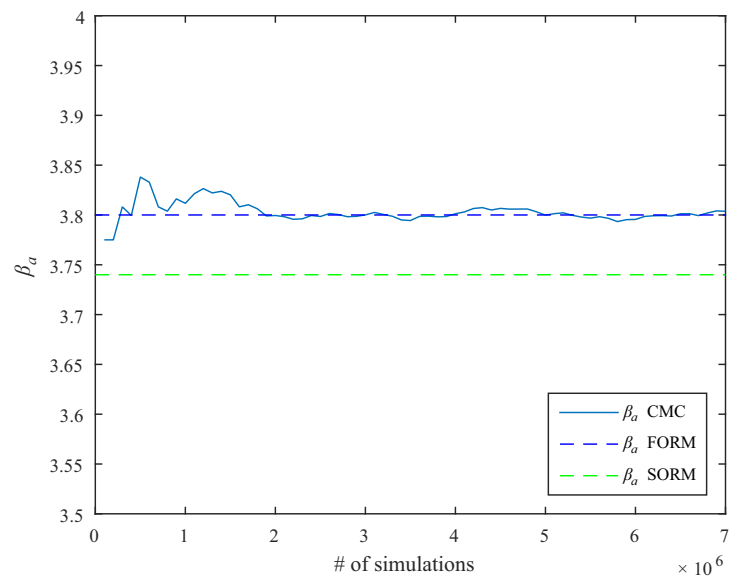


**Figure 6.11.** Comparison of annual reliabilities for FORM, SORM and CMC for Along-system.

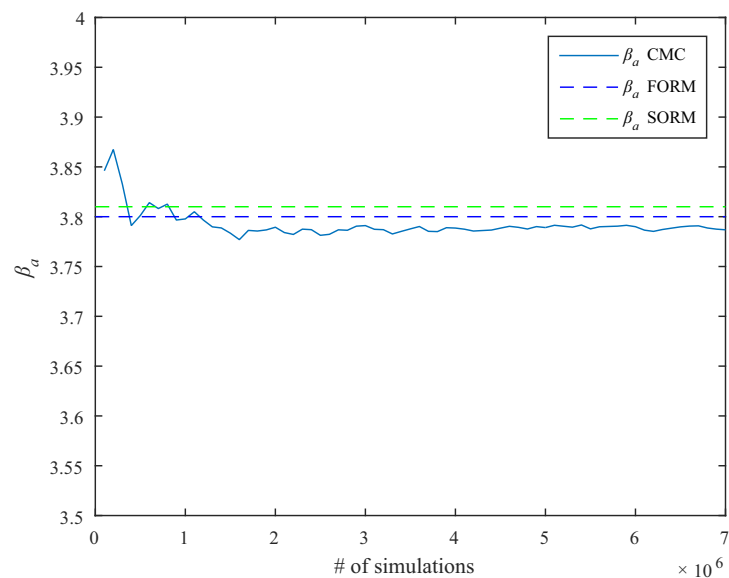


**Figure 6.12.** Comparison of annual reliabilities for FORM, SORM and CMC for Cross-system.

It can be seen from figures 6.11 and 6.12, that the simulations converges decently towards the FORM estimate. However it is slightly non-conservative to apply the FORM solution. It is clear to see that the SORM does not estimate the probability of failure well. There may be a number of reasons but the complex shape of the limit state function is likely the cause. The Hessian matrix found in the design point must indicate the shape of the limit state function poorly. Furthermore it is complicated by the non-continuous failure surface. The FORM estimate is relatively accurate at this reliability level. This tendency is assumed

to continue for reliability levels in the proximity. Henceforth, FORM will be used for the derivation of the partial safety factors under the assumption that it is precise.

Additionally, it should be noted that, increasing the number of simulations for the CMC increases the accuracy. In tables 6.10 and 6.11, the results from FORM, SORM and CMC are presented.

**Table 6.10.** Results from reliability analysis for Along-system. **Table 6.11.** Results from reliability analysis for Cross-system.

$\beta_a$			$\beta_a$		
FORM	SORM	CMC	FORM	SORM	CMC
5.20	4.87	-	5.20	5.19	-
4.80	4.48	-	4.80	4.86	-
3.80	3.74	3.80	3.80	3.81	3.79

As seen in tables 6.10 and 6.11, CMC is only simulated at  $\beta_a = 3.8$  corresponding to low consequence class according to DS/EN 1990 DK NA for structures. Ideally CMC simulations would be performed at all reliability levels, to ensure the precision the FORM calculations, however CMC simulations are quite time consuming when estimation of damage is done by DNVs method. As a million simulations of either system has an approximate duration of 6 hours, and the needed amount of simulations increase exponentially with the safety level, this will have to suffice. The duration is timed on a setup with specs as follows: Intel Core i7-4790K CPU 4.0 GHz and 16 GB of RAM.

## 6.6 Sensitivity Analysis

A sensitivity analysis is conducted on the parameters in the limit state equation presented in section 6.5. The parameters used in the limit state equation are presented in table 4.15. In the sensitivity analysis both mean and standard deviation are varied. The sensitivity analysis is a useful tool for identifying and characterizing parameters effect on the reliability index as well as evaluate the importance of various system simplifications. This knowledge can then be used when planning additional experiments. For this sensitivity analysis, three measures of the sensitivity are used.

- $\alpha$ -vector
- Reliability elasticity coefficient,  $e_p$
- Omission sensitivity factor,  $\zeta$

In tables 6.12 and 6.13, the  $\alpha$ -vector at the design point for CC3 is presented for Along-system and Cross-system. Generally, the  $\alpha$ -vector can be interpreted as a measure of the importance of the uncertainty for the corresponding stochastic variable and  $\alpha^2$  yields the percentage of the total uncertainty related with the corresponding basic stochastic variable. It is important to note that this is

only valid for uncorrelated basic variables. Otherwise, the components in the  $\alpha$ -vector can not be associated with specific stochastic variables, instead the  $\alpha^2$  components for the correlated basic stochastic variables are summed and a percentage of the total uncertainty related to the correlated basic variables combined is obtained.

$\alpha^2$		$\alpha^2$	
$\Delta$	5.51% (24.7 %)	$\Delta$	7.92% (27.2 %)
$\log K_{R=-1}$	0.00% (0.00 %)	$\log K_{R=-1}$	0.01% (0.03 %)
$\log K_{R=0.1}$	0.95% (4.28 %)	$\log K_{R=0.1}$	1.54% (3.97 %)
$\sigma_{\epsilon_{R=-1}}$	0.00% (0.00 %)	$\sigma_{\epsilon_{R=-1}}$	0.00 % (0.00 %)
$\sigma_{\epsilon_{R=0.1}}$	1.35% (6.06 %)	$\sigma_{\epsilon_{R=0.1}}$	2.12% (7.28 %)
$u_{R=-1}$	0.00% (0.00 %)	$u_{R=-1}$	0.09% (0.29 %)
$u_{R=0.1}$	14.0% (62.8 %)	$u_{R=0.1}$	17.8% (61.2%)
$X_{model}$	77.7% (- %)	$X_{model}$	70.90% (- %)
$S_{u,c}$	0.00% (0.00 %)	$S_{u,c}$	0.00% (0.00 %)
$S_{u,t}$	0.49% (2.19 %)	$S_{u,t}$	0.00% (0.00 %)

**Table 6.12.** Sensitivities for the stochastic variables for Along-system in year 100 for  $\beta_a = 5.2$ . (..) represents sensitivities when the  $\alpha$ -vector is normalized after removing  $X_{model}$ .

**Table 6.13.** Sensitivities for the stochastic variables for Cross-system in year 100 for  $\beta_a = 5.2$ . (..) represents sensitivities when the  $\alpha$ -vector is normalized after removing  $X_{model}$ .

It can be seen in tables 6.12 and 6.13 that there is a high sensitivity related to  $X_{model}$ . This is to be expected as  $X_{model}$  is raised to the power of  $m$  (respectively  $m = 8.8$  and  $m = 11.8$ ) in the limit state equation. Furthermore it is important to note that Along-system and Cross-system are loaded with different loading patterns which affects the sensitivities of the stochastic variables.

In general, it can be seen that basic variables related to  $R = 0.1$  is of higher importance to the reliability index. This is because the majority of the data is located near this  $R$ -ratio. Additionally, it is noted that even though the standard deviation of  $\Delta$  is high, it is not the parameter that affects the reliability index the most. The static compression strength has 0 % sensitivity due to the load spectrum shape. In the Along-system the tension strength has some influence, as it effects the transformation to  $S_{eq}$  for the cycles under the  $R = 0.1$ -line. In the Cross-system the effect of the static tension strength is insignificant, this is because all load cycles in this load spectrum are located near the  $R = 0.1$ -line, making its influence to the transformation to  $S_{eq}$  small. It can be seen that the physical uncertainty of  $\log K_{R=0.1}$  is of major importance, this can be seen from  $u_{R=0.1}$ .

The annual reliability elasticity coefficient,  $e_p$ , is another measure of sensitivity and is defined by eq. (6.16).

$$e_{p,i} = \frac{d\beta_a}{d p_i} \frac{p_i}{\beta_a} \quad (6.16)$$

Where the parameter,  $p_i$ , is a moment in a distribution or a constant in the limit state equation.  $e_p$  gives a measure of sensitivity as  $p$  is varied by 1% the change in  $\beta_a$  is  $e_p\%$ . Tables 6.14 and 6.15 presents  $e_p$  for the mean and standard deviation of the basic stochastic variables in the limit state equation.

	$e_{p,\mu}$	$e_{p,\sigma}$		$e_{p,\mu}$	$e_{p,\sigma}$
$\Delta$	0.15	-0.05	$\Delta$	0.19	-0.07
$\log K_{R=-1}$	0.00	0.00	$\log K_{R=-1}$	0.61	0.00
$\log K_{R=0.1}$	7.33	$-6.6 \cdot 10^{-3}$	$\log K_{R=0.1}$	8.11	-0.01
$\sigma_{\epsilon_{R=-1}}$	0.00	0.00	$\sigma_{\epsilon_{R=-1}}$	$-0.6 \cdot 10^{-3}$	0.00
$\sigma_{\epsilon_{R=0.1}}$	-0.09	$-8.4 \cdot 10^{-3}$	$\sigma_{\epsilon_{R=0.1}}$	-0.11	-0.01
$X_{model}$	-0.90	-0.52	$X_{model}$	-0.89	-0.48
$S_{u,c}$	0.00	0.00	$S_{u,c}$	0.00	0.00
$S_{u,t}$	0.26	$-3.7 \cdot 10^{-3}$	$S_{u,t}$	0.00	0.00

**Table 6.14.** Reliability elasticity coefficients for Along-system for year 100 at  $\beta_a = 5.2$ . **Table 6.15.** Reliability elasticity coefficients for Cross-system for year 100 at  $\beta_a = 5.2$ .

It can be seen from tables 6.14 and 6.15 that the mean value of  $\log K_{R=0.1}$  is of high influence. This is to be expected as it is  $K_{R=0.1}$  that is used in the limit state equation. Therefore a small change in  $\log K_{R=0.1}$  will have great effect on  $K_{R=0.1}$ . Unlike the  $\alpha^2$ -values, this analysis can also express the importance of the mean values of the input parameters. It is worth noting that the  $u_i$ -parameters are not forgotten, since they are a tool used to model the standard deviation of  $\epsilon_i$ , they are marked as changed in mean value of  $\sigma_{\epsilon_i}$ . It can be seen that the tendencies of  $e_{p,\sigma}$  match those of  $\alpha^2$  shown in tables 6.12 and 6.13.

In figures 6.13 and 6.15, the reliability index as function of the relative changes of mean and standard deviation for Along-system. In figures 6.14 and 6.16 the same is shown for Cross-system.

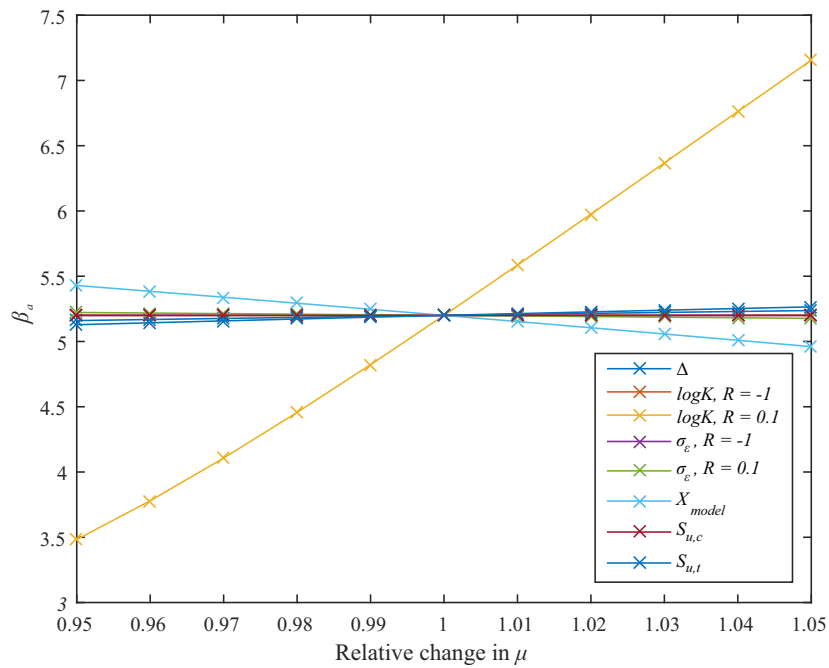


Figure 6.13.  $\beta_a$  as function of relative change in mean for basic stochastic variables in year 100 for Along-system at  $\beta_a = 5.2$ .

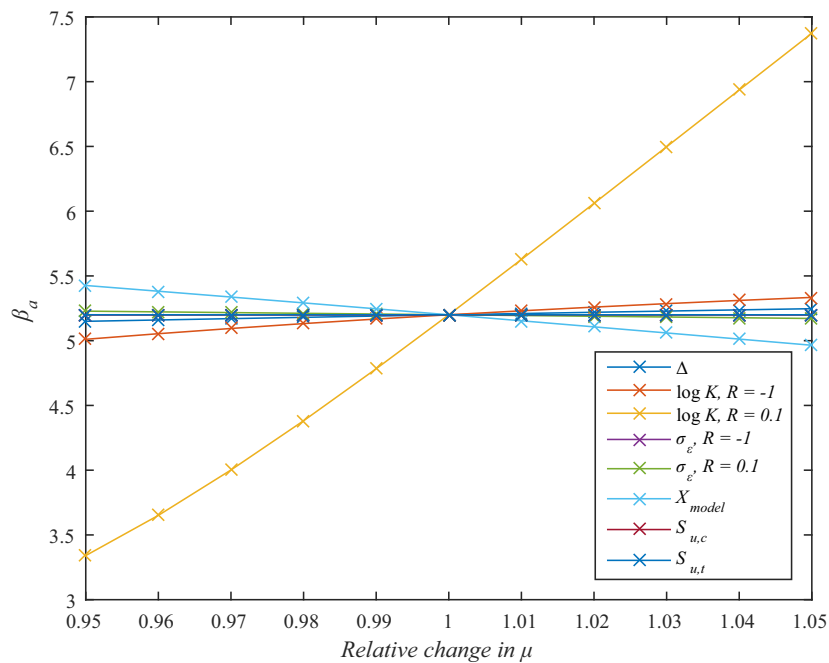


Figure 6.14.  $\beta_a$  as function of relative change in mean for basic stochastic variables in year 100 for Cross-system at  $\beta_a = 5.2$ .

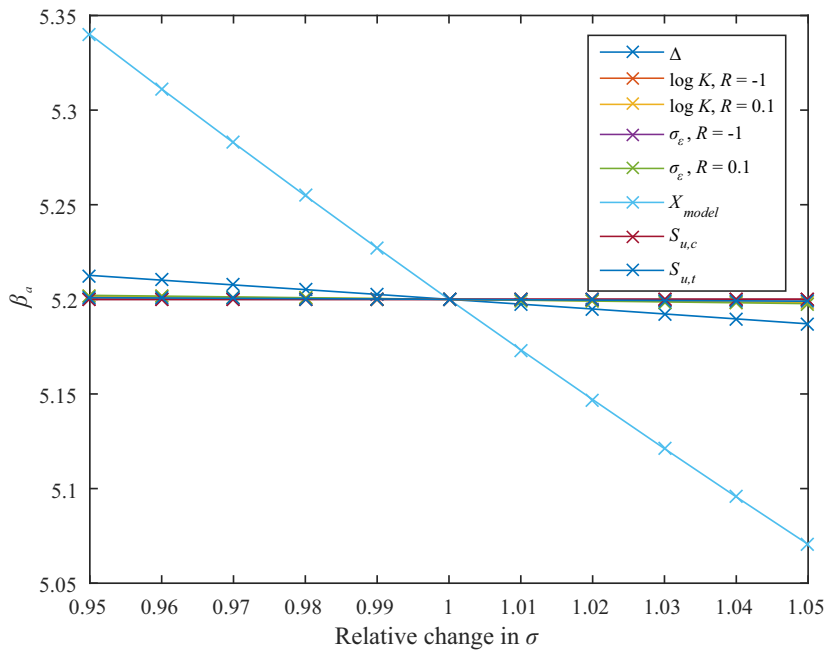


Figure 6.15.  $\beta_a$  as function of relative change in standard deviation for basic variables in year 100 for Along-system at  $\beta_a = 5.2$ .

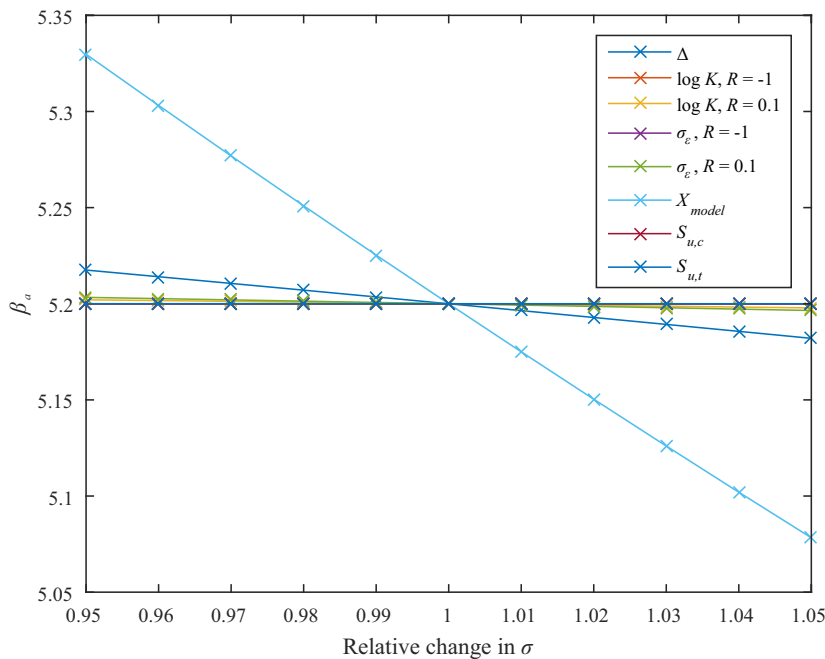


Figure 6.16.  $\beta_a$  as function of relative change in standard deviation for basic variables in year 100 for Cross-system at  $\beta_a = 5.2$ .

Figures 6.13 through 6.16, show the tendencies indicated by the reliability elasticity coefficients in tables 6.14 and 6.15 because the slopes in figures 6.13 through 6.16 are used to calculate the reliability elasticity coefficients. Regarding changes in mean values, change in  $\log K_{R=0.1}$  has the largest effect on the annual reliabil-



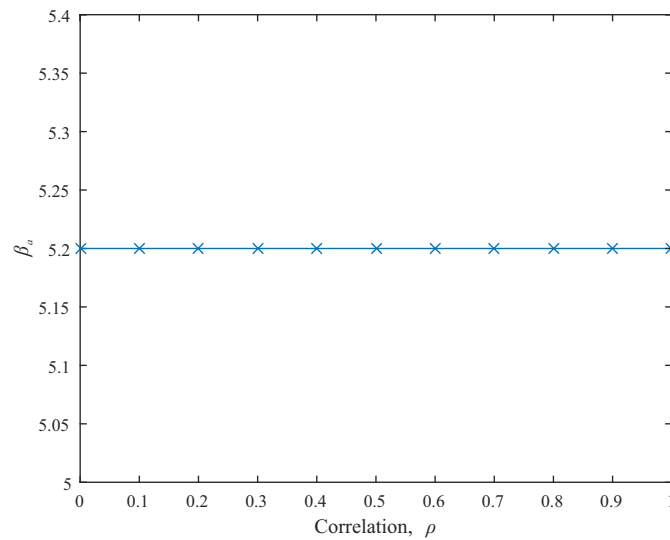


Figure 6.17. Correlation between  $\log K$  for Along-system in year 100 for CC3.

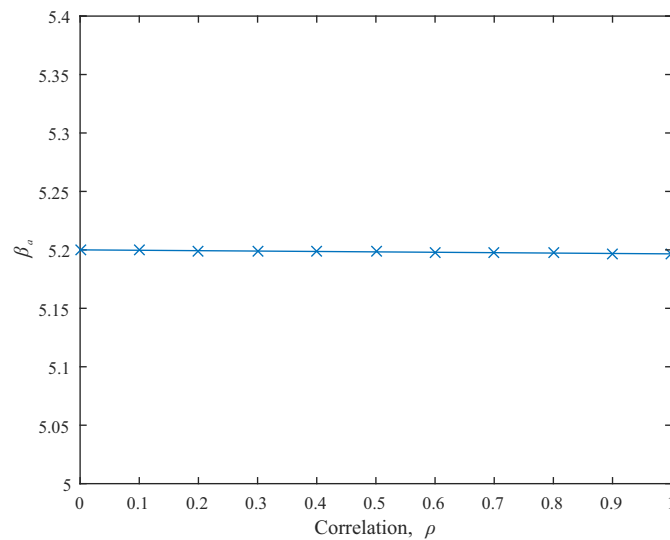


Figure 6.18. Correlation between  $\log K$  for Cross-system in year 100 for CC3.

From figures 6.17 and 6.18, that the correlation is nearly insignificant. This is because of the DNVs fatigue life prediction methods as it the load cycles to the nearest  $R$ -ratio. In both system, load cycles are moved to  $R = 0.1$ , however as seen in figure 5.7 on page 58, the S-N curve at  $R = -1$  affects the slope of the constant life lines between  $R = -1$  and  $R = 0.1$ , and therefore of minor importance.

The assumption of uncorrelated  $\log K_i$  will be maintained since the change in reliability index is below 1 %.



---

# Reliability-Based Calibration of Partial Safety Factors

In the following section, partial safety factors are calibrated for reliability levels CC2 and CC3 for bridges as presented in section 6.3. Partial safety factors are calibrated for multiple design equations depending on the constant life diagram used. The design equation consists of characteristic values of the basic variables and partial safety factors. Generally, in ultimate limit state, partial safety factors are applied to the resistance and the load, this is not the case for fatigue limit state. The partial safety factor can be applied in different ways with different levels of complexity. This section will describe three options for applying the partial safety factor to the load and their corresponding design equations. First, according to DS/INF 172 which applies partial safety factors to the cyclic stress amplitude. Second, according to the Germanischer Lloyd which applies the partial safety factors to both the cyclic stress amplitude and the cyclic mean stress. Two modifications to the application of partial safety factors for fatigue are tested, the fatigue design factor and a reduction of Miners rule in the design equation. Lastly, an adjustment to the partial safety factors is conducted based on the length of the bridge system.

All reliability calculations performed in this chapter are performed with the piecewise linear constant life diagram.

Overview of partial safety factors can be found on [Appendix-CD, *Gamma*].

## 7.1 Partial Safety Factors as DS/INF 172

As described in section 2.2, no Eurocodes are available for fiber-reinforced polymer materials, however, in DS/INF 172, the partial safety factors,  $\gamma_f \gamma_m$ , is defined and applied to the cyclic stress amplitudes for steel. If this is applied to fiber-reinforced polymer materials, the design equation becomes as shown in equations (7.1), (7.2) and (7.3) depending on which constant life diagram is used.

$$G_{PL} = 1 - t \cdot D(n, S_a \cdot \gamma_f \gamma_m, S_m, \log K_{c,R=-1}, \log K_{c,R=0.1}, m_{R=-1}, m_{R=0.1}, S_{u,c,c}, S_{u,t,c}) = 0 \quad (7.1)$$

$$G_{SGM_{R=-1}} = 1 - t \cdot D(n, S_a \cdot \gamma_f \gamma_m, S_m, \log K_{c,R=-1}, m_{R=-1}, S_{u,c,c}, S_{u,t,c}) = 0 \quad (7.2)$$

$$G_{SGM_{R=0.1}} = 1 - t \cdot D(n, S_a \cdot \gamma_f \gamma_m, S_m, \log K_{c,R=0.1}, m_{R=0.1}, S_{u,c,c}, S_{u,t,c}) = 0 \quad (7.3)$$

In equations (7.1), (7.2) and (7.3), characteristic values presented in table 4.15 on page 47.  $\gamma_f$  is partial safety factor for fatigue load and  $\gamma_m$  is partial safety factor for fatigue strength, both applied to the cyclic stress amplitude. As seen in equations (7.1), (7.2) and (7.3), the partial safety factor is applied before calculation of accumulated damage. As DS/INF 172 focus on welded steel, the cyclic mean stresses are normally not of importance, however for fiber-reinforced polymer materials the cyclic mean stresses is of importance and a suggestion could be to add the partial safety factor to the cyclic mean stresses as well. But depending on the constant life diagrams appearance this could increase the fatigue life of the structure instead of lowering it as intended.

The product of  $\gamma_f$  and  $\gamma_m$  is defined in eq. (7.4).

$$\Pi\gamma = \gamma_f \gamma_m \quad (7.4)$$

In this report,  $\gamma_f$  and  $\gamma_m$  are divided into the following partial safety factors to see the effect of the individual uncertainties have on  $\Pi\gamma$ .

$$\gamma_f = \gamma_{Model} \gamma_{Load} \quad (7.5)$$

$$\gamma_m = \gamma_{Mat} \gamma_{Stat} \quad (7.6)$$

where

$\gamma_{Model}$	Partial safety factor related to $X_{Model}$
$\gamma_{Load}$	Partial safety factor related to realized uncertainties: $X_{Load}$ , $X_{Dyn}$ and $X_{Pos}$
$\gamma_{Mat}$	Partial safety factor related to the material uncertainty
$\gamma_{Stat}$	Partial safety factor related to the statistical uncertainty

Partial safety factors are calibrated using design equations shown in equations (7.1), (7.2) and (7.3). A design parameter,  $z_d$ , estimated using the fatigue limit state for CC2 ( $\beta_a = 4.8$ ) and CC3 ( $\beta_a = 5.2$ ) is used. The partial safety factor is calibrated when the design equation is equal to zero.

In order to determine the partial safety factors defined in equations (7.5) and (7.6), a design parameter,  $z_d$ , is determined for the fatigue limit state for four cases shown in table 7.1. Table 7.1 shows which uncertainties is taken into consideration in each case. Case 1 is the case calculated in section 6.5. In Case 2,  $X_{Model}$  is assumed deterministic with its expected value of 1.0, this results in a lower  $z_d$  and as consequence a lower partial safety factor. By comparing the partial safety factors for Case 1 and 2,  $\gamma_{X_{Model}}$  can be determined.

**Table 7.1.** Cases used for estimation of partial safety factors defined in equations (7.5) and (7.6).  $\gamma_{Mat}$  is presented in table 7.6.

Uncertainties related to						
	Material	Statistical	Load range	Stress conversion	Result	Used to obtain
	$\Delta$ $\mu_{\log K}$ $\sigma_\epsilon$	$\sigma_{\log K}$ $\sigma_{\sigma_\epsilon}$	$X_{Dyn}$ $X_{Load}$ $X_{Pos}$	$X_{Model}$		
Case 1	×	×	×	×	$\gamma_{Case1}$	$\Pi\gamma$ ; tables 7.2
Case 2	×	×	×		$\gamma_{Case2}$	$\gamma_{X_{Model}}$ tables 7.3
Case 3	×	×		×	$\gamma_{Case3}$	$\gamma_{Real}$ tables 7.4
Case 4	×		×	×	$\gamma_{Case4}$	$\gamma_{Stat}$ tables 7.5

In tables 7.2, partial safety factors are presented for Case 1 for Along-system and Cross-system for CC2 and CC3 where all uncertainties are taken into consideration.

**Table 7.2.** Case 1.  $\Pi\gamma$  based on DS/INF 172 for CC2 and CC3 for Along-system and Cross-system.  $CLD_{PL}$ : Piecewise linear constant life diagram.  $CLD_{SGM_{R=-1}}$ : Shifted Goodman diagram using  $R = -1$ .  $CLD_{SGM_{R=0.1}}$ : Shifted Goodman diagram using  $R = 0.1$ .

$\Pi\gamma = \gamma_{Case1}$	Along-system			Cross-system		
	CC2	CC3	$\frac{CC3}{CC2}$	CC2	CC3	$\frac{CC3}{CC2}$
$CLD_{PL}$	2.00	2.14	1.07	1.99	2.12	1.07
$CLD_{SGM_{R=-1}}$	2.05	2.20	1.07	2.01	2.14	1.06
$CLD_{SGM_{R=0.1}}$	2.00	2.14	1.07	1.67	1.76	1.05

From tables 7.2 and 7.9, it can be seen that partial safety factors for CC2 are lower than for CC3 as expected. Additionally,  $CLD_{PL}$  and  $CLD_{SGM_{R=0.1}}$  yields the same partial safety factors in the Along-system. This is because the entire load spectrum is located between  $R = 0.1$  and  $R = 1$ , with high mean tensile stresses relative to their amplitude stresses.

Furthermore, it can be seen that the  $CLD_{SGM_{R=-1}}$  constant life diagram yields higher partial safety factors. Furthermore it can be seen that instead of defining partial safety factors for CC3, a consequence class factor,  $\frac{CC3}{CC2}$ , can be defined. Applying this to the partial safety factors for CC2 yields the appropriate safety level for CC3.  $\frac{CC3}{CC2}$  value is around 1.07 compared to the consequence class factor,  $K_{FI}$ , defined in DS/EN 1990 DK NA with a value of 1.1.

$\gamma_{Model}$  (found by Case 2) is calculated by assuming  $X_{Model}$  deterministic at its expected value of 1.0.  $\gamma_{Model}$  is shown in table 7.3.

**Table 7.3.** Case 2.  $\gamma_{Model}$  based on DS/INF 172 for CC2 and CC3 for Along-system and Cross-system.  $CLD_{PL}$ : Piecewise linear constant life diagram.  $CLD_{SGM_{R=-1}}$ : Shifted Goodman diagram using  $R = -1$ .  $CLD_{SGM_{R=0.1}}$ : Shifted Goodman diagram using  $R = 0.1$ .

$\gamma_{Model} = \frac{\gamma_{Case1}}{\gamma_{Case2}}$	Along-system		Cross-system	
	CC2	CC3	CC2	CC3
$CLD_{PL}$	1.33	1.37	1.25	1.28
$CLD_{SGM_{R=-1}}$	1.33	1.37	1.24	1.27
$CLD_{SGM_{R=0.1}}$	1.33	1.37	1.20	1.22

From table 7.3, it can be seen that  $\gamma_{Model}$  is constant in the Along-system for both CC2 and CC3, but is not constant in the Cross-system. This is due to the load spectrums placement in the constant life diagram.

$\gamma_{Load}$  (Case 3) is determined by not applying  $X_{Load}$ ,  $X_{Dyn}$  and  $X_{Pos}$  to the load spectrum and presented in table 7.4.

**Table 7.4.** Case 3.  $\gamma_{Load}$  based on DS/INF 172 for CC2 and CC3 for Along-system and Cross-system.  $CLD_{PL}$ : Piecewise linear constant life diagram.  $CLD_{SGM_{R=-1}}$ : Shifted Goodman diagram using  $R = -1$ .  $CLD_{SGM_{R=0.1}}$ : Shifted Goodman diagram using  $R = 0.1$ .

$\gamma_{Load} = \frac{\gamma_{Case1}}{\gamma_{Case3}}$	Along-system		Cross-system	
	CC2	CC3	CC2	CC3
$CLD_{PL}$	1.19	1.18	1.26	1.26
$CLD_{SGM_{R=-1}}$	1.19	1.18	1.26	1.25
$CLD_{SGM_{R=0.1}}$	1.19	1.18	1.21	1.21

It is notable that in table 7.4, CC2 yields higher partial safety factors than for CC3, but  $\Pi\gamma$  increases in table 7.2, but it should be noted that this effect is very small. Therefore the importance of the uncertainties related to  $\gamma_{Load}$  is decreased as the annual reliability index is increased.

Moreover, the partial safety factors for the Along-system are constant in both CC2 and CC3 for the different constant life diagrams. This is not the case for the Cross-system. This is likely due to the load spectrums placement for the Along-system and Cross-system in the constant life diagram.

$\gamma_{Stat}$  (Case 4) is determined by not including  $\sigma_{\log K}$  and  $\sigma_{\sigma_e}$  in the reliability calculation.  $\gamma_{Stat}$  presented in table 7.5.

**Table 7.5.** Case 4.  $\gamma_{Stat}$  based on DS/INF 172 for CC2 and CC3 for Along-system and Cross-system.  $CLD_{PL}$ : Piecewise linear constant life diagram.  $CLD_{SGM_{R=-1}}$ : Shifted Goodman diagram using  $R = -1$ .  $CLD_{SGM_{R=0.1}}$ : Shifted Goodman diagram using  $R = 0.1$ .

$\gamma_{Stat} = \frac{\gamma_{Case1}}{\gamma_{Case4}}$	Along-system		Cross-system	
	CC2	CC3	CC2	CC3
$CLD_{PL}$	1.01	1.01	1.01	1.01
$CLD_{SGM_{R=-1}}$	1.01	1.01	1.01	1.01
$CLD_{SGM_{R=0.1}}$	1.01	1.01	1.01	1.01

It can be seen from table 7.5 that the partial safety factor related to the statistical uncertainty is close to 1.0. The number of fatigue tests used in chapter 4 for each of the S-N curve (12 tests) are below the recommended amount of data (25-30 tests) needed for using Maximum-Likelihood Method. Therefore the statistical uncertainty may not have converged towards a Normal distribution, and the estimation using Maximum-Likelihood Method might not be accurate.

As  $\Pi\gamma$ ,  $\gamma_{Model}$ ,  $\gamma_{Load}$  and  $\gamma_{Stat}$  are determined,  $\gamma_{Mat}$  can be calculated.  $\gamma_{Mat}$  is presented in table 7.6.

**Table 7.6.**  $\gamma_{Mat}$  based on DS/INF 172 for CC2 and CC3 for Along-system and Cross-system.  $CLD_{PL}$ : Piecewise linear constant life diagram.  $CLD_{SGM_{R=-1}}$ : Shifted Goodman diagram using  $R = -1$ .  $CLD_{SGM_{R=0.1}}$ : Shifted Goodman diagram using  $R = 0.1$ .

$\gamma_{Mat} = \frac{\gamma_{Case1}}{\gamma_{Model}\gamma_{Load}\gamma_{Stat}}$	Along-system		Cross-system	
	CC2	CC3	CC2	CC3
$CLD_{PL}$	1.26	1.32	1.26	1.31
$CLD_{SGM_{R=-1}}$	1.29	1.35	1.28	1.33
$CLD_{SGM_{R=0.1}}$	1.26	1.32	1.15	1.19

Comparing tables 7.3, 7.4, 7.5 and 7.6,  $\gamma_{Model}$  yields the highest partial safety factors followed by  $\gamma_{Load}$  and  $\gamma_{Mat}$  indicating that  $X_{Model}$  contributes with most uncertainty which corresponds with the sensitivity analysis in section 6.6. The product of the partial safety factors in tables 7.3, 7.4, 7.5 and 7.6 result in the partial safety factors presented in table 7.2.

$\gamma_f$  and  $\gamma_m$  can now be determined from previously determined partial safety factors using equations (7.5) and (7.6) and is presented in table 7.7.

**Table 7.7.**  $\gamma_f$  and  $\gamma_m$  based on DS/INF 172 for CC2 and CC3 for Along-system and Cross-system.  $CLD_{PL}$ : Piecewise linear constant life diagram.  $CLD_{SGM_{R=-1}}$ : Shifted Goodman diagram using  $R = -1$ .  $CLD_{SGM_{R=0.1}}$ : Shifted Goodman diagram using  $R = 0.1$ . Critical design case highlighted.

	CC2		CC3	
	Along-system			
	$\gamma_f$	$\gamma_m$	$\gamma_f$	$\gamma_m$
$CLD_{PL}$	1.58	1.27	1.62	1.32
$CLD_{SGM_{R=-1}}$	<b>1.58</b>	<b>1.30</b>	<b>1.62</b>	<b>1.36</b>
$CLD_{SGM_{R=0.1}}$	1.58	1.27	1.62	1.32
	Cross-system			
$CLD_{PL}$	1.57	1.26	1.61	1.32
$CLD_{SGM_{R=-1}}$	1.56	1.29	1.59	1.34
$CLD_{SGM_{R=0.1}}$	1.44	1.16	1.47	1.20

In table 7.7, the critical design cases is highlighted. These values are used to compute recommended values for use in design by Level 1 methods. Therefore the recommended values gives the possibility of using the three constant life diagrams shown above in the design equation. The critical case is the Along-system designed by  $CLD_{SGM_{R=-1}}$ . This corresponds well with figure 4.8 on page 42. The Along-system is critical due to the significantly higher mean stresses exerted by the dead load. If the Cross-system was designed with a material with higher density compared to the composite material resulting in higher mean stresses the result may have changed.

In table 7.8, the recommended partial safety factors are shown.

**Table 7.8.** Recommended values for  $L_A = 15$  m.

Recommended partial safety factors			
	$\gamma_f$	$\gamma_m$	$K_{FI}$
CC2	1.6	1.3	1.1

The partial safety factors shown in table 7.8 is only valid when the Along-system or Cross-system is representative and when their associated uncertainties and constant life diagrams are representative.  $\gamma_f$  and  $\gamma_m$  in table 7.8 is based on the table 7.7 and is determined as the highest partial safety factor rounded to one decimal. The consequence class factor,  $K_{FI}$ , is applied as shown in eq. (7.7).  $K_{FI}$  is applied to the partial safety factors when designing for CC3. If designing for CC2,  $K_{FI}$  is 1.0. The consequence class factor is based on  $\frac{CC3}{CC2}$  relations shown in table 7.2.

$$K_{FI}\gamma_f\gamma_m \quad (7.7)$$

The product of the recommended  $\gamma_f$  and  $\gamma_m$  is calculated for CC2 and CC3.

$$\begin{aligned} \text{CC2: } & 1.6 \cdot 1.3 = 2.08 > 2.05 \\ \text{CC3: } & 1.6 \cdot 1.3 \cdot 1.1 = 2.28 > 2.20 \end{aligned} \quad (7.8)$$

Where 2.05 and 2.20 are  $\Pi\gamma$ -values from table 7.2 for  $CLD_{SGM_{R=-1}}$  for CC2 and CC3 in the Along-system.

As seen above, the recommended values yield slightly higher  $\Pi\gamma$ -values.

## 7.2 Partial Safety Factors as Germanischer Lloyd

Germanischer Lloyd applies partial safety factors on both cyclic amplitude stresses and cyclic mean stresses and the design equation becomes eq. (7.9).

$$G_{GL} = 1 - t \cdot D(n, S_a \cdot \gamma_{Mb}, S_m \cdot \gamma_{Ma}, S_{u,c,c}, S_{u,t,c}, m_{R=-1}) = 0 \quad (7.9)$$

As seen in eq. (7.9), Germanischer Lloyd applies two separate partial safety factors to respectively the cyclic stress amplitude and cyclic mean stress where Eurocode only applies partial safety factors to the cyclic stress amplitude.

The partial safety factor calibrated using the constant life diagram suggested by Germanischer Lloyd is not divided into sub partial safety factors as Germanischer Lloyd has defined in their standard which uncertainties  $\gamma_{Ma}$  and  $\gamma_{Mb}$  covers. It should be noted that the partial safety factors defined by Germanischer Lloyd in their guideline are for wind turbine blades and the target reliability level the partial safety factors are calibrated for is in accordance with reliability levels for wind turbines.  $\gamma_{Ma}$  is assumed 1.35 for fatigue analysis and only  $\gamma_{Mb}$  is calibrated.

$\gamma_{Mb}$  is calibrated using design equation shown in eq. (7.9). A design parameter,  $z_d$ , estimated using the fatigue limit state for CC2 ( $\beta_a = 4.8$ ) and CC3 ( $\beta_a = 5.2$ ) is used.

$\gamma_{Mb}$  for CC2 and CC3 for Along-system and Cross-system is presented in table 7.9.

**Table 7.9.**  $\gamma_{Mb}$  based on Germanischer Lloyd for CC2 and CC3 for Along-system and Cross-system.  $CLD_{GL}$ : Shifted Goodman diagram by Germanischer Lloyd.

$\gamma_{Mb}$	Along-system			Cross-system		
	CC2	CC3	$\frac{CC3}{CC2}$	CC2	CC3	$\frac{CC3}{CC2}$
$CLD_{GL}$	1.77	1.91	1.08	1.72	1.81	1.05

$CLD_{GL}$  yields the lower partial safety factors when compared to table 7.2. This is expected as it predicts higher damage as seen in figure 4.8 on page 42 and  $\gamma_{Ma} = 1.35$  is applied to the cyclic mean stresses. The consequence class factor,  $\frac{CC3}{CC2}$ , is intended to be applied to  $\gamma_{Mb}$  as this would achieve the require annual target reliability level. Applying the consequence class factor to  $\gamma_{Ma}$  as well would yield an annual reliability level higher than the annual target reliability according to CC3 of  $\beta_a = 5.2$ .

In table 7.10, the recommended  $\gamma_{Ma}$  and  $\gamma_{Mb}$  are shown.

**Table 7.10.** Recommended values for  $L_A = 15$  m.

Recommended partial safety factors			
	$\gamma_{Ma}$	$\gamma_{Mb}$	$K_{FI}$
CC2	1.35	1.75	1.1

The partial safety factors shown in table 7.10 is only valid when the Along-system or Cross-system is representative.  $\gamma_{Mb}$  is based on table 7.9 and is determined as the highest partial safety factor rounded to one decimal. The consequence class factor,  $K_{FI}$ , is applied as shown in eq. (7.10).  $K_{FI}$  is applied to the partial safety factors when designing for CC3. If designing for CC2,  $K_{FI}$  is 1.0. The consequence class factor is based on  $\frac{CC3}{CC2}$  relations shown in table 7.9.  $K_{FI}$  is only applied to  $\gamma_{Mb}$  as it is the partial safety factor being calibrated. Applying  $K_{FI}$  to  $\gamma_{Ma}$  would yield a higher target reliability index than that for CC3.

$$K_{FI}\gamma_{Mb} \quad (7.10)$$

The recommended  $\gamma_{Mb}$  is calculated for CC2 and CC3.

$$\begin{aligned} \text{CC2:} & \quad 1.75 & \approx & \quad \frac{1.72+1.77}{2} \\ \text{CC3:} & \quad 1.75 \cdot 1.1 = 1.93 & > & \quad 1.91 \end{aligned}$$

As seen above the recommended values yield slightly higher  $\gamma_{Mb}$ -values for CC3. This is deemed acceptable as it reduces the complexity in the Level 1 method.

### 7.3 Fatigue Design Factor as DS/INF 172

DS/INF 172 also suggest a fatigue design factor,  $FDF$ , applied to the design life as shown in equations (7.11), (7.12) and (7.13) depending on which constant life diagram is applied.

$$G_{PL} = 1 - t \cdot FDF \cdot D(n, S_a, S_m, \log K_{c,R=-1}, \log K_{c,R=0.1}, m_{R=-1}, m_{R=0.1}, S_{u,c,c}, S_{u,t,c}) = 0 \quad (7.11)$$

$$G_{SGM_{R=-1}} = 1 - t \cdot FDF \cdot D(n, S_a, S_m, \log K_{c,R=-1}, m_{R=-1}, S_{u,c,c}, S_{u,t,c}) = 0 \quad (7.12)$$

$$G_{SGM_{R=0.1}} = 1 - t \cdot FDF \cdot D(n, S_a, S_m, \log K_{c,R=0.1}, m_{R=0.1}, S_{u,c,c}, S_{u,t,c}) = 0 \quad (7.13)$$

where  $FDF$  is defined DS/INF 172 as.

$$FDF = (\gamma_f \gamma_m)^m \quad (7.14)$$

The transformation shown in eq. (7.14) is valid when one linear  $S$ - $N$  curve is used without a constant life diagram (no mean stress). Due to the complex damage estimation, and the possibility of multiple  $m$ -values, in a constant life diagram,  $FDF$  has to be defined separately and eq. (7.14) is not applied.

$FDF$  is calibrated by estimating the damage in year 100 with a design parameter corresponding to an annual target reliability level of 4.8 (CC2) and 5.2 (CC3).

In tables 7.11,  $FDF$ -values are presented.

**Table 7.11.** Fatigue design factors based on DS/INF 172 for CC2 and CC3 for Along-system and Cross-system.  $CLD_{PL}$ : Piecewise linear constant life diagram.  $CLD_{SGM_{R=-1}}$ : Shifted Goodman diagram using  $R = -1$ .  $CLD_{SGM_{R=0.1}}$ : Shifted Goodman diagram using  $R = 0.1$ .

$FDF$	Along-system		Cross-system	
	CC2	CC3	CC2	CC3
$CLD_{PL}$	1514	3248	1130	2190
$CLD_{SGM_{R=-1}}$	538	1003	465	794
$CLD_{SGM_{R=0.1}}$	1514	3248	1082	2122

In table 7.11,  $CLD_{PL}$  and yielding the highest  $FDF$ . An obvious tendency for table 7.11 is the exceptionally high numbers. It would likely feel unintuitive for an engineer to design a structure with a fatigue life of over 300 000 years ( $3248 \cdot t$ ). As a result, the fatigue design factor will not be investigated any further.

## 7.4 Reduction of Characteristic Value of Miner's Rule

Tables 7.2 through 7.11 are obtained with Miner's rule equal to 1.0 in the design equation. With regards to tables 6.6 and 6.7 on page 98 presenting design value in physical space, a lower value of Miner's rule can be suggested for the design equations. If Miner's rule equal to 0.5 is applied in the design equation instead of 1.0, the partial safety factors presented in tables 7.12 and 7.13 are obtained. Miner's rule equal to 0.5 corresponding to a safety factor of  $0.5^{-\frac{1}{m}}$  applied to the cyclic stress amplitudes.

**Table 7.12.** Case 1.  $\Pi\gamma$  based on DS/INF 172 for CC2 and CC3 for Along-system and Cross-system with Miner's rule set to 0.5.  $CLD_{PL}$ : Piecewise linear constant life diagram.  $CLD_{SGM_{R=-1}}$ : Shifted Goodman diagram using  $R = -1$ .  $CLD_{SGM_{R=0.1}}$ : Shifted Goodman diagram using  $R = 0.1$ .

$\Pi\gamma = \gamma_{Case1}$	Along-system			Cross-system		
	CC2	CC3	$\frac{CC3}{CC2}$	CC2	CC3	$\frac{CC3}{CC2}$
$CLD_{PL}$	1.87	2.00	1.07	1.85	1.96	1.06
$CLD_{SGM_{R=-1}}$	1.90	2.04	1.07	1.86	1.98	1.06
$CLD_{SGM_{R=0.1}}$	1.87	2.00	1.07	1.63	1.73	1.06

**Table 7.13.**  $\gamma_{Mb}$  based on Germanischer Lloyd for CC2 and CC3 for Along-system and Cross-system with Miner's rule set to 0.5.  $CLD_{GL}$ : Shifted Goodman diagram by Germanischer Lloyd.

$\gamma_{Mb}$	Along-system			Cross-system		
	CC2	CC3	$\frac{CC3}{CC2}$	CC2	CC3	$\frac{CC3}{CC2}$
$CLD_{GL}$	1.54	1.62	1.05	1.63	1.73	1.06

As expected tables 7.12 and 7.13 show the same tendencies as tables 7.2 and 7.9 but with lower partial safety factors. As the decrease in the partial safety factors is only slight and the impression of only using half of the fatigue life is unintuitive, the characteristic value of Miner's rule will be kept at 1.0, similar to that of steel defined in DS/EN 1993-1-9.

## 7.5 The Bridge Spans Influence on Reliability Level

In the following section, it is studied how the bridge span affect  $\Pi\gamma$  and  $\beta_a$ . Only the Along-system is investigated in this section.

In figure 7.1,  $\Pi\gamma$  as function of bridge section length is shown. At every bridge section length, a design parameter,  $z_d$ , is determined corresponding to a annual target reliability level of CC2 ( $\beta_a = 4.8$ ) and CC3 ( $\beta_a = 5.2$ ) using the piecewise linear constant life diagram to estimate fatigue life. The design parameters are used in the design equation,  $G_{PL}$ , shown in eq. (7.1) and  $\Pi\gamma$  is calibrated so that  $G_{PL} = 0$ .

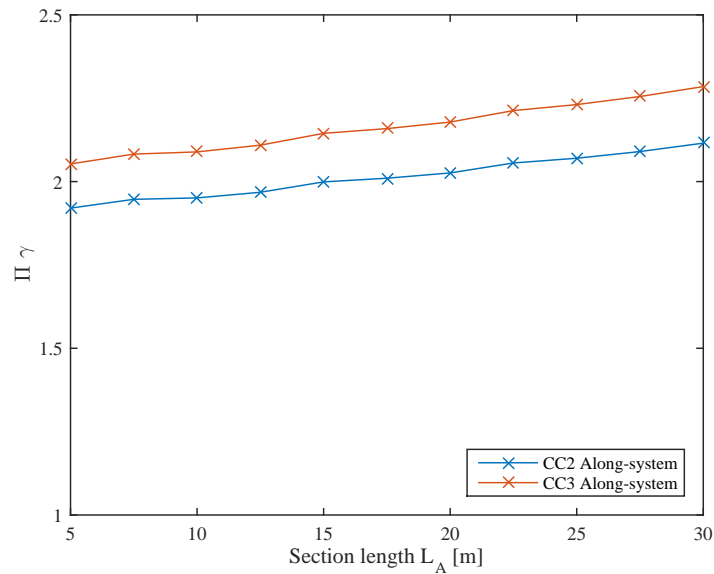
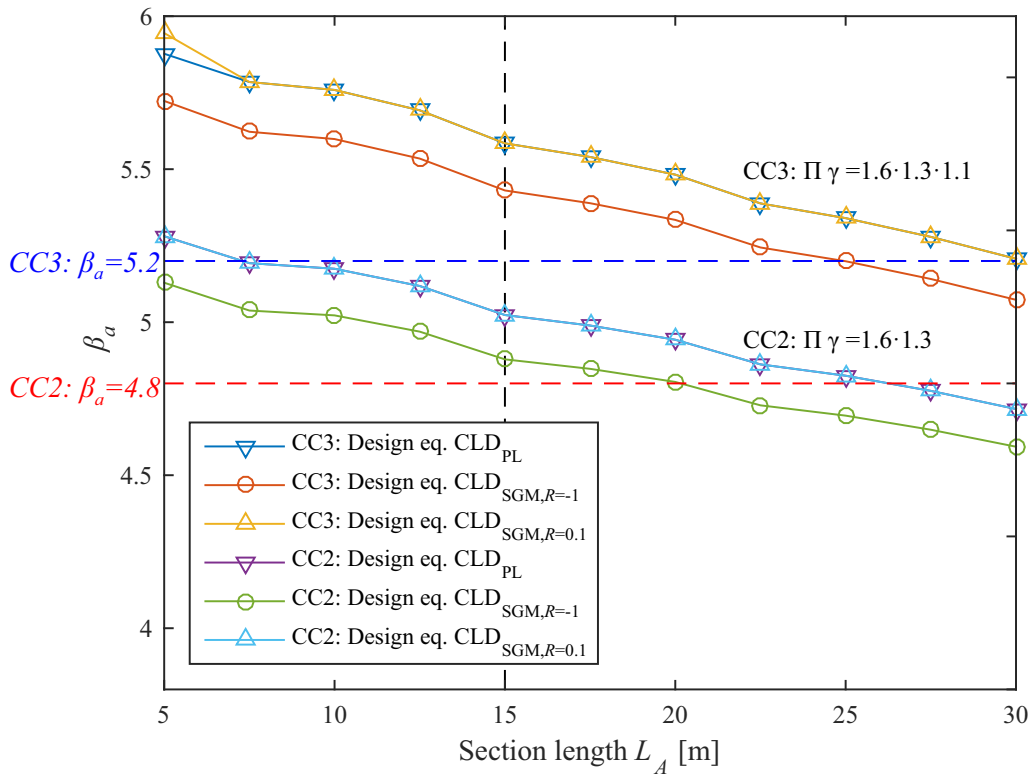


Figure 7.1.  $\Pi\gamma$  as function of bridge section length.

From figure 7.1, it can be seen that changed in bridge span has little effect on  $\Pi\gamma$ . It can be seen that the required partial safety factor increase with bridge section length. This is because higher mean stresses will be introduced when increasing the length of the bridge span.

Using the design equations (7.1), (7.2) and (7.3) as well as the recommended  $\gamma_f$  and  $\gamma_m$  from table 7.8 on page 114, the annual reliability levels as function of the bridge section length can be estimated in order to investigate the safety level obtained using Level 1 methods.

Using the design equations, a design parameter can be determined for different bridge spans so that  $G = 0$  for CC2 and CC3.  $K_{FI} = 1.1$  is used for CC3. The design parameters are used in the fatigue limit state equation estimating an annual reliability index. In figure 7.2, the annual reliability index as function of the bridge section length is shown. Additionally, the target reliability for CC2 and CC3 is plotted.



**Figure 7.2.**  $\beta_a$  as function of bridge section length.  $\beta_a$  is based on recommended  $\gamma_f$  and  $\gamma_m$ -values.

As seen from figure 7.2, the three constant life diagrams at both CC2 and CC3 are above the annual target reliability levels at  $L_A = 15$  m. This is because the recommended  $\gamma_f$  and  $\gamma_m$ -values yields a higher safety level as illustrated in eq. (7.8). For CC2 and CC3 the mean annual reliability level from the three the constant life diagrams at all presented lengths is respectively  $\bar{\beta}_a = 4.94$  and  $\bar{\beta}_a = 5.49$ . As expected the annual reliability decreases with increase in bridge section length which corresponds well with figure 7.1.

A suggestion could be made to adjust the partial safety factors so that the mean annual reliability index are approximately equal to  $\beta_a = 4.8$  and  $\beta_a = 5.2$  for CC2 and CC3 as shown in figure 7.3. By adjusting the partial safety factors to the mean reliability index, structures designed using the partial safety factors will have a mean reliability index of  $\beta_a = 4.8$  and  $\beta_a = 5.2$  for CC2 and CC3. This suits the definition of a target reliability index. In figure 7.3,  $\gamma_f$  is lowered from the recommended value of 1.6 to 1.55. The 1.55 correspond well to the mean value of all  $\gamma_f$  values presented in table 7.7 for CC2.

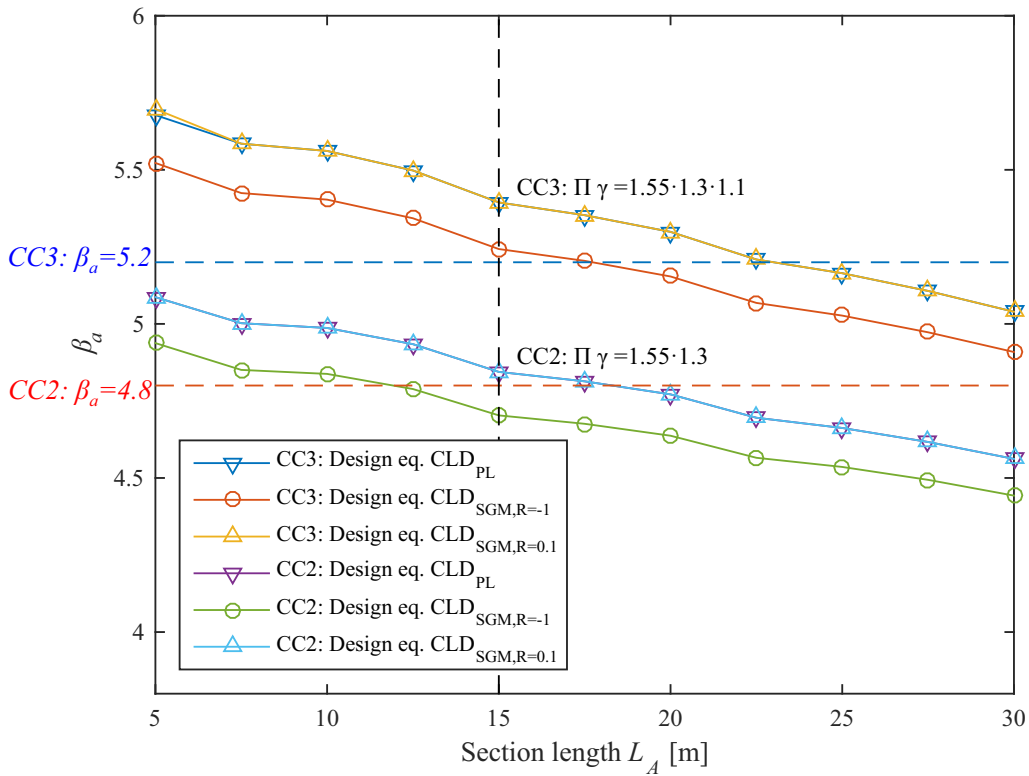


**Figure 7.3.**  $\beta_a$  as function of bridge section length.  $\beta_a$  is based on adjusted recommended  $\gamma_f$  and  $\gamma_m$ -values.

For CC2 and CC3, the mean reliability level from the three the constant life diagrams is respectively  $\bar{\beta}_a = 4.77$  and  $\bar{\beta}_a = 5.30$  using the adjusted recommended partial safety factors. By lowering  $\gamma_f$ , the mean reliability levels are more in line with the annual target reliability levels of  $\beta_a = 4.8$  and  $\beta_a = 5.2$  for CC2 and CC3. It can be seen that the mean reliability level is slightly higher than CC3, this can be lowered by reducing the consequence class factor,  $K_{FI}$ .

The lowered value of  $\gamma_f = 1.55$  will be recommended.

---

## Discussion

In the following chapter, a discussion regarding choices and assumption made in the report is conducted. Additionally, further analysis that could have improved the objectives of the report are elaborated upon.

On the subject of choosing a representative static system, two static system were investigated. To ensure that the partial safety factors are representative, more static systems could have been studied to assure that the partial safety factors are representative in all cases. Investigating more static system could change the partial safety factors. Regarding the Cross-system presented in section 3.2, a low static load (dead load) is used as the system was a composite bridge deck. If a larger dead load is used e.g. composite reinforced concrete, the partial safety factors could change.

In section 2.1, four constant life diagrams are presented. It is assumed that the linear constant life diagram describes the fatigue life best as it uses most information from different  $S-N$  curves. Optimally the investigated material would have data at more  $R$ -ratios available. Other constant life diagrams could have been studied such as the non-linear constant life diagram where a  $S_a-R$ -plane is used to derive the constant life diagram. The model uncertainty related to the constant life diagram and  $S-N$  curve can be improved by choosing a better model.

In section 4.1, characterization of static and fatigue properties of a real applicable material should have been conducted using experimental data. Unfortunately, the amount of fatigue tests received for an applicable material were insufficient for a statistical analysis. Furthermore the tests were conducted with entire specimens cast into concrete. As such the test plans have been made for fatigue in concrete, rather than for composite. Instead, experimental data for a similar composite material is used. The similar composite material has lower fiber volume which affect the mechanical properties of the material, and experimental data was performed on test coupons and not on reinforcement bars. This can change the failure mode of the test specimen.

Of the experimental data used in the report, only three static compression tests and five static tension tests are available, which is not sufficient for a statistical analysis. In order to accurately determined the static strengths of the composite

material more experimental data should be used.

The fatigue tests used in this report generally fail at a relatively low amount of stress cycles ( $10^4$ - $10^6$ ) and therefore the accuracy of the  $S$ - $N$  curves at high amount of stress cycles (low fatigue load) may be questionable. Unfortunately performing fatigue tests for stress cycles above this amount is exceptionally time consuming and therefore impractical. The tested material had 12 fatigue tests available at each of two  $R$ -ratios. This is not enough tests to determine the statistical uncertainty of the material properties properly. Furthermore a composite material used for reinforcement, should be tested for compression fatigue as well. As such, more tests at compression  $R$ -ratios would be important, as composite often do not benefit from compressive mean stresses. Furthermore, not working with a real applicable material makes the entire reliability analysis, only valid in its manner of approach. All material fatigue properties vary greatly in composites. Even advantageous/disadvantageous behavior at tension or compressive mean stresses vary in composites. Therefore a set of general partial safety factors for composites should be calibrated based on multiple materials.

In chapter 5, fatigue load model 4 according to DS/EN 1991-2 is presented. This load model may be the most extensive load model presented in DS/EN 1991-2 besides the use of traffic data, but it is still a simplification. Three uncertainties have been applied to the load model to simulate a load signal from traffic. The uncertainties take varying load of lorries, varying position and variation in exertion of force upon the bridge into account. These are all applied to single lorry crossings. At any time, no more than one lorry will be crossing the bridge, not even in the opposite lane. This simplification is significant, since many bridges are designed by a traffic jam load case, but for small traffic bridges the simplification becomes less important. Daily traffic jams, could cause fatigue more critical than that estimated by the current model. Simulating multiple lorries crossing the bridge by a Poisson process with varying traffic intensity both as a function of time of day and time of year would have been preferable. In order for this model to be accurate and representative, a study of traffic loading patterns and traffic intensity would be required. The change in load model would change the partial safety factors. This change in load model could be a valid extension of the project if more time was available. Additionally, an investigation of the precision of fatigue load model 4 for Danish traffic bridges could be determined by comparing it real traffic data.

In chapter 4 the uncertainties applied in the report are described. Many of the uncertainties and their statistical parameters are found from literature wherein they are intended for use in a similar situation or other materials. This is especially noticeable in the choice of stochastic moments for the model uncertainty in the transformation from load to stress ( $X_{model}$ ). This uncertainty accounts for over 70% of the sensitivity related to the design point (at  $\beta_a = 5.2$ ). The magnitude of the standard deviation of this parameter is very important for the entire reliability analysis.

In chapter 6, a reliability analysis using the stochastic variables presented in table 4.15 on page 47 is conducted for Along-system and Cross-system including a sensitivity analysis. The sensitivity analysis revealed that the annual reliabil-

ity index was highly dependent on  $X_{Model}$ . Both limit state equations utilized Miner's linear damage accumulation rule, use of a different damage accumulation model could have been investigated.

In order to verify the accuracy of the FORM estimate, SORM and CMC simulation at  $\beta_a = 3.8$  was performed. If more computational power and time was available performing CMC at  $\beta_a = 4.8$  and  $\beta_a = 5.2$  would have been optimal. This would ensure or disprove the accuracy of FORM at these reliability levels. Furthermore the use of other simulation techniques could have been investigated.

Partial safety factors derived in chapter 7 are derived with a mean stress level as determined in chapter 3. The partial safety factors could have been derived by varying the mean stress level within a sensible range and observe the change in annual reliability index. This would yield reliability index as a function of mean stress level. The partial safety factor that yielded a mean annual reliability index, equal the target annual reliability could then be used.



---

## Conclusion

A literature study has been conducted to investigate the fatigue behavior and fatigue life assessment of fiber-reinforced polymers. From the literature study, it can be concluded that the fatigue life of composite materials is highly dependent on the mean stresses experienced by the structure. Additionally, it can be concluded that the precision in fatigue life prediction of the constant life diagram depends on the number of  $S-N$  curves used to construct the constant life diagram. Use of more relevant experimental fatigue data for constructing the constant life diagram is preferred.

Estimation of fatigue life using constant life diagrams can not be done analytically with exception of the method suggested by Germanischer Lloyd using their constant life diagram. Therefore the fatigue life prediction method by Det Norske Veritas has been used in this report which is a step-by-step method. The method estimates an equivalent stress amplitude on the nearest  $S-N$  curve and estimate fatigue life for this stress amplitude. Det Norske Veritas method assumes linear interpolation between constant life lines to be valid and is therefore an approximation. It can be concluded that this approximation is of minor importance. The method suggested by Germanischer Lloyd is the fastest as it estimates the fatigue life analytically, but the method uses no experimental fatigue test and uses only the static strengths along with the material parameter  $m$  for the  $S-N$  curve. The method consistently overestimates damage.

As stated in the statement of intent, experimental data is used for derivation of  $S-N$  curves and constant life diagrams using classic statistical analysis for static strengths and Maximum-Likelihood Method for estimation of  $S-N$  parameters with run-outs taken into consideration. The statistical moments are shown in table 4.15.

In order to assess the fatigue loading of a traffic bridge system a load model was established based on DS/EN 1991-2 load model 4.

From the load model with the static load added it can be seen that the fatigue loading of the Along-system is with amplitudes that have a high mean value. For the Cross-system it can be seen that the cyclic mean load is lower but still occurring. This is in part due to the low density of the composite bridge deck. For all fatigue loading in this system a cyclic mean stress of equal to or greater

than the amplitude will occur.

Analysis' to estimate adequate amount of lorry crossings and allowable discretization were conducted and an appropriate load spectrum was derived.

A study of the critical fatigue points at a reasonable stress level was conducted. It was seen that the critical fatigue points were located at  $b_A = 0.4L_A$   $b_C = 0.4L_C$ . It was also noted that the location of the critical fatigue point in Along-system would vary if the stress level changed significantly.

In chapter 6, a reliability analysis was conducted for the Along-system and the Cross-system using different reliability techniques. Two limit state equations were established for respectively the Along-system and the Cross-system. Design parameters are estimated corresponding to annual target reliability levels for bridges according to DK NA using FORM. The design parameters are shown in table 6.5 on page 98. As FORM is the simplest reliability technique, SORM and CMC have been used to estimate the annual reliability level using the design parameters found by FORM. It can be concluded that at an annual target reliability index of 3.8, FORM, SORM and CMC estimate similar annual reliability levels, see tables 6.10 and 6.11 on page 101.

At  $\beta_a = 5.2$ , a sensitivity analysis was carried out for Along-system and Cross-system. The sensitivity analysis showed that the stochastic variable,  $X_{Model}$ , highly affected the reliability index.

Moreover, it can be concluded that correlation between  $\log K$  at  $R = -1$  and  $R = 0.1$  had very little influence for this load spectrum.

In chapter 7, partial safety factors are calibrated using design parameters found using the fatigue limit state equation. Different applications of partial safety factors were investigated.

- Partial safety factors as DS/INF 172
- Partial safety factors as Germanischer Lloyd
- Fatigue design factors as DS/INF 172

A set of partial safety factors were applied as DS/EN 1990 suggests. Three design equations were investigated each using different constant life diagrams; the piecewise linear constant life diagram and the shifted Goodman diagrams. This was done to ensure that the derived partial safety factors can be applied to a design equation using any of the investigated constant life diagrams. The recommended partial safety factors are shown in table 9.1. The partial safety factors can be applied to tension reinforcement bars in traffic bridges wherein the expected load spectrum can be represented by the load spectrum presented in this report. Furthermore the tension reinforcement bar material should be alike that presented in this report.

**Table 9.1.** Recommended values of partial safety factors for composite tension reinforcement bars in traffic bridges in fatigue limit state.

Recommended partial safety factors			
	$\gamma_f$	$\gamma_m$	$K_{FI}$
CC2	1.55	1.3	1.1

A second set of partial safety factors were applied as Germanischer Lloyd suggests. Germanischer Lloyds constant life diagram simplifies the estimation of fatigue life and thereby simplifies the design equation. This simplification makes the design equation very applicable for the common engineer. The recommended partial safety factors are shown in table 9.2.

**Table 9.2.** Recommended values of partial safety factors for composite tension reinforcement bars in traffic bridges in fatigue limit state.

Recommended partial safety factors			
	$\gamma_{Ma}$	$\gamma_{Mb}$	$K_{FI}$
CC2	1.35	1.65	1.1

Only  $\gamma_{Mb}$  has been calibrated.  $\gamma_{Ma}$  is chosen as recommended by Germanischer Lloyd in their guideline.

Fatigue design factors were applied as DS/INF 172 suggests. The fatigue design factors are shown in table 7.11 on page 116. The numeric values of the fatigue design factors are exceptionally high, it would likely feel unintuitive for an engineer to design a structure with a fatigue life of over 300000 years ( $3248 \cdot t$ ). Therefore the fatigue design factor is not recommended for practical use.

Comparing the design parameters determined using the fatigue limit state for the Along-system presented in table 6.5 on page 98 with the design parameter for the Along-system in ultimate limit state shown in table 3.3 on page 27, it can be concluded that the fatigue limit state is not the design limit state for the Along-system as the design parameters determined by fatigue limit state are approximately 10 times smaller than the design parameter of ultimate limit state.



---

# Bibliography

- Allah, Abdin, Selmy, and Khashaba, 1996.** M. H. Abd Allah, Enayat M. Abdin, A. I. Selmy, and U. A. Khashaba. *Effect of Fibre Volume Fraction on the Fatigue Behaviour of GRP Pultruded Rod Composites*. URL: [http://ac.els-cdn.com/0266353895001255/1-s2.0-0266353895001255-main.pdf?\\_tid=5af154e8-f964-11e4-948f-00000aab0f26&acdnat=1431517194\\_c34de6c2a6effecaa9f7c12e24782211](http://ac.els-cdn.com/0266353895001255/1-s2.0-0266353895001255-main.pdf?_tid=5af154e8-f964-11e4-948f-00000aab0f26&acdnat=1431517194_c34de6c2a6effecaa9f7c12e24782211), 1996.
- Alsayed, Al-Salloum, and Almusallam, 2015.** S.H. Alsayed, Y.A. Al-Salloum, and T.H. Almusallam. *Performance of glass fiber reinforced plastic bars as a reinforcing material for concrete structures*. URL: <http://faculty.ksu.edu.sa/yallsoum/Documents/Performance-2000.pdf>, 2015.
- Asfaltindustrien, 2004.** Asfaltindustrien. *Lærebog for vejasfaltarbejde*. URL: [http://materialeplatform.emu.dk/materialer/public\\_downloadfile.do?mat=140366&id=22563535](http://materialeplatform.emu.dk/materialer/public_downloadfile.do?mat=140366&id=22563535), 2004.
- CEN/TC 250, 2014.** CEN/TC 250. *Fibre Reinforced Polymer Structures*. 2014.
- Det Norske Veritas, 2006.** Det Norske Veritas. *Design And Manufacture of Wind Turbine Blades, Offshore and Onshore Wind Turbines*. Det Norske Veritas, 2006.
- DS/EN 1990, 2007.** DS/EN 1990. *Eurocode 0: Basis of structural design*. 2. edition. Danish Standards Association, 2007.
- DS/EN 1990 DK NA, 2009.** DS/EN 1990 DK NA. *EN 1990/A1 DK NA:2009 - Nationalt Anneks til Eurocode 0: Projekteringsgrundlag for bærende konstruktioner Annex A2 Application for bridges*. 2009. Vejdirektoratet, 2009.
- DS/EN 1991-2, 2003.** DS/EN 1991-2. *Eurocode 1: Actions on structures - Part 2: Traffic loads on bridges*. 1. edition. Danish Standards Association, 2003.
- Fiberline Composites A/S, 2014.** Fiberline Composites A/S. *Gang- og cykelbro i Nørre Aaby på Fyn*. URL: <http://fiberline.dk/gang-og-cykelbro-i-noerre-aaby-paa-fyn>, 2014.
- Fiberline Composites A/S, 2003.** Fiberline Composites A/S. *Fiberline Konstruktionshåndbog*. Fiberline Composites A/S, 2003.

- Fiberline Composites A/S, 2015.** Fiberline Composites A/S. *Fiberline.com*. URL: <http://www.fiberline.com/>, 2015. Fiberline Composites A/S.
- Harries and Moses, 2007.** K. A. Harries and J. Moses. *Replacing a composite RC bridge deck with an FRP deck - The effect on superstructure stresses*. URL: <http://www.iifc-hq.org/wp-content/uploads/2011/01/APFIS-032-Harries-and-Moses.pdf>, 2007.
- JCSS, 2014.** JCSS. *JCSS Probabilistic Model Code*. URL: [http://www.jcss.byg.dtu.dk/Publications/Probabilistic\\_Model\\_Code](http://www.jcss.byg.dtu.dk/Publications/Probabilistic_Model_Code), 2014.
- Potyrala, 2011.** Pawel Bernard Potyrala. *Use of Fibre Reinforced Polymers in Bridge Construction. State of the Art in Hybrid and All-Composite Structures*. URL: <http://upcommons.upc.edu/pfc/bitstream/2099.1/12353/1/Use%20of%20Fibre%20Reinforced%20Polymer%20Composites%20in%20Bridge%20Construction.%20State%20of%20the%20Art%20in%20Hybrid%20and%20All-Composite%20Structures..pdf>, 2011.
- Premier Composite Technologies, 2015.** Premier Composite Technologies. *The Benefits of Building with Advanced Composites*. URL: <http://www.pct.ae/composites.php?section=35>, 2015.
- Road Directorate, Scholten, Enevoldsen, Arnbjerg-Nielsen, Randrup-Thomsen, Sloth, Engelund, and Faber, 2004.** Road Directorate, Charlotte von Scholten, Ib Enevoldsen, Torben Arnbjerg-Nielsen, Søren Randrup-Thomsen, Mette Sloth, Svend Engelund, and Michael Faber. *Reliability Based Classification of the Load Carrying Capacity of Existing Bridges*. ISBN: 87-7923-774-6, Report 291. Road Directorate, 2004.
- Schöck, 2014.** Schöck. *Technical Information*. 1. edition. Schöck, 2014.
- Shave, 2014.** Jon Shave. *The future of Fibre Reinforced Polymer structures*. URL: <http://www.nce.co.uk/opinion/the-future-of-fibre-reinforced-polymer-structures/8655487.article>, 2014.
- Sørensen, 2011a.** John Dalsgaard Sørensen. *Statistical analysis using the Maximum-Likelihood method*. Lecture Notes 2014, 2011.
- Sørensen, 2011b.** John Dalsgaard Sørensen. *Notes in Structural Reliability Theory And Risk Analysis*. Aalborg University, 2011.
- Sørensen, 2009.** John Dalsgaard Sørensen. *Baggrundsundersøgelser ifm. udarbejdelse af brospecifikke Nationale Annekser til Eurocodes EN1990 og EN1991*, 2009.
- Toft and Sørensen, 2009.** Henrik Stensgaard Toft and John Dalsgaard Sørensen. *Uncertainty on Fatigue Damage Accumulation for Composite Materials*. Aalborg University, 2009.
- Université libre de Bruxelles, 1996.** Université libre de Bruxelles. *Composite Structures*. URL: [http://ac.els-cdn.com/0266353895001255/1-s2.0-0266353895001255-main.pdf?\\_tid=5af154e8-f964-11e4-948f-00000aab0f26&acdnat=1431517194\\_c34de6c2a6effecaa9f7c12e24782211](http://ac.els-cdn.com/0266353895001255/1-s2.0-0266353895001255-main.pdf?_tid=5af154e8-f964-11e4-948f-00000aab0f26&acdnat=1431517194_c34de6c2a6effecaa9f7c12e24782211), 1996.

**V. M. Karbhari, 2000.** V. M. Karbhari. *Determination of materials design values for the use of fibre-reinforced polymer composites in civil infrastructure*. URL: <http://pil.sagepub.com/content/214/3/163.full.pdf+html>, 2000.

**Vassilopoulos and Keller, 2011.** Anastasios P. Vassilopoulos and Thomas Keller. *Fatigue in Fiber-reinforced Composites*. ISBN: 978-1-84996-180-6. Springer, 2011.



# Appendix



## Comparison of Fatigue Life Prediction Methods

In the following chapter, two methods for predicting fatigue life will be compared to evaluate their accuracy and performance. One of them being Det Norske Veritas (DNV) method for estimating fatigue life is presented in DNV-OS-J102 Annex H. The other being a method describing constant life diagram and  $S-N$  curves in a spatial plane, referred to as the spatial plane method.

First DNVs method is presented and its assumptions is defined. Hereafter the method using spatial planes is presented with associated assumptions. Lastly, the methods are compared based on accuracy and CPU time.

Both methods are tested using data found in [Vassilopoulos and Keller, 2011]. The parameters for these  $S-N$  curves and their corresponding  $R$ -ratios are shown below in table A.1

**Table A.1.**  $S-N$  curve parameters used for the comparison of life estimation methods. [Vassilopoulos and Keller, 2011].

	$\log K$	$m$
$R=10$	40.45	18.83
$R=-1$	42.85	19.34
$R=0.1$	23.32	9.55

### A.1 Fatigue Life Prediction by DNV

DNVs method uses the constant life diagram constructed from available  $S-N$  curves typically  $R = 10$ ,  $R = -1$  and  $R = 0.1$  to obtain fatigue lifetimes for cycles obtained from Rainflow counting with different mean and amplitude strains. DNV assumes a piecewise linear constant life diagram and constant life lines are drawn for lifetimes of 10, 100, 1000... cycles. Furthermore it assumes that all constant life lines are connected to the static tensile and compressive strains at failure as shown in figure A.1.

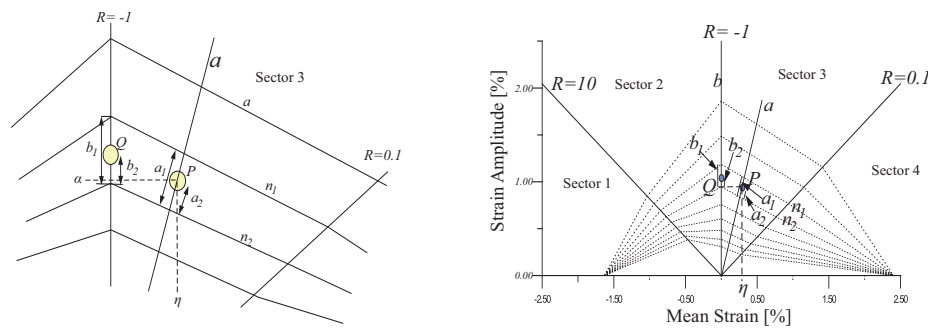


Figure A.1. Principle of DNV's fatigue life prediction method. [Det Norske Veritas, 2006]

With the before mentioned assumptions established DNV presents a procedure estimating the expected lifetime  $N^{exp}$  for a given cyclic mean strain and cyclic strain amplitude presented below and shown in figure A.1.

1. Draw the point  $P$  in the constant amplitude life diagram representing the given stress amplitude,  $\alpha$ , and mean,  $\eta$ .
2. Draw a line  $a$  from the origin of the constant amplitude life diagram (0 mean, 0 amplitude) through and beyond the point  $P$ .
3. Identify the two closest constant life lines nearest to  $P$ ,  $n_1$  and  $n_2$ , where  $n_2$  is the line with the higher number of cycles to failure.
4. Measure the length  $a_1$  on line  $a$  between the two constant life lines  $n_1$  and  $n_2$  nearest to  $P$ .
5. Measure the length  $a_2$  on line  $a$  between point  $P$  and the constant line  $n_2$  with the higher number of cycles nearest to  $P$ .
6. Find the line  $b$  nearest to  $P$  representing fatigue life of a measured  $R$ -ratio, e.g.  $R = 10$ , or  $R = -1$ , or  $R = 0.1$ .
7. Measure the length  $b_1$  on  $b$  between  $n_1$  and  $n_2$ .
8. Calculate  $b_2 = b_1 \frac{a_2}{a_1}$ .
9. Find the strain amplitude,  $\epsilon_{CLD}$ , corresponding to point  $Q$  that lies on  $b$  at a distance  $b_2$  away from the intersection of  $b$  and  $n_2$ .
10. Obtain the characteristic value of the expected number of cycles  $N^{exp}$  for  $\epsilon_{CLD}$  using the measured characteristic  $S$ - $N$  curve.

[Det Norske Veritas, 2006]

Besides the before mentioned assumptions, the expected lifetime,  $N^{exp}$ , determined by this approach is an approximation and not the exact solution. The method is described for strains, it will however be applied for stresses in this report. This is no approximation as the  $S$ - $N$  curves are derived for stresses, and the transformation between stress and strain is linear. The step size between

the constant life lines is an important factor for improving the accuracy of the method. To illustrate this, the step size,  $i$ , defined as eq. (A.1).

$$10^{i_{step}}, 10^{i_{step} \cdot 1}, \dots, 10^{i_{step} \cdot (n-1)}, 10^{i_{step} \cdot n_{step}} \quad i_{step} \in \mathfrak{R} > 0 \quad (A.1)$$

Where

$i_{step}$	Step size
$n_{step}$	Number of steps

In figure A.2 constant life diagrams are shown with different step sizes.

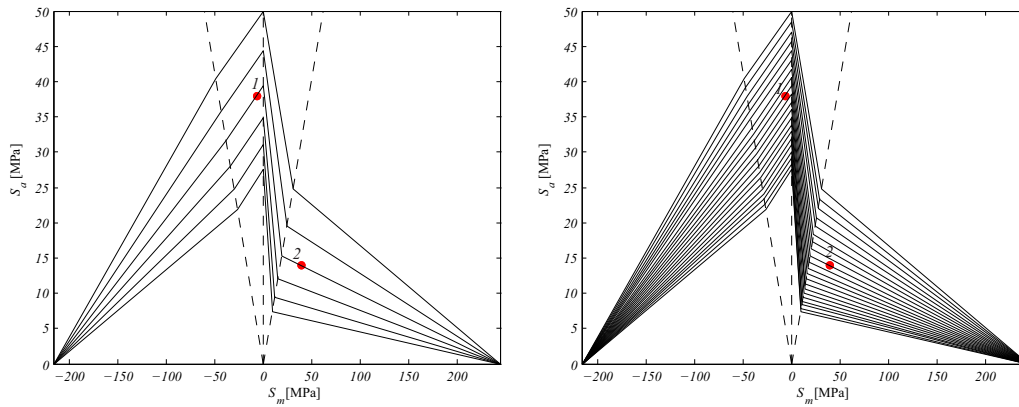
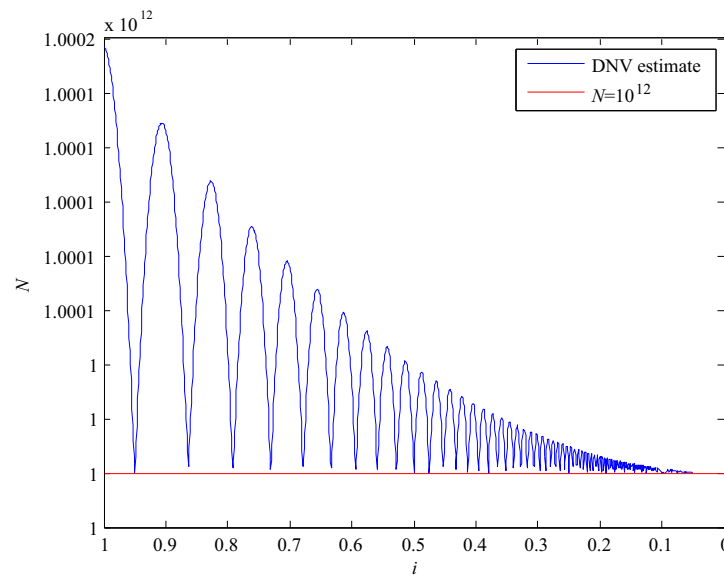
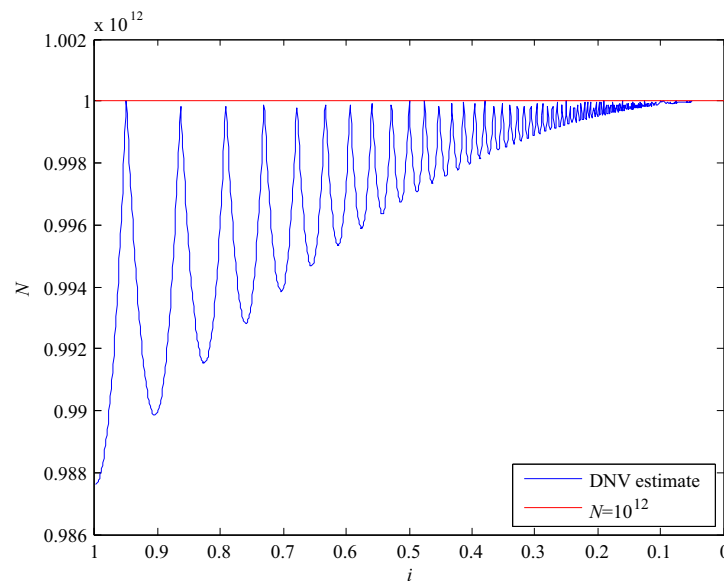


Figure A.2. Constant life diagrams with step sizes,  $i$ , of respectively 1 and 0.25.

The two points shown in figure A.2 are used for a convergence analysis. Both points are located on the  $10^{12}$  constant life line. The convergence analysis is used to determine the require step size needed for the approximate solution is equal to the exact solution. The convergence analysis is shown in figures A.3 and A.4, where the step size starts at 1 in relation to DNVs method and is decreased. The first constant life line is drawn at  $10^{1.5}$ .



**Figure A.3.** Convergence analysis of step size between constant life lines used in DNVs method for point 1.



**Figure A.4.** Convergence analysis of step size between constant life lines used in DNVs method for point 2.

It is seen from both figures A.4 and A.3, that as the step size decreases both points converges towards  $N = 10^{12}$ . It is important to note, that the relative deviation is small, at about  $i_{step} = 1$  is 0.02 % for the point 1 and 1.2 % for point 2, and it can be concluded from this that DNVs decision of a step size of 1 is appropriate for this case. As seen on the figures, point 1 is estimated conservatively at all step sizes, and the opposite is the case for point 2. This means that in a large series of data, some of the precision of the end result will be a product of the errors counteracting each other. The varying precision is due to the mechan-

ics of the analysis. As the step size is decreased, the placement of the constant life lines will vary, and the distance from the points to the nearest constant life line will behave in a sinusoidal manner. Hence the precision will be high when the a constant life line is placed on top of the point, and low when the point is in-between two constant life lines.

## A.2 Fatigue Life Prediction using Spatial Planes

An alternate method for determining number of cycles to failure,  $N$ , is to describe the constant life diagram and  $S$ - $N$  curves with a spatial plane. The advantage of this compared to DNVs method is that  $N$  is determined more accurately. In the following, section the derivation of the spatial planes is presented. The method is derived for piecewise linear constant life diagrams as shown in figure A.5 where a simple constant life diagram with only one  $R$ -ratio ( $R = -1$ ) is presented. Furthermore, it is assumed that all constant life lines are connected to the tensile and compressive yield stress.

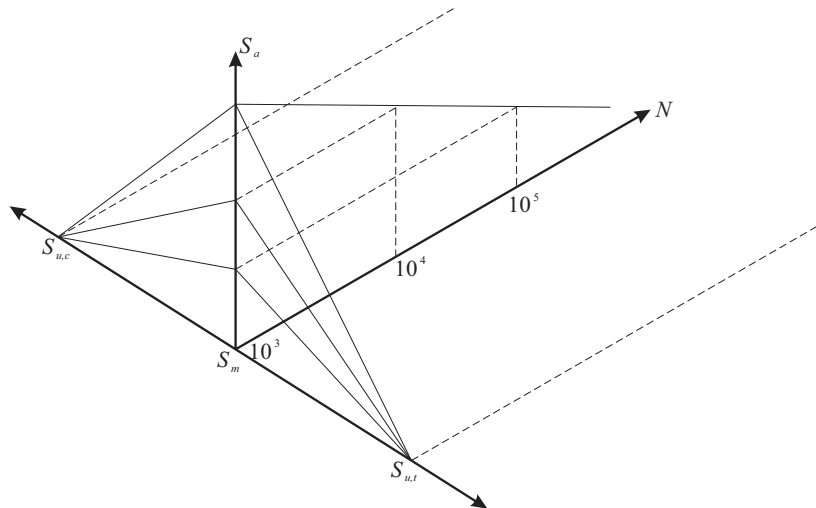


Figure A.5. Spatial illustration of a constant life diagram combined with a  $S$ - $N$  curve.

In order to describe a constant life diagram using planes, two points are considered as shown in figure A.6 illustrating a constant life lines between two  $R$ -ratios at a certain  $N$ .

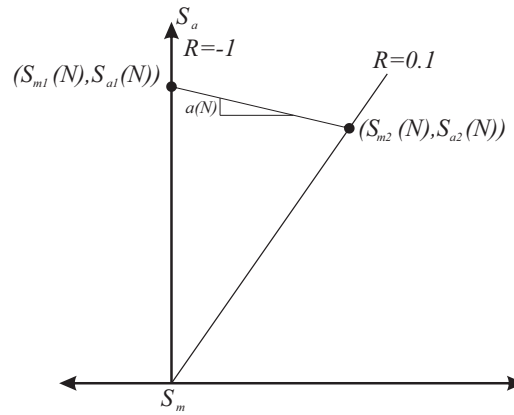


Figure A.6. Principle sketch of CL line.

Since a piecewise linear constant life diagram is considered, the constant life line can be described using a linear equation shown in eq. (A.2).

$$\begin{aligned}
 S_a(S_m, N) &= a(N) \cdot S_m + b(N) \\
 &= \frac{\Delta S_a(N)}{\Delta S_m(N)} \cdot S_m + b(N) \\
 &= \frac{S_{a2}(N) - S_{a1}(N)}{S_{m2}(N) - S_{m1}(N)} \cdot S_m + b(N) \quad (A.2)
 \end{aligned}$$

where

$$\begin{array}{l|l}
 a(N) & \text{Slope of the line} \\
 b(N) & \text{y-intercept}
 \end{array}$$

The cyclic mean stress and cyclic stress amplitude at the two points is determined from the  $S$ - $N$  curve and the relation between the cyclic mean stress and cyclic stress amplitude presented in eq. (A.3) and (A.4).

$$S_a = \left( \frac{K}{N} \right)^{\frac{1}{m}} \quad (A.3)$$

$$S_m = \left( \frac{1+R}{1-R} \right) S_a \quad (A.4)$$

$b(N)$  is determined using the following consideration.

$$\begin{aligned}
 S_a(S_m, N) &= a(N) \cdot S_m + b(N) \\
 b(N) &= S_a(S_m, N) - a(N) \cdot S_m
 \end{aligned}$$

The linear equation describing the line between two  $R$ -ratio can now be ex-

pressed shown in eq. (A.5).

$$S_a(S_m, N) = a(N) \cdot S_m + b(N) \quad (\text{A.5})$$

$$a(N) = \left[ \frac{\left(\frac{K_2}{N}\right)^{\frac{1}{m_2}} - \left(\frac{K_1}{N}\right)^{\frac{1}{m_1}}}{\left(\frac{1+R_2}{1-R_2}\right)\left(\frac{K_2}{N}\right)^{\frac{1}{m_2}} - \left(\frac{1+R_1}{1-R_1}\right)\left(\frac{K_1}{N}\right)^{\frac{1}{m_1}}} \right]$$

$$b(N) = \left[ \left(\frac{K_2}{N}\right)^{\frac{1}{m_2}} - a(N) \cdot \left(\frac{1+R_2}{1-R_2}\right)\left(\frac{K_2}{N}\right)^{\frac{1}{m_2}} \right]$$

Above equation cannot be solved for  $N$ , and iteration has to be applied. For example if a point,  $P$ , is known ( $S_m$  and  $S_a$  is known),  $N$  is obtained by inserting the mean cyclic stress and iterating  $N$  until a relative deviation of the cyclic stress amplitude is obtained.

A qualitative initial guess is made before iteration.  $P$  is located between two  $R$ -ratio (two  $S$ - $N$  curves) and  $S_a$  for point  $P$  is inserted in both  $S$ - $N$  curves and the average of  $N$  is taken and used as initial guess.

It should be noted that eq. (A.5) has to be established between every  $R$ -ratio that forms the constant life diagram. Additionally a modification has to be made when one of the  $R$ -ratio used in the equation is  $R = 1$ .

This is done by equating the cyclic mean stress equal to the ultimate compressive or tensile stress and the cyclic stress amplitude to zero.

In figures A.7 and A.8 a convergence analysis is shown for the same points used in the DNV method. A relative error of  $10^{-7}$  of  $S_a$  is chosen. The convergence analysis measure the number of iterations needed until they converge.

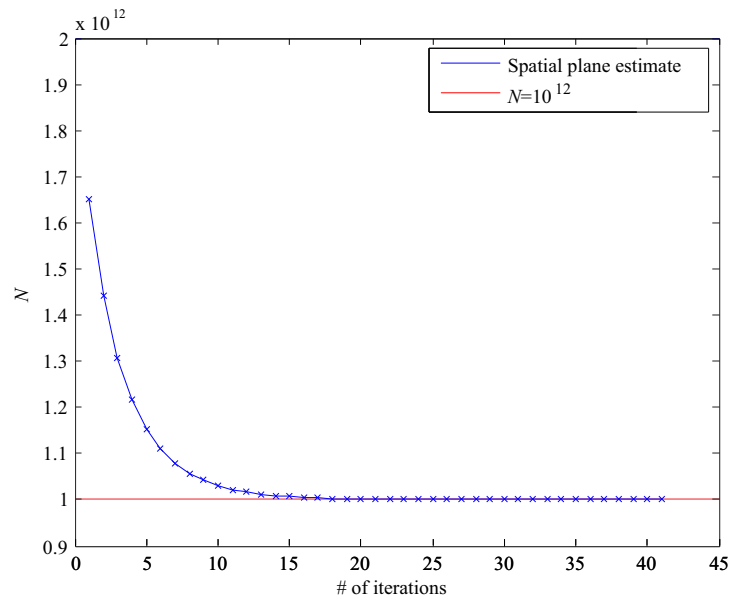


Figure A.7. Convergence analysis for point 1.

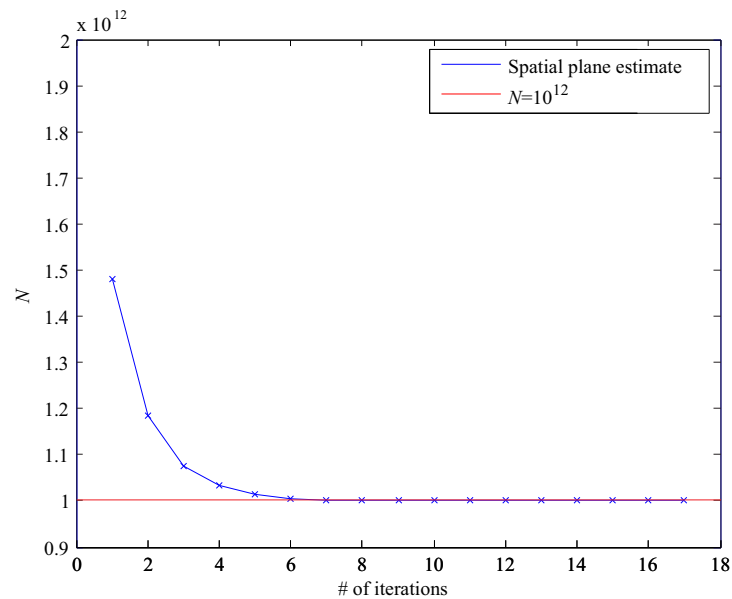


Figure A.8. Convergence analysis for point 2.

It is seen from figures A.7 and A.8 converge after respectively 25 and 10 iterations. The number of iterations needed highly depends on the initial guess and the relative deviation selected.

### A.3 Concluding Remarks

A notable point of comparison besides accuracy is computational time. However, as neither of the programs were optimized and their input parameters vary and their precision differ, such a comparison would be inadequate. When testing the programs at a low amount of cycles with high accuracy it yielded a favorable result for the spatial plane method, as it was both faster and more accurate. However, when a sample pool of 500,000 was tested the DNV-method was superior. Their total damage calculated differed minimally and the DNV-program was more than 20 times faster. These exact numbers may not be replicable with other programs, but the tendency will remain. It is worth noting that some of the DNV-methods' precision is due to the conservatism and non-conservatism of the individual cycles counteracting each other. At an unrealistically low amount of cycles, the spatial plane method will be faster as the large amount of calculations per cycle is still less than the calculations needed from the DNV method in order to assess the nearest constant life lines. When the sample size is increased, the number of calculations from the spatial plane method will increase linearly with the number of cycles. However, the DNV-method will still need approximately the same amount of calculations for assessing the nearest constant life line and then only a single set of calculations for determining the fatigue life of the cycles. In conclusion, the DNV-method is preferable in most cases, as the precision is decent at the recommended level and can be improved significantly by e.g. using 10 times more constant life lines. If exceptionally large precision is needed and large computational power was available, the method of spatial planes could prove useful.

---

## Calculation of Concrete Beam

In order to determine the dead load of the bridge, the dead load of the Along-system has to be determined based on the static system presented in figure 3.2 in ultimate limit state. Furthermore the first moment of area from ultimate limit state is compared to the first moment of area in fatigue limit state in section 6.5. A rough calculation according to DS/EN 1992-1 is carried out with loads applied in accordance with DS/EN 1991-2. Load Model 1 (LM1) is applied as DS/EN 1991-2 states that this model should be used for general and local verifications in ultimate limit state. The load model consist of two partial systems: A double concentrated load,  $Q_k$  defined as.

$$\alpha_Q Q_k$$

A uniformly distributed load,  $q_k$ , defined as.

$$\alpha_q q_k$$

Both loads are applied simultaneously.  $\alpha_Q$  and  $\alpha_q$  is dependent on expected traffic and possibly on different classes of routes. Due to no information regarding these factors,  $\alpha_Q$  and  $\alpha_q$  are set to 1.0. Additionally, the uniformly distributed load should be applied only in unfavorable parts of the beam. Partial safety factors on the loads are applied according to DS/EN 1990 DK NA [DS/EN 1990 DK NA, 2009]. It is concluded from a simple check that the load combination with the variable load is always critical. Therefore the following partial safety factors are used.

**Table B.1.** Partial safety factors from DS/EN 1990-1-1 DK NA applied.

$\gamma_Q$	1.4
$\gamma_G$	1.0

1.4 is for traffic load on bridges. And  $\gamma_G$  is for the dead load where variable loads are dominant.

The characteristic values of  $Q_k$  and  $q_k$  are taken from table B.2.

Table B.2. Load model 1: characteristic values. [DS/EN 1991-2, 2003]

	Axle loads $Q_{ik}$ [kN]	$q_{ik}$ [kN/m <sup>2</sup> ]
Lane Number 1	300	9
Lane Number 2	200	2.5
Lane Number 3	100	2.5
Other lanes	0	2.5
Remaining area $q_{rk}$	0	2.5

As the bridge system in this report has two lanes only loads for "Lane Number 1" is used together with the load for "Remaining area". The load model 1 is illustrated in figure B.1.

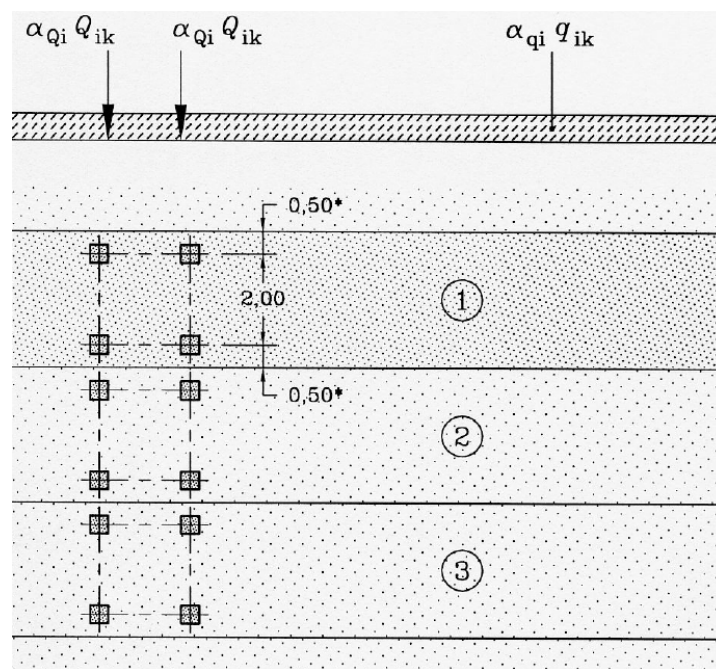


Figure B.1. Application of load model 1.

The point and distributed loads are applied directly to the Cross-system as shown in figure B.2.

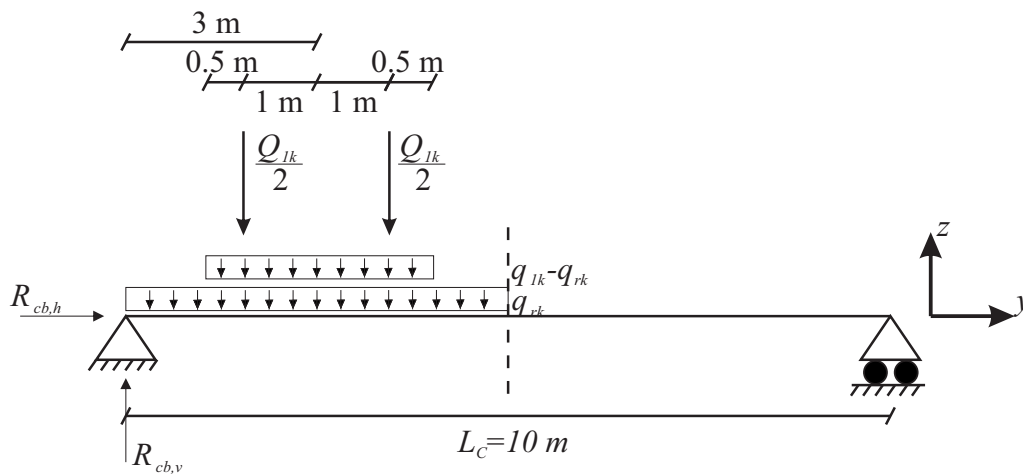


Figure B.2. Static system and applied loads of Cross-system.

Only one axle is shown in figure B.2 as it is assumed in chapter 5 that only one axle loads the Cross-system at any time. The reaction from the cross beam with point loads becomes a line load in the Along-system.

$$\begin{aligned}
 R_{cb,v} &= q_{rk} \cdot 5 \text{ m} + (q_{1k} - q_{rk}) \cdot 3 \text{ m} + (5 \text{ kN/m}^2 + 1 \text{ kN/m}^2) \cdot 5 \text{ m} \\
 &= q_{rk} \cdot 5 \text{ m} + (q_{1k} - q_{rk}) \cdot 3 \text{ m} + (G_{Asphalt} + G_{Deck}) \cdot 5 \text{ m} \\
 &= 62 \text{ kN/m}
 \end{aligned}$$

As the distributed loads should only be applied in unfavorable parts of the system a reaction with only the dead load from the deck and the asphalt is calculated.

$$\begin{aligned}
 R_{cb,v,\text{no dist. load}} &= (G_{Asphalt} + G_{Deck}) \cdot 5 \text{ m} \\
 &= (5 \text{ kN/m}^2 + 1 \text{ kN/m}^2) \cdot 5 \text{ m} \\
 &= 30 \text{ kN/m}
 \end{aligned}$$

Furthermore the reaction from the point load is found as.

$$\begin{aligned}
 R_{cb,v,\text{point load}} &= \frac{Q_{1k}}{2} \left(1 - \frac{2 \text{ m}}{L_c}\right) + \frac{Q_{1k}}{2} \left(1 - \frac{4 \text{ m}}{L_c}\right) \\
 &= \frac{300 \text{ kN}}{2} \left(1 - \frac{2 \text{ m}}{10 \text{ m}}\right) + \frac{300 \text{ kN}}{2} \left(1 - \frac{4 \text{ m}}{10 \text{ m}}\right) \\
 &= 210 \text{ kN}
 \end{aligned}$$

The above calculated reactions are applied to the Along-system as shown in figure B.3. The point loads are positioned at the most critical point on the static system determined by FEM analysis. Furthermore it can be concluded from FEM analysis that it is favorable to apply distributed load to the right side of the Along-system.

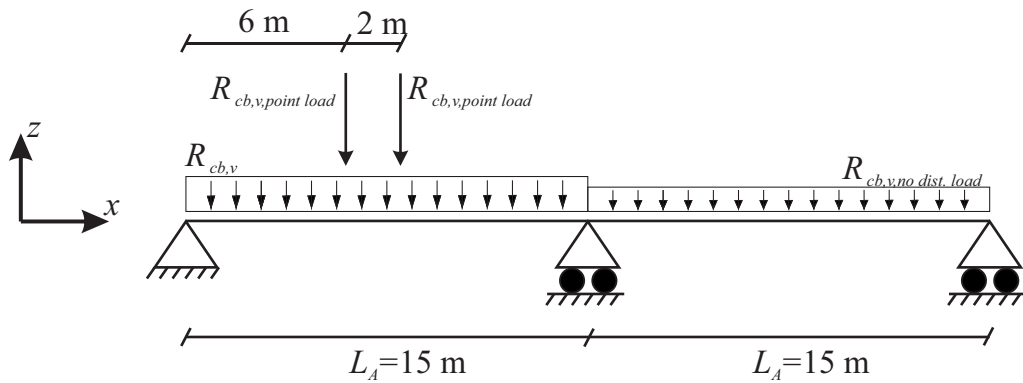


Figure B.3. Static system and applied loads of Along-system.

As seen from figure B.3, the point loads are applied as stated by the load model in figure B.1. The maximum moment is found to be 3091 kNm with the variable load being the dominant load. This is the moment the Along-system are designed for. The bending moment along the beam is shown in figure B.4

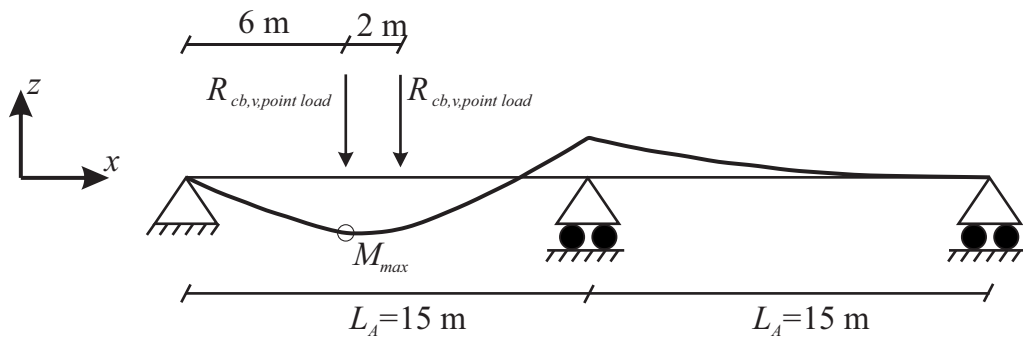


Figure B.4. Bending moment distribution for the beam.

Additionally, an added moment from the dead load of the beam is taken into account. If the weight density of reinforced concrete is  $25 \text{ kN/m}^3$ , the member distributed load can be determined as shown in eq. (B.1).

$$q_{dead} = 25 \text{ kN/m}^3 \cdot \left( \frac{800 \text{ mm} \cdot 1000 \text{ mm}}{10^6} \right) = 20 \text{ kN/m} \quad (\text{B.1})$$

where 800 mm is the width and 1000 mm is the height of a qualitative guess of the design of the reinforced concrete beam presented in figure B.5 and table B.3. The added load gives a total moment of 3564 kNm using the dimensions presented in table B.3.

The beams are designed for pure bending with equal amount of compression and tension reinforcement bars. Calculation with compression reinforcement is basically the same as without, the only change is that the compressive zone changes due to the contribution from the reinforcement. The stresses are found using Navier's equation as well as the assumption that the horizontal projection needs to be zero. A cracked cross-section is assumed. Based on figure B.5, the stresses can be found as shown below.

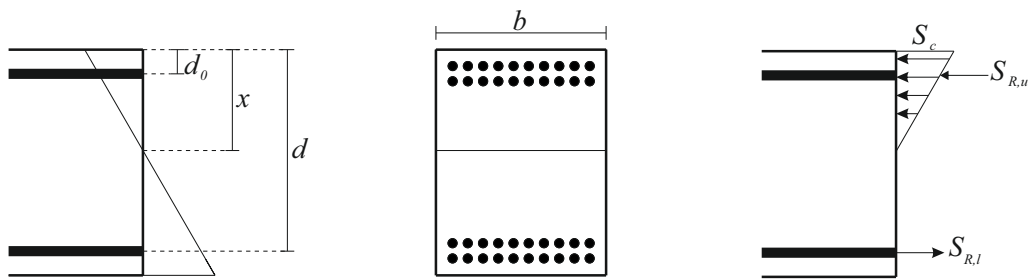


Figure B.5. Cross-section of the beam.

A qualitative guess of the design of the reinforced concrete beam is also presented in figure B.5.

The cross-section consists of a total of 40 reinforcement bars, 20 in the top and 20 in the bottom of the cross-section with a diameter of 20 mm. A concrete C60 is chosen and characteristic values are given in table B.3

Table B.3. Characteristic values.

Reinforcement bar diameter		$\varnothing 20$
Characteristic concrete strength	$f_{ck}$	60 MPa
Elasticity modulus of concrete at failure	$E_{ck}$	7.3 GPa
Elasticity modulus of composite rebar $E_R$	41.3 GPa	
Elasticity ratio	$\alpha \left( = \frac{E_R}{E_{ck}} \right)$	5.7
Height of beam	$h$	1000 mm
Width of beam	$b$	800 mm
Area of reinforcement, upper half	$A_{R,u}$	6283 mm <sup>2</sup>
Area of reinforcement, lower half	$A_{R,l}$	6283 mm <sup>2</sup>
Distance, top to upper reinforcement	$d_0$	50 mm
Distance, top to lower reinforcement	$d$	950 mm
Rebar characteristic ultimate tension strength	$S_{u,t,c}$	988 MPa
Rebar characteristic ultimate compression strength	$S_{u,c,c}$	-718 MPa

In order to make the characteristic values design values, partial safety factors have to be applied to the modulus of elasticity and the strengths. It is assumed that the reinforced concrete beams are in-situ cast and are carried out in normal consequence class. The partial safety factors are presented in table B.4.

Table B.4. Partial safety factors.

$\gamma_c$	1.45
$\gamma_3$	1.0

The design values for the concrete are found using eq. (B.2).

$$f_{cd} = \frac{f_{ck}}{\gamma_c \gamma_3} = 41.4 \text{ MPa} \quad (\text{B.2})$$

The design values for composite reinforcement bars are determined as the 5 % quantile of the distributions presented in table 4.5 on page 35.

The compressive zone height,  $x$ , is found using horizontal projection.

$$A_c \frac{1}{2} x + \alpha A_{so} (x - d_0) = \alpha A_{sn} (d - x)$$

$$800 \text{ mm} \cdot x \cdot \frac{1}{2} + 5.7 \cdot 6283 \text{ mm}^2 (x - 50 \text{ mm}) = 5.7 \cdot 6283 \text{ mm}^2 (950 \text{ mm} - x)$$

$$x = 222 \text{ mm}$$

Next, the moment of inertia of determined.

$$I_t = \frac{1}{3} b x^3 + \alpha A_{so} (x - d_0)^2 + \alpha A_{sn} (d - x)^2$$

$$= \frac{1}{3} \cdot 800 \text{ mm} \cdot (222 \text{ mm})^3 + 5.7 \cdot 6283 \text{ mm}^2 (222 \text{ mm} - 50 \text{ mm})^2$$

$$+ 5.7 \cdot 6283 \text{ mm}^2 (950 \text{ mm} - 222 \text{ mm})^2$$

$$= 228 \cdot 10^8 \text{ mm}^4$$

The stresses in the concrete and the reinforcement bars can now be calculated.

$$S_c = \frac{M}{I_t} x = \frac{3564 \text{ kNm} \cdot 10^6}{228 \cdot 10^8 \text{ mm}^4} \cdot 222 \text{ mm}$$

$$= 34.8 \text{ MPa} < 41.4 \text{ MPa} \quad \text{OK!}$$

$$S_{R,l} = \alpha \frac{M}{I_t} (d - x) = 5.7 \cdot \frac{3564 \text{ kNm} \cdot 10^6}{228 \cdot 10^8 \text{ mm}^4} \cdot (950 \text{ mm} - 222 \text{ mm})$$

$$= 643 \text{ MPa} < 988 \text{ MPa} \quad \text{OK!}$$

$$S_{R,u} = -\alpha \frac{M}{I_t} (x - d_0) = -5.7 \cdot \frac{3564 \text{ kNm} \cdot 10^6}{228 \cdot 10^8 \text{ mm}^4} \cdot (222 \text{ mm} - 50 \text{ mm})$$

$$= -152 \text{ MPa} > -718 \text{ MPa} \quad \text{OK!}$$

The stresses are below the ultimate stresses. This design will be used as an estimate of the dead load of the concrete beams with a value of 20 kN/m. The design first area of moment for ultimate limit state at the tension reinforcement bars is.

$$z_d = \frac{I_t}{d - x} = 31 \cdot 10^6 \text{ mm}^3$$

Calculation of the concrete beam can be found on [Appendix-CD, *Concrete Beam*].

## Approximate Fatigue Design

When analyzing the stress spectrum a design parameter will determine the stress levels. This would not be an issue in a material unaffected by mean stresses with a single  $S-N$  curve. However in a piecewise linear constant life diagram calculated with the approximated method proposed by DNV the tendencies and the importance of the mean stress versus the amplitude stresses will vary with the stress level. This can be seen from the findings in section 2.1. A fitting first area of moment will be found by iteration. The fatigue loads will be assessed by Load model 4 shown in chapter 5. The amount of traffic will correspond to traffic category 2, shown in table 5.1. The calculation will be performed deterministically with all parameters at their characteristic value presented in table 4.15 on page 47. The design equation is shown in equation (7.1).

$$0 = 1 - t \cdot D_{PL}(z)$$

where

$D_{PL}$	Annual damage from load spectrum found by the piecewise linear constant life diagram
$t$	Design life, 100 years
$z$	First area of moment relating to the reinforcement bar

The design first area of moment is found to be  $z_d = 2.6 \cdot 10^6 \text{ mm}^3$ . This is for the Along-system designed with for a design life of a 100 years. Since this design parameter was found without the use of any partial coefficients, which would usually be applied in a Level 1 analysis, the design parameter is rounded up to  $z_d = 3 \cdot 10^6 \text{ mm}^3$ . This value will be used for estimating stress levels in the main report, for both the Along-system and the Cross-system.